# Using radiocarbon to trace methane emissions from natural and anthropogenic sources in two Canadian ecosystems.

Regina Gonzalez Moguel

Department of Earth and Planetary Sciences

McGill University, Montreal

May 2022

A thesis submitted to McGill University in partial fulfillment of requirements of the degree of Doctor of Philosophy.

**Contents**

**List of Figures**

## List of tables

## Abstract

Global methane ($CH_4$) emissions originating from natural ecosystems are expected to increase as a result of climate change and human activities. The magnitude of this increase is highly uncertain because we do not fully understand how ecosystems that are vulnerable to climate variability will respond to environmental changes. Given the large global warming potential of $CH_4$, it is crucial to know how these environmental changes, including increased temperature and permafrost thaw, will affect the production, consumption, transport, and emissions of $CH_4$ in vulnerable ecosystems. In this thesis I used carbon-14 ($^{14}C$) and carbon-13 ($^{13}C$), two tracers of methane sources and methane formation process, to investigate the sources of $CH_4$ from two rapidly changing regions in Canada: Nunavik or the region of Northern Quebec, and the Athabasca Oil Sands Region in Alberta. In the first manuscript, I evaluated the main sources of inorganic carbon, organic carbon, and methane in five subarctic lakes in Nunavik formed by the thaw of permafrost and determined the extent to which reservoirs of long dormant carbon from permafrost and deep peat contribute to these carbon pools. In the second manuscript, I used laboratory experiments to assess how temperature changes affect the rate of $CH_4$ production in the lake's sediments and the contribution of different carbon pools as sources of methanogenesis. In the third manuscript, I determined the regional sources of $CH_4$ emissions in the vicinity of the Athabasca oil sands mines in Alberta, one of the largest deposits of oil globally and a region with very high $CH_4$ emissions.

## Résumé

Les émissions mondiales de méthane ($CH_4$) provenant des écosystèmes naturels devraient augmenter en raison du changement climatique et des activités anthropogéniques. L'ampleur de cette augmentation est grandement incertain, car nous ne comprenons pas pleinement de quelle façon les écosystèmes qui sont vulnérables à la variabilité climatique répondront aux changement environnementaux. Étant donné le potentiel important du $CH_4$ comme gaz à effet de serre, il est crucial de connaitre par quels moyens ces changements environnementaux, notamment le réchauffement, le dégel du pergélisol et les activités d'extraction des ressources naturelles, affecteront la production, la consommation, le transport et les émissions de $CH_4$ dans les écosystèmes vulnérables. Dans cette thèse, j'ai utilisé le carbone-14 et le carbone-13, deux traceurs de l'origine du méthane et de leurs processus de formation, pour étudier l'origine du $CH_4$ de deux régions en rapide évolution au Canada: celle du Nunavik, dans le nord du Québec, et celle de la région des sables bitumineux de l'Athabasca en Alberta. Dans le premier manuscrit, j'ai évalué les principales sources de carbone inorganique, de carbone organique et de méthane dans cinq lacs subarctiques du Nunavik qui ont été formés par la fonte du pergélisol. Ensuite, j'ai déterminé dans quelles mesures les réservoirs de carbone emmagasiné dans le pergélisol et dans la tourbe profonde contribuent aux principales sources de carbone mentionnés plus haut. Dans le deuxième manuscrit, j'ai effectué des expériences en laboratoire pour évaluer comment le changement de température affecte le taux de production de $CH_4$ dans les sédiments de lac ainsi que la contribution de différents réservoirs de carbone en tant que sources de méthanogenèse. Dans le troisième manuscrit, j'ai déterminé les sources régionales d'émissions de méthane à proximité des mines de

sables bitumineux en Alberta, l'un des plus grands gisements de pétrole au monde et une région avec des émissions de $CH_4$ très élevées.

## Acknowledgements

I would like to express my deepest gratitude to my supervisor Peter Douglas who patiently guided me, frequently encouraged me on my research, and always genuinely supported my decisions. I would also like to thank my committee members Irene Gregory Eaves and Nagissa Mahmoudi for their valuable feedback on my projects.

This project would not have been possible without my co-authors (mentioned in author contributions) and a number of other collaborators including Isabelle Laurion, Warwick Vincent, Stephanie Arnold, Richard Petagumskum, Thi Hao Bui, Melanie Burnett, Kathryn Rico, Lauren Rosenthal, Audrey Laberge-Carignan, Raoul-Marie Couture, the Centre d'Etudes Nordiques field station team, Lauriant Giroux, Tony Bromley, Sally Gray, Rowena Moss and Ross Martin, the Rafter Radiocarbon Lab team, Ralf Staebler, and Doug Worthy.

I would like to thank the EPS administrative staff (Anne, Kristy, and Angela) and to the members of the Adams Club for all the afternoons at Thomson House, wine and cheeses, barbecues, and wizard Fridays. I'm also grateful with my friends and family (especially to Angelica and Pedro) for their unconditional support through challenging periods of my PhD.

Finally, I could have not done completed this thesis without the support from Mexican National Council of Science and Technology (CONACYT), the Fonds Québécois de la recherche sur la nature et les technologies (FRQNT), the Trottier Institute for Science and Public Policy, and the NSERC Northern Research Supplements Program who financed part of my PhD program, field work, and research projects.

## Contribution to original knowledge

This thesis is composed of three manuscripts which contain original research and have been formatted to be published in peer-reviewed journals. The first two manuscripts of the thesis advance our understanding on how climate change induced degradation of permafrost environments affects carbon cycling, and more specifically $CH_4$ production, in lakes. When we published Chapter 3, our article was one of the first to present a dataset with $^{14}C$ measurements for all significant carbon fractions involved in the carbon cycling in thermokarst lakes. Some of the key findings that were revealed from this dataset was that the pathway of $CH_4$ emission in the lakes that we sampled largely determines $^{14}C$ ages of $CH_4$, that particulate organic matter has a larger contribution of old carbon pools compared to dissolved organic carbon, and that the dissolved gases have a larger contribution of contemporary carbon pools compared to the particulate and dissolved organic carbon fractions.

When we wrote Chapter 4, there was very limited information on $CH_4$ production rates from lake sediments, especially from Canadian ecosystems, and even less radiocarbon data. We generated, to our knowledge, the first measurements of $^{14}C$ in $CH_4$ produced from thermokarst lake sediment incubations. One of our main findings was that microbial communities in lake sediment incubations respond to warming by producing $CH_4$ from contemporary carbon pools at faster rates.

Lastly, at the time of publication of Chapter 5, there were very few published papers in which both $^{13}C$ and $^{14}C$ had been implemented simultaneously in atmospheric $CH_4$ samples for emissions source attribution. We were one of the firsts groups to apply this technique to source appointment of $CH_4$ emissions at a regional level. The key finding for this chapter was that most of the atmospheric $CH_4$ in the region is from anthropogenic origin, with surface mines as the largest source of $CH_4$.

## Author contributions

I am the first author in all three manuscripts that compose this thesis' chapters with several colleagues as co-authors. I contributed with the project development, manuscript writing and editing, fieldwork, and data processing. Peter Douglas, my PhD supervisor, was a coauthor in all three manuscripts and was jointly responsible for the project design, idea development, manuscript editing, organizing and conducting fieldwork, and analyzing data.

The first manuscript (Chapter 3) was published in the *Journal of Geophysical Research: Biogeosciences* in 2020. Adrian Bass contributed to fieldwork, manuscript editing, and scientific discussions. Martine Pilote, Benjamin Keenan, and Alex Matveev contributed to fieldwork. Mark H Garnett contributed with advice on methane gas collection and extraction techniques, and in the collection and analysis of $^{14}C$ data.

The second manuscript (Chapter 4) is being prepared for submission to *Biogeosciences* or *Global biogeochemical cycles*. Nagissa Mahmoudi contributed to experimental design and manuscript editing.

The third manuscript (Chapter 5) was published in *Atmospheric Chemistry and Physics* in 2021. Felix Vogel collaborated with designing the research study and collecting the samples. Hinrich Schaefer and Jocelyn Turnbull analyzed the samples. Sebastien Ars helped with modelling air mass trajectories. All the coauthors contributed with the manuscript editing and discussions of ideas.

## 1. Introduction

The atmospheric dry air mole fraction of methane ($CH_4$) has been rising since industrialization (~1750 CE), largely due to anthropogenic activities, primarily agriculture, fossil fuel extraction and transport, and waste, but also from climate change induced feedbacks from natural sources (IPCC, 2013). In August 2021, $CH_4$ levels reached 1891 ppb, 2.7 times larger than pre-industrial levels, and continue to rise rapidly (Dlugokencky, 2021). Because of the large capacity of $CH_4$ to absorb energy, its short atmospheric lifetime (~9 years), and its indirect effects on climate, $CH_4$ is estimated to have 28 to 36 times the warming potential of $CO_2$ on a 100-year timescale (IPCC, 2013). The indirect effects of $CH_4$ in climate include the production of ozone, the production of water vapor (a powerful greenhouse gas) in the stratosphere, and the production of $CO_2$ when $CH_4$ is oxidized. As a result, even though $CH_4$ global emissions are only 4% of $CO_2$ global emissions on a molar basis, atmospheric $CH_4$ has contributed 20% of the additional radiative forcing accumulated in the lower atmosphere since 1750 (IPCC, 2013). However, the short atmospheric life of $CH_4$ also means that a reduction of $CH_4$ emissions could rapidly lead to a reduction on the global radiative forcing, making $CH_4$ a good target for short-term climate change mitigation.

Current methods for the quantification of $CH_4$ emissions are broadly categorized in bottom-up (BU) methods, based on inventories, process models, and site measurements, and top-down (TD) methods, which are based on atmospheric observations and inversion models. Limitations in both approaches can lead to large discrepancies in their estimations of $CH_4$ emissions (up to 30%), with BU approaches usually overestimating emissions (Kirschke, et al., 2013; Saunois, et al., 2016; Saunois, et al., 2020). In BU approaches, these limitations include uncertainty when upscaling, the lack of representative data, double counting of sources, and uncertainty in land cover, specially of wetlands. For TD approaches, limitations include the need to use a priori estimates, and errors in transport models. Recently, several research groups have made significant combined efforts to gather data from both approaches to develop global methane budgets (Kirschke, et al., 2013; Saunois, et al., 2016; Saunois, et al., 2020) and analyze $CH_4$ trends (Schaefer, 2019; Fletcher & Schaefer, 2019; Turner, Frankerburg , & Kort, 2019). Currently, the Global Carbon Project decadal budget is one of the most comprehensive syntheses of recent global methane budgets (Saunois, et al., 2020). In this budget (2008–2017; based on TD estimates), ~62% of the global methane emissions, estimated to be ~576 Tg $CH_4$ $yr^{-1}$, originated from anthropogenic sources, specifically from agriculture and waste ( ~37%), fossil fuels (~19 %), and biomass and biofuel burning (~5%). Natural emissions represented the remaining ~38% of global emissions, originating mainly from wetlands (~31%) but also from other land sources such as freshwaters and geological sources (~6%). From all these categories, wetlands tend to have the largest $CH_4$ emission uncertainty, and it is highly difficult to accurately distinguish them from other freshwater sources (Kirschke, et al., 2013).

While current $CH_4$ budgets have large uncertainties, future changes in emissions are even more uncertain (Dean, et al., 2018). Wetlands, inland waters, and permafrost ecosystems store large amounts of organic matter because freezing temperatures, low oxygen content, or a high saturation of water slows degradation. At the same time, these environments are especially susceptible to disturbances caused by the effects of climate change and human activities (Trumbore, 2009). Therefore, they are expected to respond to the increasing global temperatures by increasing their $CH_4$ emissions to the atmosphere and creating positive feedbacks to climate change (Dean, et al., 2018; O'Connor, et al., 2010). Methane emissions from these ecosystems are mainly controlled by the microbial production of $CH_4$ through the decomposition of organic matter, and the counteracting microbial consumption, or oxidation, of $CH_4$ (Conrad R. , 2020; Le Mer & Roger, 2001). As a result, climate change is expected to affect their $CH_4$ emissions through changes in the environmental factors that control $CH_4$ production and oxidation, such as temperature, precipitation, and the availability of organic substrates (Dean, et al., 2018; O'Connor, et al., 2010).

Temperature increases might enhance the rates of both microbial $CH_4$ production and oxidation; lengthen productive seasons for both primary production and microbial metabolisms; lower the solubility of $CH_4$ leading to increased formation of $CH_4$ bubbles that escape oxidation zones; and contribute to the thawing of permafrost that will release organic carbon and nutrients to aquatic environments (Gudasz, et al., 2010; Thornton, Wik, & Crill, 2015; Schuur, et al., 2015; Prowse, et al., 2002). The availability of organic substrates in wetlands and inland waters is expected to increase through a variety of processes such as eutrophication, dredging, sediment dumping, vegetation changes, permafrost thaw, reduction of sea ice cover, and coastal erosion (Parmentier, et al., 2013; Christensen, Johansson, Akerman, & Mastepanov, 2004; McCalley, et al., 2014; Vonk, et al., 2012; Sinha, Michalak, & Balaji, 2017). Hydrological changes like changes in precipitation can alter water table levels; modify wetland and lake areas; change the rate of leaching and the delivery of thaw organic materials from permafrost to aquatic systems; and increase soil moisture leading to increased microbial activity (Cook, Smerdon, Seager, & Coats, 2014; Chang, Xu, Fang, Li, & Nie, 2021; Tank, Striegl, McClelland, & Kokelj, 2016; Berg, Sheffield, & Milly, 2016). Overall, these mechanisms are complex and predicting how $CH_4$

emissions will respond to climate change requires improving our understanding and modelling of carbon cycling processes within ecosystems that are vulnerable to climate change.

Two tools used to study the carbon cycling in a diverse range of environments are measurements of the two heavy rare isotopes of carbon, $^{13}C$ and $^{14}C$. The distribution of $^{13}C$ in $CH_4$ is controlled by the mass-dependent fractionation of biological processes (e.g., $CH_4$ production and consumption) and the isotopic signal of the precursor of $CH_4$. The distribution of $^{14}C$ is controlled by the fractionation during biological and physical processes, the isotopic signal of the precursor of $CH_4$, and radioactive decay. However, in most cases $^{14}C$ measurements are corrected using $^{13}C$ in order to eliminate the effects of mass-dependent fractionation. Consequently, by knowing how different formation processes fractionate $^{13}C$ it is possible to know what was the process by which $CH_4$ was formed, and by knowing the rate of $^{14}C$ decay, it is possible to know what the characteristics of the precursors of $CH_4$ are. Given these properties, one of the main applications of $^{13}C$ and $^{14}C$ measurements in $CH_4$ has been to trace sources of $CH_4$, indicating whether $CH_4$ originated from natural or anthropogenic sources, and further indicating what the process of formation was. My goal in this thesis is to then, to apply the capability of $^{13}C$ and $^{14}C$ as $CH_4$ source tracers in three case studies (formatted as research articles) to increase our understanding of how global climate change and human activities have affected $CH_4$ cycling in two vulnerable Canadian environments.

In the first two case studies, my collaborators and I evaluated how permafrost thaw in two subarctic valleys of Northern Quebec (Eastern Canada) has affected the production and emission of $CH_4$ from lakes. Previous studies have identified lakes formed from permafrost thaw as processing sites of soil organic matter and significant global sources of $CH_4$ emissions (Wik, Varner, Walter Anthony, MacIntyre, & Batsviken , 2016). However, strong geographical variations in the composition of permafrost thaw and lakes characteristics have left gaps in our understanding of the availability of permafrost soil organic matter to methanogenesis. Based on these gaps, our main goal in the first case study (Chapter 3) was to use $^{14}C$ to test if $CH_4$ and other carbon fractions in the lakes were sourced by permafrost soil organic matter or by other carbon pools that can be characterized by their radiocarbon age. We hypothesized that permafrost-aged carbon would be a major source of organic carbon, inorganic carbon, and $CH_4$ in the lakes; and that the radiocarbon age would vary between lake types, $CH_4$ emission pathway, and season.

In the second case study (Chapter 4), we aimed to determine how carbon pools of different ages influence $CH_4$ production and what carbon pools would be used to produce $CH_4$ when incubating lake sediments at increased temperatures. We hypothesized that warming would increase $CH_4$ production rates and would allow microbial communities to utilize older carbon pools to produce $CH_4$. We also hypothesized that we would observe lower $CH_4$ production rates and $^{14}C$ ages of $CH_4$ in incubations from lakes that were recently formed by the collapse of palsas, or permafrost peat mounds, as peat tends to contain old and relatively unreactive organic carbon.

In the third case study (Chapter 5) we used the ability of $\delta^{13}C$ and $\Delta^{14}C$ measurements to distinguish fossil fuel and biogenic sources to determine the contributions from key sources to atmospheric $CH_4$ in the Athabasca oil sands region in Alberta. This region, containing one of the largest deposits of oil globally, is a major source of greenhouse gas emissions to the atmosphere in Canada, but the sources of $CH_4$ have not been well characterized in recent years. The previous study in the region found a large contribution of $CH_4$ emissions from tailings ponds and surface mines (Baray , et al., 2018), but no other study has corroborated or updated these findings. Because tailings ponds are surface mines are both formed through different processes and from carbon substrates with distinct $^{14}C$ values, we tested if using $^{13}C$ and $^{14}C$ in atmospheric measurements of $CH_4$ would allow us to estimate the contribution of tailings ponds and surface mines to $CH_4$ emissions. Our hypothesis was that $CH_4$ emissions from the tailings ponds would constitute the major source of $CH_4$ to the atmosphere, as abundant methanogenic activity has been previously detected in the ponds (Small, Cho, Hashisho , & Ulrich, 2015).

Lastly, in Chapter 6, I discuss the gaps that these three study cases covered in the context of the existing literature, as well as the limitations of these studies, the significance of the results and the future research directions that arise from these results.

# 2. Literature review

## 2.1. Carbon-13 as a tracer of $CH_4$ formation

One tool used to study the carbon cycling in a diverse range of environments are the natural abundances of the heavy stable and radioactive isotopes of carbon, $^{13}C$ and $^{14}C$ respectively. The heavy stable isotope $^{13}C$ is a useful tracer of carbon cycling and different biochemical pathways because its distribution across carbon reservoirs varies as a result of isotopic fractionation during physical, chemical, and biological processes (Harmon, 1953; Harmon, 1954). The $^{13}C$ content is commonly expressed as delta $^{13}C$ ($\delta^{13}C$), denoting the ratio of $^{13}C$ relative to $^{12}C$ compared to the Pee Dee Belemnite (PDB) standard and reported in parts per thousand (‰). In terrestrial environments, most of the variation of $\delta^{13}C$ is a result of fractionation resulting from photosynthesis, in which autotrophs transfer $CO_2$ from in the atmosphere to the biosphere (Harmon, 1954; Park & Epstein, 1960). This $\delta^{13}C$ variation is further regulated by the photosynthetic pathway, as well as environmental and physiological influences (Farquhar, 1989). For example, $C_3$ plants consistently express a lower $\delta^{13}C$ value than $C_4$ plants. As autotrophs constitute one of the largest sources of soil organic matter, the $\delta^{13}C$ of soil organic matter range $\delta^{13}C$ values that reflect the $\delta^{13}C$ of the autotrophs that form the soil (Bowling, Pataki, & Randerson, 2008). These $\delta^{13}C$ values are modified with time as certain components of the soils are degraded by microbial metabolisms (Zhu, Di, Ma , & Shi, 2019).

When organic matter is broken down by microbial communities, the $\delta^{13}C$ signal of the source component is carried over the decomposition products and further modified by the different metabolic processes. The $\delta^{13}C$ value of $CH_4$, which is ultimately a product of organic matter breakdown in most natural ecosystems, is determined by the isotopic signal of the $CH_4$ source organic material and the fractionation of carbon induced by different pathways of methanogenesis. In most freshwater systems, the two main pathways of $CH_4$ production are through 1) the reduction of the methyl group in acetate and 2) through the reduction of $CO_2$ (Bethke, Sanford, Kirk , Jin , & Flynn, 2011). The result of this is that a common application of $\delta^{13}C$ measurements in aquatic systems has been to quantify the contribution of the different methanogenic pathways to $CH_4$ production. It is generally agreed that fractionation is larger during the reduction of $CO_2$ compared to the reduction of the methyl group in acetate, meaning that the $CO_2$ reduction produces a $CH_4$ that has a lower $\delta^{13}C$ value. (Whiticar, 1999; Conrad R. , 2005). In many cases however, it is very challenging to provide an accurate quantification of the contribution of the different $CH_4$ production pathways because fractionation factors can vary to a great extent with microbial taxa, substrate availability, growth phase of the microbes, and temperature (Conrad R. , 2005).

The production of $CH_4$ is not the only process that fractionates the carbon isotopic composition of $CH_4$ in aquatic systems. Significant fractionation also occurs during the consumption of $CH_4$, wherein $CH_4$ is microbially oxidized into $HCO_3^-$ , which can occur in both aerobic and anaerobic environments. During both the anaerobic and aerobic oxidation of $CH_4$, there is an increase in $\delta^{13}CH_4$ values and a decrease in $\delta^{13}C$ values of DIC because methanotrophs oxidize $^{12}C$ preferentially, forming isotopically light $HCO_3^-$ and leaving behind isotopically enriched $CH_4$ (Valentine & Reeburgh, 2000). Altogether, $\delta^{13}CH_4$ can provide information on the production and consumption of $CH_4$, although there are important limitations associated to this method. Some of these limitations are that the range of empirical $\delta^{13}CH_4$ values for the production and oxidation pathways are loosely defined, there is significant overlap between these values, and the empirical values in general are based on field data that might not be exclusively representative of the emission pathways in the first place (Conrad R. , 2005). To overcome these challenges, the use of additional tracers such as concentration profiles, $CO_2$ to $CH_4$ ratios, and hydrogen isotopes, as well as the use of laboratory cultures and experiments can help improve the understanding of $CH_4$ production pathways.

The microbial production of $CH_4$ is the main formation process of $CH_4$ in freshwater aquatic systems but it is not the only $CH_4$ formation process. Methane can be formed from other processes such as the thermal decomposition of organic matter as in fossil fuels, and as the product of incomplete combustion. Each of these formation processes have distinct fractionations and therefore result in $CH_4$ with different $\delta^{13}C$ values (Sherwood, Schwietzke, Arling, & Etiope, 2017). Methane formed by the microbial degradation of organic matter in anaerobic conditions, including in lakes and wetlands, is characterized by values around -61.7 ± 6.2 ‰ (Figure 2.1). Methane formed by the thermal and pressure breakdown of organic molecules, otherwise known as thermogenic $CH_4$, is characterized by values around -44.8 ± 10.7 ‰ (Figure 2.1). Methane produced by incomplete combustion is characterized by values around -26.2 ± 15 ‰ (Figure 2.1). Further separation exists within these categories, and distinct $\delta^{13}C$ values can even be linked to a specific $CH_4$ source or geographic region. For example, the $CH_4$ from different fossil fuels (e.g., oil, coal, and natural gas) tend to have different isotopic signatures, and the combustion of $C_3$ plants yield different isotopic values than the combustion of $C_4$ plants (Sherwood, Schwietzke, Arling, & Etiope, 2017).

In the atmosphere, the $\delta^{13}C$ isotopic signature of $CH_4$ is largely controlled by the emissions of $CH_4$ from isotopically distinct sources, and by the fractionation of $CH_4$ sinks. For this reason, a common application of $\delta^{13}C$ measurements in atmospheric $CH_4$ is to constrain $CH_4$ budgets. In particular, the ability of $\delta^{13}C$ to partition microbial $CH_4$ sources from thermogenic sources of $CH_4$, usually deriving from the use of fossil fuels, has been useful in top-down studies that constrain fossil fuel $CH_4$ emissions from regional to global scales (Schaefer, et al., 2016; Lowry, Holmes, Rata , O Brien , & Nisbet, 2001; Townsend-Small, Tyler, Pataki, Xu, & Christensen , 2012; Lopez, et al., 2017; Maazallahi, et al., 2020). Some disadvantages of this method are that there is not a clear separation between the microbial and thermogenic isotopic source signatures, that there are strong spatial differences between $CH_4$ sources, and that some sources might not be exclusive to one category. For example, some fossil fuel reservoirs contain a mixture of thermogenic and microbial $CH_4$ (Head, Jones, & Larter, 2003). To overcome these disadvantages, some source-partitioning studies incorporate the use of additional tracers, such as methane-ethane ratios, hydrogen isotopes, and radiocarbon measurements (Townsend-Small, et al., 2016; Sherwood, Schwietzke, Arling, & Etiope, 2017).

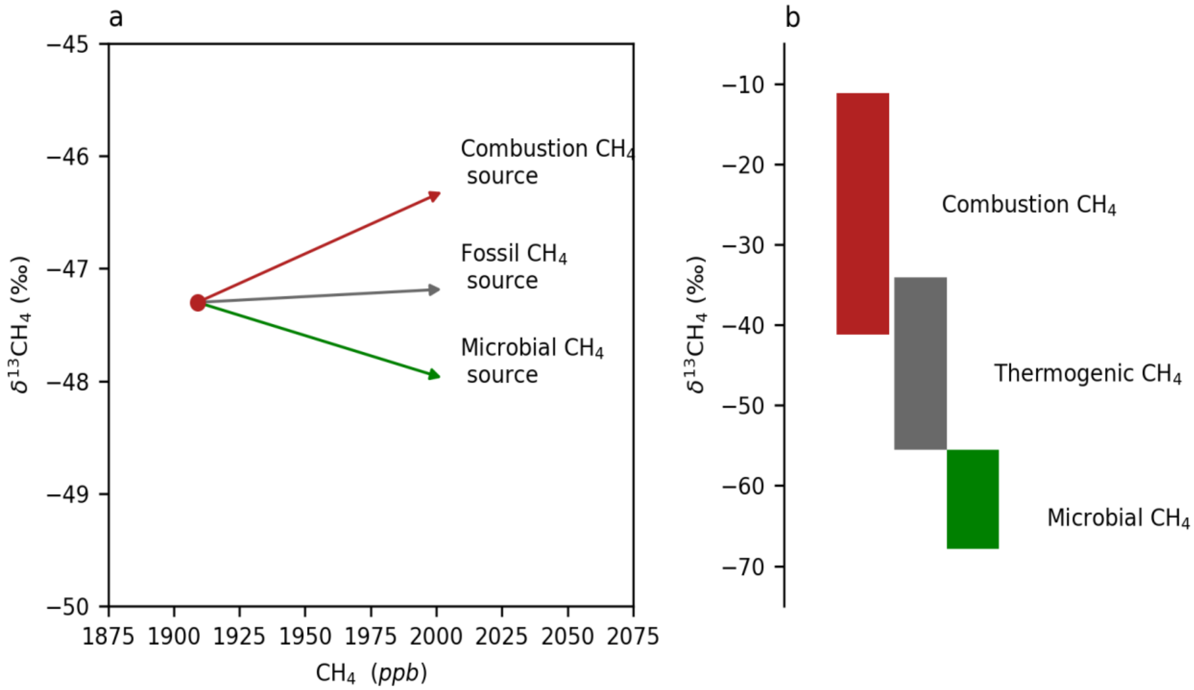

**Figure 2.1 Using $\delta^{13}$CH4 for source partitioning.** a) The diagram shows the theoretical expected changes in $CH_4$ mole fraction and $\delta^{13}CH_4$ from an atmospheric background (red dot) when adding exclusively thermogenic $CH_4$, microbial $CH_4$, and combustion $CH_4$. For example, the addition of microbial $CH_4$ would increase $CH_4$ mixing ratio and shift the $\delta^{13}CH_4$ towards lower values, as microbially produced $\delta^{13}CH_4$ tend to range around -62 ± 6‰ (Sherwood, Schwietzke, Arling, and Etiope, 2017). Regionally, the effects of the sinks are assumed to be zero as atmospheric transport is faster than the $CH_4$ half-life in the atmosphere. b) $\delta^{13}CH_4$ values from different sources can vary greatly regionally, although most values fall within these three category ranges compiled by Sherwood, Schwietzke, Arling, and Etiope (2017).

## 2.2. Radiocarbon as a tracer of $CH_4$ sources and the cycling of carbon

Radiocarbon ($^{14}C$) is another tool used to trace the carbon cycling because it provides information about the precursors of $CH_4$. As with $^{13}C$, the distribution of $^{14}C$ depends on the mass-dependent fractionation of biological and physical processes, but unlike $^{13}C$, it is also affected by radioactive decay (Trumbore, 2009). Radiocarbon is synthesized in the atmosphere by the interaction of cosmic rays with atmospheric gases and enters the carbon cycle and terrestrial systems through photosynthesis, as plants and other autotrophs uptake $CO_2$ from the atmosphere to produce energy. When plants die their $^{14}C$ distribution is preserved in organic matter, and because radiocarbon is not stable, it decays into Nitrogen-14 with a half life of 5730 years. In most cases, $^{14}C$ is normalized to a standard $\delta^{13}C$ of -25 per mil (‰) when reported, which eliminates the effects of mass dependent fractionation. A consequence of this is that by calculating how much the fractionation-corrected $^{14}C$ to $^{12}C$ ratio has decreased due to decay and comparing it with the original atmospheric ratio, it is possible to determine the time that has passed since the component was incorporated to the terrestrial system from the atmosphere.

One of the more common current ways to measure radiocarbon content is through an accelerator mass spectrometer, in which a detector measures the ratio of $^{14}C$ to $^{12}C$ atoms, and the ratio of $^{13}C$ to $^{12}C$ atoms in a sample. There are several ways of reporting radiocarbon, following the conventions of Stuiver and Polach (1977). The notation fraction of modern carbon (FMC) compares the ratio of $^{14}C$ to $^{12}C$ to a “modern” standard, and then normalizes it to a $\delta^{13}C$ of -25 ‰. “Modern” in this case is defined as 95% the radiocarbon content of NBS Oxalic Acid normalized to a $\delta^{13}C$ of -19 ‰ (Olson, 1970). The radiocarbon age is a notation derived from the FMC that uses the Libby’s half-life of 5568 years to calculate the time in years that spanned before the “present”, where the “present” is the year 1950. The formula used to make this calculation is $Age = -8033\ln(FMC)$. Because the half-life of $^{14}C$ is 5730 years, the oldest radiocarbon dates that can be accurately measured in samples are around 50000 years. The notation delta $^{14}C$ ($\Delta^{14}C$) reports the ratio of $^{14}C$ to $^{12}C$, compared to a decay-corrected standard (corrected to the year 1950), and normalized to a $\delta^{13}C$ of -25 ‰. Unlike FMC, $\Delta^{14}C$ is corrected to account for the decay since the sample was collected to when it was measured.

A relevant application of radiocarbon measurements in terrestrial ecosystems is to track the cycling of organic matter in soils and sediments. Soils are a very complex mixture of chemical components that receive a constant input of dead organic matter while at the same time losing carbon as certain components are respired to $CO_2$ or transformed into different compounds that can be metabolized by a range of microorganism including methanogens, or leached as dissolved organic carbon (Trumbore, 2009). Because these processes operate at different timescales in different components, radiocarbon can be used to inform on the loss and decomposition rates of certain components (fixed before 1960) and the accumulation of other components. Commonly, scientists conceptualize soil as being separated in “pools” for simplicity and use radiocarbon abundances to make inferences about the turnover rates of these pools. This separation in “pools” is also useful to determine what are the main soil horizons that contribute to respiration or other microbial processes in different ecosystems. For example, radiocarbon measurements have helped determine that the main source of surface soil heterotrophic respiration is soil with decadal residence times (Schuur, Carbone, Hicks Pries, Hopkins, & Natali, 2016).

Certain components of the organic material in soils and sediments are sometimes stabilized by chemical, physical, or climatic mechanisms such as freezing, sorption, or by having a chemical structure that is resistant to decomposition (Trumbore, 2009). In these cases, the components that are stabilized in the soils or sediments will have a distinct $^{14}C$ age that depends on the decomposition rates and the time since the component was fixed in the stabilized reservoir. These properties are particularly useful in permafrost ecosystems, where thaw can allow the mobilization, export, and decomposition of previously preserved soil carbon deposits. These soil deposits will transmit their unique $^{14}C$ age to other carbon components when mobilized as dissolved organic carbon (DOC), particulate organic carbon (POC), or mineralized into other components such as $CO_2$ and $CH_4$. As a result, one important application of $^{14}C$ measurements in terrestrial systems has been to trace the contribution of previously frozen soil organic carbon in actively cycling components such as $CH_4$, $CO_2$, DOC, POC, simply by comparing the isotopic values of these fractions with the radiocarbon age of the soil deposits and other potential sources (Estop-Aragonés, et al., 2020). For example, in recent years several research groups have focused on using $^{14}C$ measurements to assess the transport of thawing permafrost soil organic carbon through arctic aquatic networks in the form of DOC and POC (Wild, et al., 2019; Dean, et al., 2018). Similarly, a growing body of literature seeks to understand to what extent permafrost soil organic carbon can contribute to $CH_4$ and $CO_2$ emissions from wetlands and lakes (Elder, et al., 2018; Walter Anthony , et al., 2016; Estop-Aragonés, et al., 2020).

Another application of $\Delta^{14}C$ measurements deriving from the distinct $\Delta^{14}C$ values in different reservoirs is the partitioning of sources of $CH_4$ and $CO_2$ to the atmosphere. The principle is that we can compare the isotopic values of atmospheric $CO_2$ or $CH_4$ with the contrasting isotopic values of the potential sources to determine what source contributes the most. The value of $\Delta^{14}C$ in atmospheric $CH_4$ is given by the biogenic $CH_4$ emissions, fossil fuel $CH_4$ emissions, and $CH_4$

from nuclear emissions (Figure 2.2). Globally, the large influence of nuclear emissions in background atmospheric $CH_4$ stems from the release of large amounts of $^{14}C$ during the testing of nuclear weapons in the 1950s and 1960s (Lassey, Lowe, & Smith, 2007). Regionally, the effect of nuclear emissions is dependant in the region of study, the proximity to the nuclear power plants, and the uncertainty on the magnitude of nuclear power plant emissions (Graven , Hocking, & Zazzeri, 2019). In the case of atmospheric $CO_2$, the value of $\Delta^{14}C$ is mainly influenced by biogenic $CO_2$ emissions and fossil fuel $CO_2$ emissions. Fossil fuels lack $^{14}C$ because they are millions of years old, and as a result $CO_2$ and $CH_4$ produced from fossil fuel precursors will have a $\Delta^{14}C$ value of -1000 ‰. Conversely, the isotopic value of biogenic emissions of both $CO_2$ and $CH_4$ approximates the $\Delta^{14}C$ value of atmospheric $CO_2$, but due to the anthropogenic addition of fossil fuel-derived carbon to the atmosphere, this value is constantly decreasing. In 2021, the atmospheric $\Delta^{14}CO_2$ value was around -5‰ in the northern atmosphere (Hammer & Levin, 2017), but in a business-as-usual emissions scenario $\Delta^{14}CO_2$ could reach -250 ‰ in 2100 (Graven H. , 2015).

The use of radiocarbon to partition $CH_4$ sources in atmospheric samples is relatively recent, and therefore there are only few studies applying this technique. Globally, radiocarbon measurements in $CH_4$ have been used to constrain the current contribution from fossil fuels to atmospheric $CH_4$ (Lowe, Brenninkmeijer, Manning, Sparks, & Wallace, 1998), but also to constrain the pre-industrial fossil $CH_4$ emissions using $CH_4$ in ice-core records (Hmiel, et al., 2020). At a regional level, a few studies have used radiocarbon to identify the main sources of $CH_4$ emissions in European and North American cities but found several challenges when implementing this method (Eisma, Vermeulen, & Van der Borg, 1995; Townsend-Small, Tyler, Pataki, Xu, & Christensen , 2012). Some of these challenges are a lack of a $\Delta^{14}CH_4$ background measurement record, the lack of clear correlations between the mole fraction of $CH_4$ and its radiocarbon signal in samples, and the difficulty of constraining regional radiocarbon sources to the atmosphere (Graven , Hocking, & Zazzeri, 2019). For example, the emissions of $^{14}CH_4$ from nuclear power plants to the atmosphere are largely unquantified in certain regions such as continental Europe (Graven , Hocking, & Zazzeri, 2019; Eisma, Vermeulen, & Van der Borg, 1995). Other challenges for the implementation of this method are technical, such as the need for very large air samples in order to obtain accurate $^{14}C$ measurements and the expensiveness of analyzing samples in the accelerator mass spectrometer (Zazzeri, Xu, & Graven H., 2021).

Considerable effort has been made in recent years to overcome these challenges. Some of the advances related to $^{14}C$ seek to improve the sampling systems to reduce the volume of sample needed to get reliable $^{14}C$ measurements (Zazzeri, Xu, & Graven H., 2021). Other advances have focused on improving the interpretation of $^{14}C$ data. For example, Graven, Hocking, and Zazzeri (2019) developed a framework for the regional analysis of radiocarbon data, re-analyzed the data from Townsend-Small, Tyler, Pataki, Xu, & Christensen (2012), and added a constrain to nuclear emissions from the American city of Los Angeles, allowing to better partition the $CH_4$ sources in the region. Lastly, including measurements of additional tracers such as ethane, $\delta^{13}C$, and $\delta D$ could help improve the estimation of $CH_4$ emissions from the different sources.

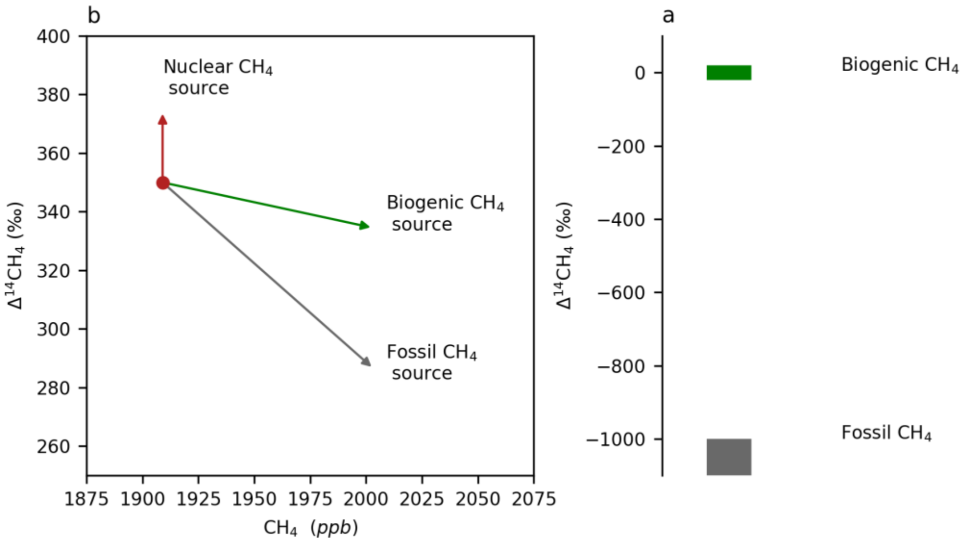

**Figure 2.2. Using $\Delta^{14}CH_4$ as a source tracer.** a) The diagram, adapted from Graven et al., (2019), shows the theoretical expected changes in $CH_4$ concentration and isotopic values from the background (red dot) when adding exclusively a fossil fuel source, biogenic source, or nuclear source. Here, the effect of nuclear emissions varies regionally and depends on the emission rate, although the concentration increase is negligible. As for $\delta^{13}C$ (Fig. 2.1), the effects of $CH_4$ sinks are assumed zero. b) Radiocarbon values of the two main sources of $CH_4$. $\Delta^{14}CH_4$ biogenic equals the $\Delta^{14}C$ value of atmospheric $CO_2$, which decreases annually due to the effect of adding fossil fuel derived $CO_2$ to the atmosphere.

### 2.3. $CH_4$ cycling in northern lakes

The $CH_4$ cycle in northern lakes has two main components that are the microbial production of $CH_4$ and the microbial consumption of $CH_4$ (Figure 2.3). However, before the production of $CH_4$ can happen, the organic matter (OM) that is in the lake or that is imported to the lake has to be broken down to simpler substrates. For this reason, the complexity and composition of the organic matter (OM) as well as its cycling are an essential part of lake $CH_4$ dynamics. In the water column, dissolved organic carbon (DOC) is generally the largest carbon pool and because of this it largely impacts the lake's physical, chemical, and biological characteristics (Seekel, Lapierre, & Cheruvelil, 2018). The particulate organic carbon (POC) is also an important carbon pool in the water column which is involved in the movement of carbon between the water column and the sediments (Kharbush, et al., 2020). In the sediment, a mixture of components that include a variety of organic compounds is transformed by a series of physical, chemical, and biological processes on timescales of days to years and therefore its composition also affects the production of $CH_4$ in the lake.

The decomposition of organic matter involves several steps and groups of microbial communities, that start with the hydrolysis of organic macromolecules, and follows with either 1) respiration or 2) the partial breakdown of OM through the glycolysis and fermentation of components such as sugars, fatty acids, and aminoacids (Bridgham, Cadillo-Quiroz, Keller, & Zhuang, 2013). In the second pathway, fermentation can convert pyruvate, a product of glycolysis, into a variety of end products such as acetate, lactate, and ethanol depending on the type of microorganisms involved in the process. In the first pathway (respiration), an electron acceptor is used to reduce an organic substrate to generate energy for the cell. The process that generates the most energy is aerobic respiration, in which $O_2$ is used as oxidizing agent in a series of complex processes that involve glycolysis, acetyl-CoA formation, and the citric acid cycle (Konhauser, 2007). Once oxygen is depleted, competing metabolisms work as electron acceptors in a series of redox zones that yield progressively less energy and is therefore less thermodynamically favorable (Bethke, Sanford, Kirk , Jin , & Flynn, 2011). In order, these metabolisms are denitrification ($NO_3^-$

), iron reduction (Fe (III)), manganese reduction (Mn (IV)), sulfate reduction ($SO_4^{2-}$), and methanogenesis.

The production of $CH_4$ in the sediments occurs as the final stage in the decomposition of organic matter, after essentially all other electron donors for other competing metabolisms are depleted. Methanogens can only use few substrates to produce methane, including hydrogen, methyl groups, formate, and few alcohols (Conrad R. , 2020). In most freshwater environments, most $CH_4$ is produced by hyrogenotrophic methanogenesis, where $H_2$ is used as an electron donor to reduce $CO_2$ into $CH_4$, or by acetotrophic methanogenesis, where the methyl group of acetate is reduced to $CH_4$ and the carboxyl group of acetate oxidized to $CO_2$ (Conrad R. , 2020). The proportion of $CH_4$ produced from each of these two main pathways varies in different lake environments, influenced by factors such as temperature, pH, vegetation, degree of eutrophication, and the type of substrates available in the sediments. For example, some previous studies in peatlands have suggested that substrates from thawing palsas (frozen peat mounds) and older peat material are linked to an increase contribution from hydrogenotrophic methanogenesis while younger substrates are linked to acetotrophic methanogenesis (McCalley, et al., 2014; Chanton, et al., 2008). An ongoing question is how the methanogenic communities in northern lakes will adapt to changes in organic substrates and physicochemical lake conditions resulting from permafrost thaw in terms of the dominant methanogenic pathway.

The $CH_4$ that is produced in the anoxic and reduced zones of the sediment diffuses towards other redox zones where it can theoretically be used as an electron donor for sulfate, nitrite, iron, and manganese (Valentine & Reeburgh, 2000). The most studied anaerobic oxidation process in aquatic systems is the anaerobic oxidation of $CH_4$ to $HCO_3^-$ coupled to sulfate reduction, where sulfate ($SO_4^{2-}$) accepts an electron from $CH_4$ and is reduced to $HS^-$ (Knittel & Boetius, 2009). Although common in marine systems, this process is less widespread in freshwater systems because sulfate concentrations tend to be low. In the oxic-anoxic interface, methanotrophic bacteria use dissolved oxygen as an electron acceptor to aerobically oxidate $CH_4$ into $HCO_3^-$. Rates are higher for aerobic methanotrophy in thermokarst lake's water column and sediments compared to anaerobic methanotrophy (Heslop J. , et al., 2020). Ultimately, the rates of $CH_4$ oxidation depend mainly on the concentration of substrates, that in the case of aerobic methanotrophy are oxygen and methane, and to lesser extent on temperature (Lofton , Whalen, & Hershey, 2014).

The $CH_4$ emissions from northern lakes are largely determined by the amount of $CH_4$ produced in the sediment and the amount of $CH_4$ oxidized to $HCO_3^-$. This balance is strongly influenced by the processes in which $CH_4$ is transported and emitted to the atmosphere, which in turn varies geographically and seasonally, and is dependent on lake morphology, lake origin, and the composition of the permafrost that underlies the lake (Kuhn, et al., 2021). During the ice-free season, $CH_4$ oversaturates the water column and diffuses to the atmosphere, while in the sediment pore-water $CH_4$ accumulates in bubbles that are released to the atmosphere in a process termed ebullition (Bastviken, Cole, Pace, & Tranvik, 2004). Compared to ebullition, diffusion is a slower process and is therefore more susceptible to microbial oxidation. During the ice-covered season, ebullition bubbles are trapped in ice or under the ice, where they can diffuse to the water column (Greene, Walter Anthony, Archer, Sepulveda-Jauregui, & Martinez Cruz, 2014). Both the $CH_4$ stored in bubbles and the diffused $CH_4$ are released to the atmosphere when the ice melts in spring. Other release mechanisms are the release of $CH_4$ using plants as conduits to the atmosphere (Bastviken, Cole, Pace, & Tranvik, 2004), although this process is less studied in northern lakes.

The balance of $CH_4$ production rates, $CH_4$ oxidation rates, and transport processes is highly variable across aquatic ecosystems, and for this reason one of the most important current challenges related to $CH_4$ budgets of northern ecosystems is estimating $CH_4$ emissions from lakes. Globally, the current estimations of northern lakes $CH_4$ emissions are between 7 to 25 Tg $CH_4$ $yr^{-1}$ through all pathways (Wik, Varner, Walter Anthony, MacIntyre, & Batsviken , 2016), encompassing a large range of emission and high uncertainty. Some of this large uncertainty stems from the poor representation of ebullition fluxes compared to diffusive fluxes, of certain regions or lake types, and seasons (e.g., from spring ice melt), and lack of differentiation between wetlands and lakes. Additionally, measuring ebullition fluxes accurately is highly challenging because ebullition occurs at irregular time intervals and is heterogeneous in space, and the current sampling techniques capture short time periods. To date, one of the most complete compilation of northern lakes (above 50° N) $CH_4$ flux data comes from the work of Kuhn et al. (2021). Results from this compilation suggest that winter fluxes tend to be lower than fluxes from ice-free seasons, ebullition fluxes tend to be higher than diffusion fluxes, and that lakes in permafrost sporadic zones have the highest diffusive and ebullitive fluxes compared to lakes in zones with discontinuous and continuous permafrost cover.

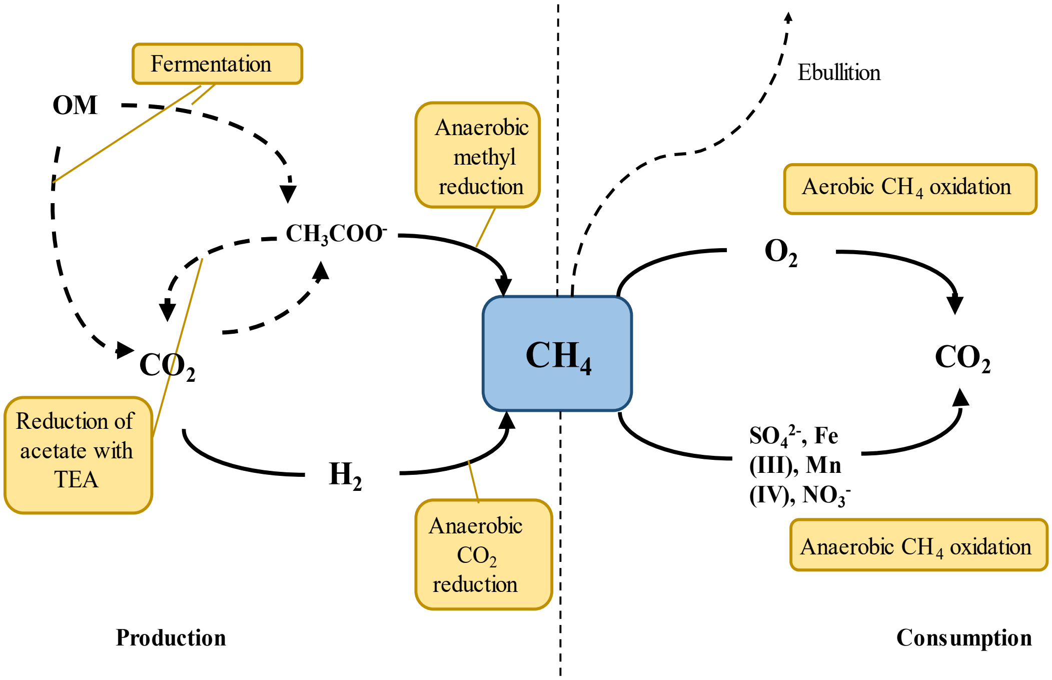

**Figure 2.3 Methane cycle in lakes.** The methane budget in a lake, represented in this diagram, is controlled by the production of $CH_4$ (left panel), and $CH_4$ consumption (right panel). In the right panel, representing the sinks of $CH_4$, the $CH_4$ is oxidized into $CO_2$ through the aerobic oxidation of $CH_4$ with $O_2$ or the anaerobic oxidation of $CH_4$ with other inorganic components, but it can also be removed from the lake by physical processes such as ebullition (dashed line). In the left panel, representing the sources of $CH_4$, $CH_4$ is produced through the reduction of $CO_2$ with $H_2$ or by the reduction of methyl group with the carboxyl group of acetate. Both acetate and $CO_2$ are products of the fermentation of organic matter, and $CO_2$ is also formed from the reduction of acetate during terminal electron acceptor (TEA) processes.

## 2.4 Variability of $CH_4$ dynamics in different types of northern lakes

One challenge in the study of $CH_4$ and $CO_2$ emissions from northern lakes is the difficulty of upscaling fluxes and making generalizations about the processing of different carbon pools because there is a wide diversity of water systems in northern latitudes. There are many factors that influence the distribution of different types of lakes throughout the North including substrate geology, climate, the mechanisms of lake formation, landscape relief, and drainage (Smith, Sheng, & MacDonald, 2007). At the same time, these factors strongly influence the pathway and magnitude of the $CH_4$ fluxes from the lake to the atmosphere (Kuhn, et al., 2021). In terms of radiocarbon, since the lake methane cycle is largely controlled by the transfer of organic substrates through the terrestrial landscape and into aquatic systems, the composition of the surrounding permafrost soil carbon can strongly influence the response in the magnitude and radiocarbon age of the greenhouse gas emissions from northern lakes (Tank, et al., 2020; Elder, et al., 2018).

In the two recent synthesis of $CH_4$ fluxes from Northern lakes, the authors estimated that most $CH_4$ emissions originate from three dominant lake types: peatland ponds, glacial and post-glacial lakes, and thermokarst ponds and lakes (Wik, Varner, Walter Anthony, MacIntyre, & Batsviken , 2016; Kuhn, et al., 2021). In this section I will very briefly introduce each category and highlight the main characteristics of each type of lake. It is important to mention that the results from this synthesis are based on the current existing datasets of lake fluxes, which have a low representation from certain types of lakes, and that there are some limitations with separating lakes in these categories, such as accounting for lakes fitting more than one category. An example of this limitation is that most of the compiled $CH_4$ measurements from thermokarst lakes are restricted to water bodies in Pleistocene loess deposits in Siberia and Alaska, while measurements from thermokarst lakes underlying other types of deposits are underrepresented.

Thermokarst landscapes are estimated to cover ~20% of the northern permafrost region, from which around ~7% are thermokarst lakes (Olefeldt , et al., 2016). Thermokarst ponds and lakes are formed as a direct result of permafrost thaw as the melting of ground ice can leave depressions filled by water (Smith, Sheng, & MacDonald, 2007). The development of these lakes is heavily influenced by topography, ground ice content, extent of permafrost cover, and the composition of the sediments (Olefeldt , et al., 2016). Commonly, the highest thermokarst lake coverages are linked to areas with lower drainage due to an extensive permafrost cover acting as a barrier against water infiltration, and flat topographies in lowland regions such as the Alaskan North Slope or the Yukon delta. Due to the extensive coverage of thermokarst lakes in these regions, some of the better studied thermokarst lakes are those developed in Yedoma deposits, deposits formed in the Pleistoscene by the simultaneous sedimentation of loess and development of permafrost in areas of low topographic relief in Siberia, Alaska, and Canada (Tank, et al., 2020).

A high ice content, high organic carbon content, a low decomposition of the organic carbon, and an abundance of labile compounds such as low molecular weigh compounds are some characteristics that make Yedoma deposits highly labile (reactive). For this reasons, Yedoma lakes have particularly high ebullition fluxes compared to other lakes, and $CH_4$ ebullition “hotspots” are common and persistent even through the ice in winter (Kuhn, et al., 2021). Radiocarbon measurements of ebullition $CH_4$ released from these lakes have found that $CH_4$ is derived from Pleistocene-aged carbon (Estop-Aragonés, et al., 2020), although a subset of measurements showed that for Yedoma lakes in Alaska diffusive $CH_4$ emissions ranged from modern to 3,000 years BP, substantially younger than the soil organic carbon deposits (Elder, et al., 2018). Contrastingly, non-Yedoma thermokarst lakes, frequently with underlying Holocene deposits, have found to emit $CH_4$ bubbles ranging ages of modern to approximately ~3,800 years BP, or Holocene-aged (Estop-Aragonés, et al., 2020).

The advance of ice sheets during the Last Glacial Maximum (LGM) in the northern latitudes resulted in the formation of a large number of lakes by the effect of glacial erosion and deposition (Pienitz, Doran , & Lamoureux, 2008). Glacial processes work through a number of mechanisms that favor the formation of lakes and rivers that include modifying the topographic relieve, eroding substrates, changing drainage patterns, and the emplacement of low-permeability tills, and kettling (Smith, Sheng, & MacDonald, 2007). From all northern lakes, glacial and post-glacial lakes have the largest area coverage and therefore constitute most of the ice-free $CH_4$ fluxes, although the average $CH_4$ and $CO_2$ flux by surface area tends to be the lowest for this lake type (Wik, Varner, Walter Anthony, MacIntyre, & Batsviken , 2016). In the two compilations, glacial lakes tended to have a comparable ebullition and diffusive $CH_4$ fluxes, likely because they tended to be deeper than other types of lakes and to be thermally stratified, which can alter the transport of ebullition and diffusive $CH_4$ to the surface.

Previous studies measuring the radiocarbon in $CH_4$ and $CO_2$ fluxes from glacial lakes have found that $CH_4$ and $CO_2$ fluxes have ages comparable to the radiocarbon ages to SOC, indicating the emission of SOC through $CH_4$ and $CO_2$ (Bouchard, et al., 2015; Preskenis, et al., 2021). When measurements were available, the results showed that there were spatial differences within the lakes, with the oldest $CH_4$ ages originating from emissions in the center of the lakes (Bouchard, et al., 2015). However, the glacial lakes in these two studies tended to be larger and deeper than other types of lakes, and therefore it is likely that the observed results were influenced by the morphological characteristics of these lakes (i.e., the depth).

Wetlands are abundant in the north because certain organic-rich soils, glacio-marine and lacustrine clays impede infiltration of rainwater and snowmelt allowing water to accumulate, and the presence of permafrost can add an additional barrier to infiltration (Pienitz, Doran , & Lamoureux, 2008). Peatlands in particular have poor drainage and low permeability that favor the pooling of surface water and formation of ponds and lakes (Smith, Sheng, & MacDonald, 2007). Peatland lakes are frequently small and shallow, favoring the heating of sediments, and have organic-rich sediments and high concentration of dissolved organic carbon (Wik, Varner, Walter Anthony, MacIntyre, & Batsviken , 2016). $CH_4$ measurements from peatland lakes are scarce, but it is estimated that this type of lake tends to have the highest diffusive $CH_4$ fluxes compared to other types of lakes (Kuhn, et al., 2021). In fact, peatland lakes have the highest fluxes by area unit of all the lake types, but this might be influenced by the small size of these type of lakes compared to other types of lakes (Wik, Varner, Walter Anthony, MacIntyre, & Batsviken , 2016). Radiocarbon measurements in peatland lakes have shown that DOC and POC approach SOC ages but dissolved $CH_4$ and $CO_2$ tend to be younger than organic carbon (Chanton, et al., 2008).

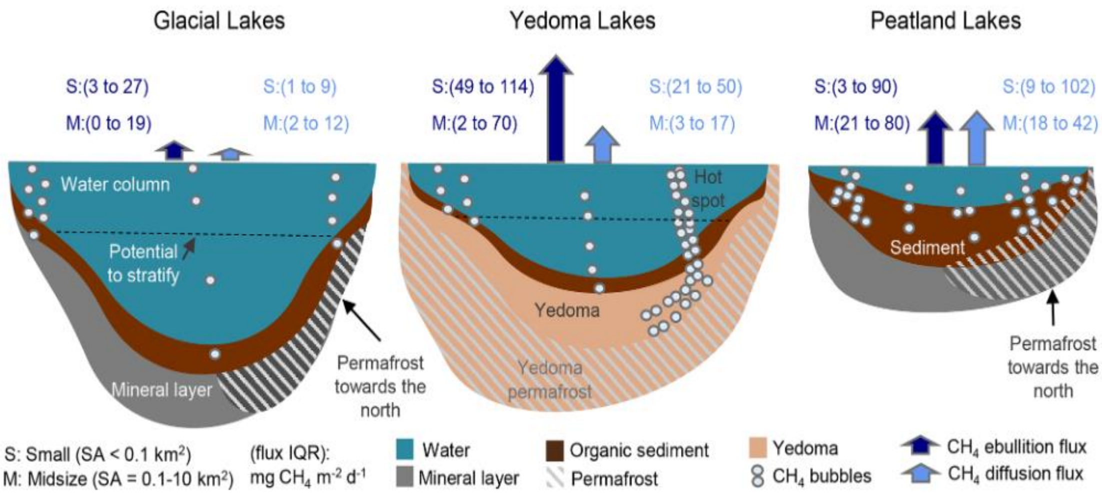

**Figure 2.4 Effect of northern lake types in $CH_4$ emissions.** Lake morphology, substrate geology, permafrost composition, and process of lake formation are some of the factors that could influence the $CH_4$ flux magnitude and age. The diagram, taken from Kuhn et al. (2021), shows three common types of northern and the relative sizes of their diffusive and ebullition $CH_4$ emissions, with the size of the arrows is scaled based on the flux magnitude. Glacial lakes have the lowest emissions, Yedoma lakes have the highest ebullition fluxes, and peatland lakes have the highest diffusive fluxes.

## 3. Radiocarbon data reveal contrasting sources for carbon fractions in thermokarst lakes and rivers of Eastern Canada (Nunavik, Quebec)

Authors and affiliations: Regina Gonzalez Moguel[1], Adrian M. Bass[2], Mark H Garnett[3], Martin Pilote[4,6], Benjamin Keenan[1], Alex Matveev[5,6], Peter M. J. Douglas[1]

1. McGill University, Earth and Planetary Sciences; Geotop Research Centre
2. University of Glasgow, School of Geographical and Earth Sciences
3. NEIF Radiocarbon Laboratory
4. Environment and Climate Change Canada
5. Concordia University, Department of Geography and Environment
6. Centre d'études nordiques, Université Laval

### 3.1. Context within the thesis

High latitudes are warming at faster rates than the rest of the globe, contributing to the extensive degradation of permafrost in subarctic environments of Canada in the last decades. One consequence of permafrost loss in the subarctic landscapes has been the extensive formation of thaw lakes due to the collapse of permafrost features and subsequent infilling by water. These lakes have been shown to be active sites of carbon processing, and they emit large amounts of $CH_4$ and $CO_2$ to the atmosphere, but little is known about what substrates sustain methanogenesis. A hypothesis that has been proposed in recent years is that the organic carbon previously stored in permafrost becomes available upon thaw and drives $CH_4$ production. An alternative hypothesis suggests that as permafrost disappears, the development of vegetation and delivery of vegetation products to lakes drives the $CH_4$ production. Because radiocarbon is an excellent tracer of permafrost carbon in $CH_4$ and other carbon fractions, we used it in this chapter to test these two alternate hypotheses. In addition, $\delta^{13}C$ can further inform on $CH_4$ production pathways, which could help us understand at a microbial community level how different sources are processed in the lake. In this chapter, published in 2020 in the *Journal of Geophysical Research: Biogeosciences*, we aimed to evaluate the contribution of different carbon pools to DOC, POC, $CH_4$, and $CO_2$ contained in the thaw lakes of two rapidly degrading subarctic valleys in Quebec, Canada.

### 3.2. Abstract

Greenhouse gas (GHG) emissions from permafrost organic carbon decomposition in lakes and rivers can accelerate global warming. We used radiocarbon ($^{14}C$) measurements to determine the predominant sources of dissolved organic carbon (DOC), particulate organic carbon (POC), dissolved inorganic carbon (DIC), and methane ($CH_4$) in five thermokarst lakes and three rivers in an area of widespread permafrost degradation in Northern Quebec to assess contributions from thawing permafrost and other old carbon (fixed before CE 1950) reservoirs. We compared emission pathways (dissolved gas and ebullition), seasons (summer and winter), and surface soil type (mineral and peat soils). Modern carbon (fixed after CE 1950) was the dominant source of DOC, DIC, and $CH_4$ of non-peatland aquatic systems, while POC and sediment carbon were predominantly fixed in the last millennia. In the peatland systems, modern and permafrost carbon were important sources of DOC, lake DIC, lake ebullition $CO_2$, and lake dissolved $CH_4$. In contrast, POC, lake ebullition $CH_4$, and river DIC were dominated by millennial-old carbon. In winter, the $^{14}C$ age of DOC, DIC, and POC in the peatland lakes increased, but the $^{14}C$ age of dissolved $CH_4$ did not change. Our results point to a clearly older overall carbon source for

ebullition $CH_4$ relative to dissolved $CH_4$ in the peatland lakes, but not the non-peatland lakes. The younger ages of diffusive $CH_4$ and DIC relative to DOC and POC in all lakes suggest that recent primary productivity strongly influences the large total lake $CH_4$ emissions in this area, as diffusion fluxes greatly exceed ebullition fluxes.

## 3.3. Introduction

Warming-induced permafrost thaw enables the transport of large stocks of previously frozen soil organic carbon through aquatic systems as dissolved organic carbon (DOC) and particulate organic carbon (POC), and its subsequent microbial mineralization to methane ($CH_4$) and carbon dioxide ($CO_2$) (Kling et al., 1991; Schuur et al., 2015). Permafrost-derived $CH_4$ and $CO_2$ represent a net input of carbon to the atmosphere and a positive feedback to climate change, but there is a large uncertainty on the extent of this feedback as variations in landscape relief, permafrost extent, ice content, composition and degree of processing of permafrost material, vegetation, and hydrological factors all influence how aquatic system carbon-cycling responds to thaw (Tank et al., 2020). Radiocarbon ($^{14}C$) measurements are used to estimate the contribution of permafrost carbon to DOC, POC, and $CH_4$ and $CO_2$, as the storage of soil carbon in permafrost for hundreds to thousands of years results in distinct $^{14}C$ ages (Estop-Aragonés et al., 2020, Dean et al., 2018, Elder et al., 2018, 2019). The $^{14}C$ content of the carbon fraction indicates the weighted sum of the $^{14}C$ signals of the carbon sources, which means that the approximate relative contribution from each carbon source can be estimated with a mass balance if the $^{14}C$ content of the endmembers is known.

Analyses of $^{14}C$-DOC and $^{14}C$-POC have shown that previously frozen organic carbon is exported from thawed permafrost soils and transported and mineralized in Arctic rivers (Estop-

Aragonés et al., 2020). In these studies, aged soil organic carbon represented most of the river POC, while modern carbon constituted the majority of river DOC except for a few sites where labile and highly depleted $^{14}$C-DOC was present (Guo and Macdonald, 2006; Guo et al., 2007; Lamoureux and Lafreniere, 2014; Mann et al., 2015, Spencer et al., 2015, Wang et al., 2018; Wild et al., 2019). Despite the potential for DOC and POC to transport permafrost organic carbon across the Arctic and Subarctic landscapes and increase potential mineralization in aquatic systems, there are very few studies analyzing $^{14}$C of DOC and POC in lakes (Dean et al., 2018).

Thermokarst lakes are widespread across the circumpolar north (Olefeldt et al., 2016) and are sites of intense microbial activity that favors the degradation of organic carbon to $CH_4$ and $CO_2$, which are typically emitted through diffusive, ebullition (bubbles), and plant-mediated fluxes (Bastviken et al., 2004). Radiocarbon age measurements of $CH_4$ and $CO_2$ from thermokarst lakes span wide ranges (modern to 50 000 yrs BP), varying greatly between different geological settings and emissions pathways (Estop-Aragonés et al., 2020). Ebullition $CH_4$ has frequently been shown to transport permafrost organic carbon to the atmosphere, with the specific $^{14}CH_4$ ages depending on the age of local soil organic carbon deposits (Bouchard et al., 2015; Walter et al., 2006; Walter et al., 2016; Zimov, et al. 1997). In contrast, more limited datasets have found dissolved $^{14}CH_4$ and $^{14}CO_2$ ages to be younger relative to local soil organic carbon deposits, implying that modern carbon is largely incorporated to $CH_4$ and $CO_2$ diffusive fluxes (Dean et al., 2018; Elder et al., 2018, 2019). Overall, most $^{14}$C data from thermokarst systems is from a few sites in Alaska, Eastern Siberia, and Western Canada (Estop-Aragonés et al., 2020), with relatively limited datasets from Eastern Canada (Bouchard et al., 2015; Matveev et al., 2016, 2018; Preskeinis et al., 2021).

Only two of these studies directly compared diffusive and ebullition $CH_4$ fluxes in the same site (Elder et al., 2019; Preskeinis et al., 2021)

Rapid warming and a widespread decrease in permafrost area and degradation of permafrost landforms has been recorded in Northern Quebec (Eastern Canada) in the last 30 years (Bouchard et al., 2014; Smith et al., 2010; Laberge and Payette, 1995; Vallée and Payette, 2007). The collapse of peat permafrost mounds (palsas) and mineral permafrost mounds (lithalsas) has led to the formation of thermokarst lakes and the subsequent release of $CH_4$ and $CO_2$. Particularly high $CH_4$ and $CO_2$ diffusive fluxes have been measured in thermokarst lakes in the southernmost permafrost border, where degradation is more advanced (Matveev et al., 2016, 2018). However, it is not clear if the higher diffusive fluxes in more southerly lakes is due to the enhanced mineralization of permafrost carbon, or alternately to increased primary productivity and bioavailable plant-derived carbon (Wang and Roulet, 2017).

In this study, we aimed to determine what the predominant carbon sources of DOC, DIC, POC, and $CH_4$ are in five thermokarst lakes and three rivers in the sporadic permafrost region of Northern Quebec. We specifically examined whether carbon sources differed between: (1) lakes and rivers in different soil types (peatland and non-peatland), (2) the ice-free and ice-covered seasons, and (3) dissolved and ebullition $CH_4$ and $CO_2$. To address these questions, we measured the $^{14}C$ content, $\delta^{13}C$, and concentration of: ebullition $CH_4$ and $CO_2$, dissolved $CH_4$, DIC, DOC, POC, and surficial sediments from three palsa-associated lakes and two lithalsa-associated lakes in summer; dissolved $CH_4$, DIC, DOC and POC from the palsa lakes in winter; and DIC, DOC, and POC in two non-peatland rivers (sampled in summer) and one peatland river (sampled in winter). We also used a $^{14}C$ end-member mixing model to estimate the relative contribution of potential carbon sources to DOC, POC, DIC, and $CH_4$ fluxes in the different lakes and rivers.

### 3.4. Study Site

All the sampled lakes and rivers are located in the sporadic permafrost region near the Hudson Bay, within 15 km of Kuujjuarapik-Whapmagoostui (K-W) in Nunavik, Quebec, Canada (Figure 3.1). The Tyrell Sea submerged this area after regional deglaciation roughly after around 8,000 yrs BP (Hillaire-Marcel, 1976). The end of the Tyrell Sea transgression, resulting from isostatic uplift, initiated the deposition of organic soils and the widespread formation of peatlands over marine clays after around 5,700 cal. yrs BP, or approximately 5,000 $^{14}C$ yrs BP (Arlen-Pouliot and Bhiry, 2005). Although the time of permafrost aggradation in the sampling sites is not completely constrained, it has been inferred from stratigraphic, microfossil, and $^{14}C$ analyses that permafrost development and the formation of palsas and lithalsas in the Great Whale River area initiated as early as 1,600 yrs BP, and probably intensified during the Little Ice Age (500–100 yrs BP) (Bhiry and Robert, 2006; Arlen-Pouliot and Bhiry, 2005; Fillon et al., 2014). After the Little Ice Age, the degradation of permafrost and collapse of palsas and lithalsas resulted in the formation of thermokarst lakes and an increase of the vegetation cover in the area (Arlen-Pouliot & Bhiry, 2005; Bouchard et al., 2014), a process that continues to the present. Regional vegetation is classified as forest tundra, with different areas dominated by grasses, lichen, shrubs, and spruce forests (Bhiry et al., 2011), as well as sedges in peatlands (Wang & Roulet, 2017).

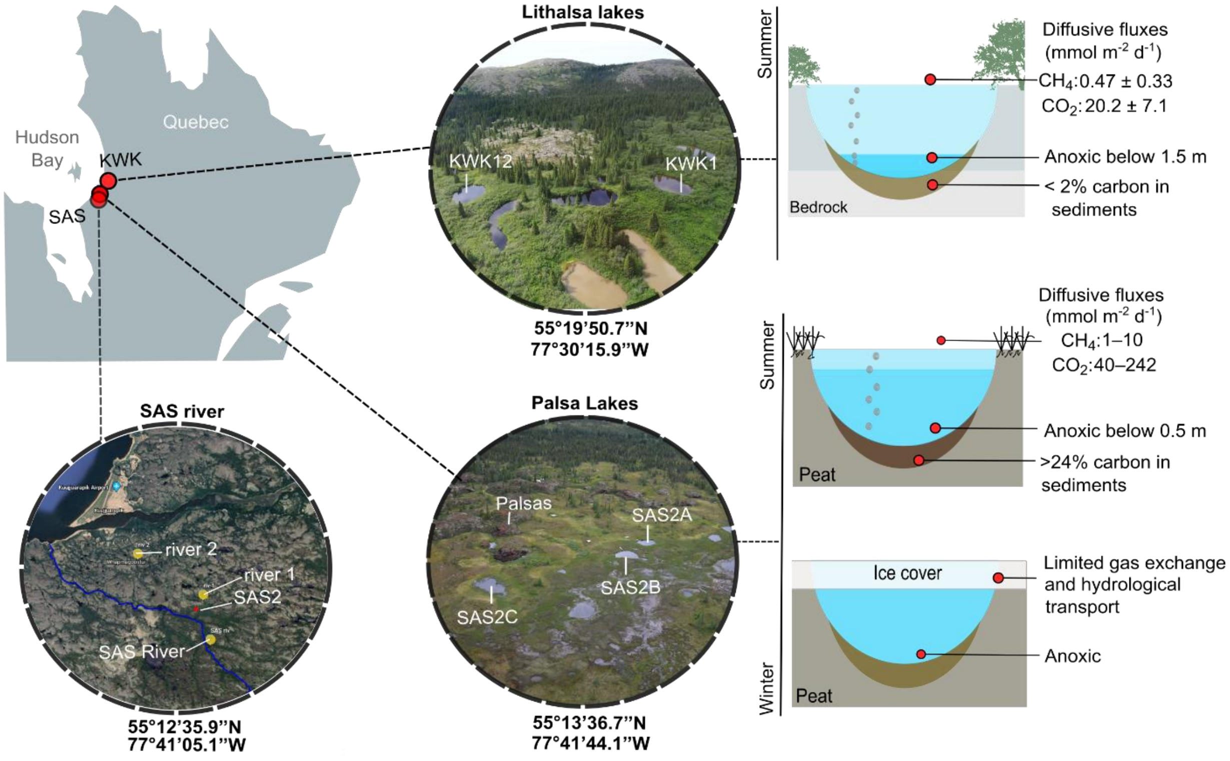

**Figure 3.1 Study site location and characteristics.** Location, aerial photographs, and schematics of the KWK lithalsa lakes (summer) and SAS2 palsa lakes (summer and winter) showing the diffusive fluxes magnitude (Matveev et al., 2016, 2018) and oxygenation patterns; and satellite image of the rivers sampling locations in yellow (Google Earth, 2020). KWK, Kwakwatanikapistikw River; SAS, Sasapimakwananisikw River.

### 3.4.1. Palsa lakes

We sampled three palsa-associated thermokarst lakes located southeast of K-W in a peatland adjacent to the Sasapimakwananisikw River (known as the SAS2 peatland) in two consecutive summers (August 2018 and 2019) and one winter (February 2019; Figure 3.1). Permafrost in the SAS2 peatland underlies the palsa mounds, but there is a rapid transition to permafrost-free soil towards the bog and lakes (Vincent et al., 2017). The area close to the palsas is vegetated by deciduous and ericaceous shrubs (*Betula glandulosa, Kalmia polifolia, Ledum groenlandicum*), the permafrost-free soil by peat moss (*Sphaghnum* spp.), and sedges (*Carex* spp.) are dominant close to the lakes (Wang & Roulet, 2017). The three sampled lakes -SAS2A, SAS2B, and SAS2C- are less than 2.8 meters deep and have surface areas between 115 and 230 $m^2$ (Matveev et al., 2020). All lakes stratify in summer, becoming anoxic below 0.5–1 meter (Figure 3.1). The measured summer diffusive fluxes in these lakes are high relative to other thermokarst lakes in the region, ranging 1–10 mmol $CH_4$ $m^{-2}$ $day^{-1}$ and 40–242 mmol $CO_2$ $m^{-2}$ $day^{-1}$ (Matveev et al., 2016). In contrast, ebullition fluxes range 0.01–0.5 mmol $CH_4$ $m^{-2}$ $day^{-1}$ and from less than 0.001 to 0.1 mmol $CO_2$ $m^{-2}$ $day^{-1}$ (Matveev et al., 2016). Ice covers the lakes from mid-October to May, and the entire water column becomes anoxic during this period (Deshpande et al., 2015; Matveev et al., 2016, 2019).

### 3.4.2. Lithalsa lakes

We sampled two lithalsa-associated thermokarst lakes located northeast of K-W in a once-glaciated valley adjacent to the Kwakwatanikapistikw River (KWK valley) in two consecutive summers (August 2018 and 2019; Figure 3.1). Due to the difficulty of site access, we were not able to sample in winter. Bouchard et al. (2014) calculated that the permafrost surface cover in the KWK valley decreased by 96% from 1959 to 2006, leaving only one visible lithalsa. In 2019, we observed that the remaining lithalsa had disappeared. The permafrost degradation in the valley resulted in the increase of vegetation cover and growth of shrubs (*Salix* spp., *Alnus crispa, Myrica gale*), mosses (*Sphaghnum* spp.), and herbaceous plants such as sedges (*Carex* spp.) between the lakes (Bouchard et al., 2014). The two sampled lakes – KWK1 and KWK12 – are less than 2.8 meters deep and have areas of 390 and 480 $m^2$ (Matveev et al., 2020). Both lakes stratify in summer, developing anoxic conditions below 1.5 meters (Laurion et al., 2010). Measured diffusive fluxes in these lakes are lower than in the SAS2 lakes, averaging 0.47 ± 0.33 mmol $CH_4$ $m^{-2}$ $day^{-1}$ and 20.2 ± 7.1 mmol $CO_2$ $m^{-2}$ $day^{-1}$ (Matveev et al., 2018). Ebullition fluxes average 0.016 mmol $CH_4$ $m^{-2}$ $day^{-1}$ and 0.06 mmol $CO_2$ $m^{-2}$ $day^{-1}$ (Matveev et al., 2018).

### 3.4.3. Rivers

We sampled the Sasapimakwananisikw River (SAS River) in winter (February 2019) from two locations adjacent to each other (55°12'35.9"N, 77°41'05.1"W). The SAS River runs Southeast to Northwest and its course is parallel to the Great Whale River (Figure 3.1). The river drains several peatlands, including SAS2, before flowing into the Hudson Bay, approximately 1 km SW of the mouth of the Great Whale River. To our knowledge, there are no studies exploring the limnological characteristics of the SAS River. In summer (August 2019), we sampled two smaller rivers in catchments that do not drain peatlands: a small tributary of the SAS River (55°13'53.4"N, 77°41'22.6"W) and a small river that flows parallel to the Great Whale River (55°15'05.2"N, 77°44'26.1"W). Due to logistical and access constraints, we were only able to sample the two non-peatland rivers in the summer of 2019, and the SAS River in winter of 2019.

## 3.5. Methods

### 3.5.1. Sample collection

#### 3.5.1.1. Ebullition gas (bubbles)

We placed one to three gas-tight submerged funnels, described in Matveev et al. (2016), attached to a 140 mL syringe close to the center of the lakes and fixed them with a rope staked to the lake shore to limit movement. Five to eight days later, we recorded the collected gas volume and transferred the gas from the syringe to an evacuated 120 mL vial sealed with a crimped butyl stopper. We stored the vials at room temperature until analysis. In winter 2019, the SAS2 palsa lakes were completely covered with ice and ebullition was not observed and therefore not collected. In summer 2019, bubbles were only collected in the SAS2 palsa lakes.

#### 3.5.1.2. Dissolved methane

To collect dissolved $CH_4$, we used the technique described in Garnett et al. (2016). We added 400–600 mL of water from a depth of 1–1.5 m below the surface to a 1.1 L bottle, shook the bottle for 3 minutes, and analyzed the headspace concentration using a Sensit Technologies SENSIT PMD portable methane detector. We used the concentration of $CH_4$ in the headspace to calculate the volume of water needed to produce 5–10 mL of $CH_4$. We then pumped the required volume of water (2–14 liters) into an ‘accordion water carrier’ using a Proactive Environmental ALEXIS peristaltic pump or a hand pump. In the winter, we drilled through the ice before pumping the water. Then, we used a syringe to add 1–2 L of ambient air to the accordion and shook for three minutes. Lastly, we transferred the accordion headspace to a 6 L pre-evacuated canister (Silonite Canister, Entech Instruments, USA), using a hydrophobic filter to prevent water from entering the canister.

#### 3.5.1.3. Water sampling

We collected water samples for DIC, DOC, and POC analyses from 1 to 1.5 meters below the lake surface using the peristaltic pump or the hand pump. We filtered the water with a 0.7 µm (47 mm diameter) pre-baked glass fiber filter and transferred it to a pre-baked and acid washed 1 L vial (for $^{14}C$ analysis) and to three 40 mL pre-cleaned borosilicate amber vials with extra septa (for concentration and $\delta^{13}C$ analyses). We freeze-dried the filters and kept them refrigerated at 4°

C until analysis. In winter, we transported the collected water to the research station in 3 L acid rinsed Nalgene bottles and performed the filtration the same day. All water samples were stored at 4 °C with no fixing agent added and were delivered for analysis within 15 days of collection. It is possible that during these 15 days a small portion of DOC was respired to DIC, resulting in DIC ages shifting towards DOC ages.

We did not collect dissolved $CO_2$ but we assumed that that DIC and dissolved $CO_2$ have a similar $^{14}C$ signal (Mayorga et al., 2005), because carbon exchange within the DIC pool is rapid (Zhang et al., 1995) and any isotopic fractionation effects are corrected when normalizing the radiocarbon results. Additionally, the relatively low pH of the lakes at the sampled depth, ranging from approximately 5 to 6.5, indicates that the predominant DIC species is dissolved $CO_2$ in most lakes (Figure A1.1).

#### 3.5.1.4. Sediments

In summer 2018, we collected sediments from close to the center of the lakes using a Wildco hand corer. In the SAS2 palsa lakes, roughly the first 10–15 cm of the core were composed of organic rich lacustrine mud (gyttja). Below the gyttja layer the cores consisted of clay. These sediment samples represent a spectrum of depositional ages that are not constrained as we do not know the accumulation rates of the sites. In the KWK lithalsa lakes, only about 4–6 cm of the core was gyttja, and the rest was clay. Previous sediment analyses in these lakes measured $^{14}C$ ages of up to 1000 cal. yrs BP in the upper sediments (gyttja) and determined that most of the upper sediment was deposited in the last 150 years based on $^{210}Pb$ and $^{137}Cs$ measurements (Bouchard et al., 2011). In both sites we sampled and homogenized the gyttja from the cores and discarded the clay, as we aimed to estimate an average $^{14}C$ age of the shallow sediments that could be contributing to ebullition $CH_4$ and $CO_2$ production. We freeze-dried and stored the sediments at 4 °C until analysis.

### 3.5.2. Concentration and $\delta^{13}$C analysis

#### 3.5.2.1. Dissolved and ebullition $CH_4$ and $CO_2$

The ebullition $CH_4$ and $CO_2$ concentrations were measured alongside two standards (5,000 ppm $CO_2$ and 2,000 ppm $CH_4$) at McGill University using a Shimadzu 2014 gas chromatograph (GC) with a flame ionization detector (FID) and a methanizer. The 2019 ebullition $\delta^{13}C\text{-}CH_4$ and $\delta^{13}C\text{-}CO_2$ were measured in the Ján Veizer Stable Isotope Laboratory (University of Ottawa, Canada) using a GC Isolink system interfaced via a Conflo 4 to a Delta V Isotope Ratio Mass spectrometer and normalized using the international standards USGS HCG-1, USGS HCG-2, and USGS HCG-3 (U.S. Geological Survey Hydrocarbon Gas). The dissolved $\delta^{13}C\text{-}CH_4$ and 2018 ebullition $\delta^{13}C\text{-}CH_4$ were measured at the NEIF Radiocarbon Laboratory (East Kilbride, UK), using a dual inlet stable isotope mass spectrometer (Thermo Fisher Delta V) in the pre-prepared sample. To calculate the concentration of dissolved $CH_4$, we divided the mass of $CH_4$, calculated from the volume of $CH_4$ recovered from the canister using the ideal gas law, by the volume of water (in L) that we degassed in the accordion water carrier. We did not calculate the dissolved $CH_4$ concentrations in winter 2019, as the formation of ice in the accordion system led to unreliable water volume estimations.

#### 3.5.2.2. DIC and DOC

The concentration and $\delta^{13}$C of DOC and DIC in the water samples were measured in the Ján Veizer Stable Isotope Laboratory (University of Ottawa, Canada) as described in Lalonde et al. (2014). The samples in the 40 mL amber vials and two standard solutions (KHP and sucrose) were loaded into a carousel. Then, an aliquot was injected into a reaction chamber and acidified with 5% $H_3PO_4$. The released gas was carried using ultra-pure helium. Water was removed and the $CO_2$ (DIC) concentration in the gas measured by a nondispersive infrared sensor (NDIR). Subsequently, the $\delta^{13}C$-$CO_2$ (DIC) was measured using a Thermo Finnigan DeltaPlus XP isotope ratio mass spectrometer (IRMS). After the inorganic carbon was removed, a persulfate reagent was added to the aliquot to oxidize the organic carbon (DOC) to $CO_2$, which was measured for concentration and $\delta^{13}C$ as described above. The 2σ analytical precision is 0.5 mg $L^{-1}$ for the concentration, and ±0.2 ‰ for the isotopes.

#### 3.5.2.3. POC and sediments

The concentration and $\delta^{13}C$ of the filters and the sediments were measured in the GEOTOP Light Stable Isotope Geochemistry Laboratory (Montreal, Canada). Samples were weighed in tin cups and analyzed alongside two internal reference standards with a Micromass model Isoprime 100 Isotope Ratio Mass Spectrometer coupled to an Elementar Vario MicroCube elemental analyzer in continuous flow mode. A third reference material was analyzed to assess the uncertainty of the normalization. The results were normalized to the NBS19-LSVEC scale and expressed in delta units against VPDB. Analytical uncertainty (2σ) was <±0.2‰. To calculate POC concentration, we multiplied the measured carbon fraction in the filter (%) by the total weight of the sample (mg), which was calculated as the difference of the dry weight of the filter before and after sampling. Then, we divided the carbon mass in the filter (mg) by the volume of water filtered (L). Water volumes, and therefore concentrations, were only recorded for summer 2019.

Because the filters and sediment were not acidified prior to analysis, we used two residual filter and sediment samples to test whether acidification (24 hours with 36% HCl) changed the concentration and $\delta^{13}C$ of POC and sediment carbon. The differences in $\delta^{13}C$ between the acidified and unacidified sediments (collected from the surface organic rich layer) and filters were within the range of analytical uncertainty ($2\sigma \sim \pm 0.2‰$). Therefore, we reported the $\delta^{13}C$ of unacidified samples as the $\delta^{13}C$ of sedimentary organic carbon and POC. In the case of concentration, the difference between acidified and unacidified filters (0.9–2 mg $L^{-1}$) and sediments (0.7–1.13%) were both outside the uncertainty range. Therefore, we report the concentrations of unacidified samples as the concentrations of total sedimentary carbon and total particulate carbon.

### 3.5.3. $^{14}C$ sample preparation and analysis

The DOC, DIC, POC, sediments, and 2019 ebullition samples were prepared and analyzed in the A.E. Lalonde AMS Laboratory (University of Ottawa, Canada) according to the methods described in Crann et al. (2017), Murseli et al. (2019), and Pack et al. (2015). For DIC, phosphoric acid (85%) was added to the sample in a pre-baked borosilicate bottle at 60°C and the resulting gas was cryogenically separated in a breakseal. Then, for DOC, around 8 mL of sodium persulfate solution (400 g $L^{-1}$) and 1 mL of $AgNO_3$ catalyst (0.5 N) were added to the same sample, the mixture was heated to 95 °C for at least one hour, and the resulting gas was again separated in a breakseal. The POC and sediment samples were treated with an acid wash to remove carbonates (HCl, 1N, 80°C, 30 min), freeze-dried, weighed in tin cups, combusted to $CO_2$ using a Thermo Flash 1112 elemental analyzer (EA), and the $CO_2$ was cryogenically separated in a breakseal.

To separate the $CH_4$ from the ebullition samples, the sample was transferred to a combustion line with an ultra-zero gas carrier at a flow of 10 mL $min^{-1}$, where $CO_2$ was separated cryogenically, CO was oxidized to $CO_2$ in a 300°C oven with CuO and separated cryogenically. Then, $CH_4$ was combusted to $CO_2$ in a 975°C tube furnace packed with CuO and stored in a pre-baked breakseal. To separate the $CO_2$, the sample was extracted and flushed 10 times at 200 ml $min^{-1}$ with Helium, $CO_2$ was trapped cryogenically on a U-trap packed with Silver wool, then transferred to a vacuum line for cryogenic purification with a -80 °C ethanol slurry to remove water and other non-condensable gases, and lastly transferred to a pre-baked breakseal. All the breakseals, containing grains of silvered cobaltous/cobaltic oxide, were baked at 200°C to remove sulfur and halogens. The $CO_2$ in the breakseals was reduced to graphite in the presence of Fe-H. $^{14}C$ of the resulting graphite was analyzed on a 3MV tandem accelerator mass spectrometer (AMS). The results were background-corrected.

The 2018 ebullition samples ($CO_2$ and $CH_4$) and all the dissolved gas samples ($CH_4$) were prepared at the NEIF Radiocarbon Laboratory (East Kilbride, UK) using the methods described in Garnett et al. (2012). In the case of $CH_4$ analysis, $CO_2$ was removed from the sample using soda lime and zeolite molecular sieve. The $CH_4$ was then combusted on 950°C Pt/Al beads to $CO_2$. The resulting $CO_2$ was separated cryogenically and reduced to graphite using Fe/Zn reduction. For ebullition $CO_2$ analysis, $CO_2$ was separated cryogenically and reduced to graphite as described above. The $^{14}C$ analyses of these samples were performed at the Scottish Universities Environmental Research Centre (SUERC) AMS laboratory, or the Keck Carbon Cycle AMS Facility (University of California, Irvine, USA).

In all cases the results were normalized to $\delta^{13}$C-VPDB‰ = -25 using the IRMS-measured $^{13}C/^{12}C$ ratios in samples analyzed in the SUERC AMS Laboratory and using the AMS-measured $^{13}C/^{12}C$ ratios in samples analyzed in the Keck Carbon Cycle AMS Laboratory and A.E. Lalonde AMS Laboratory. All the results were reported as Fraction Modern Carbon (FMC) and conventional radiocarbon ages (years BP, where 0 BP = AD 1950) at the ± 1$\sigma$ level. In this document, we report the radiocarbon ($^{14}$C) age averages, but include the FMC averages where the age is modern (FMC > 1.0). In data that contain both modern and pre-1850 ages, we report the range of $^{14}$C ages, rounded to the closest hundred.

### 3.5.4. Isotope separation factor $\varepsilon_c$ calculation

We calculated the ebullition and dissolved isotope separation factor $\varepsilon_c$ for ebullition and dissolved $CO_2$ and $CH_4$ using the equation $\varepsilon_c = \delta^{13}C_{CO2} - \delta^{13}C_{CH4}$, after Whiticar (1999). To derive the dissolved $\delta^{13}$C-$CO_2$ from $\delta^{13}$C-DIC, we first calculated the distribution of the $CO_2$ (dissolved), $HCO_3^-$, and $CO_3^{2-}$ species at a depth of 1.5 meters using the pH values and DIC concentrations at that depth. The winter pH and temperature values were obtained from Matveev et al. (2019, 2020). Then, we used a mass balance equation and the isotope fractionation factors ($\alpha_{A\text{-}B} = R_A/R_B$), obtained from Zhang et al. (1995), between pure $CO_2$ (gas) and $CO_2$ (dissolved), bicarbonate ($HCO_3^-$), and carbonate ($CO_3^{2-}$) to calculate the dissolved $\delta^{13}$C-$CO_2$. The complete calculations are available in the Appendix 1.

### 3.5.5. Carbon source $^{14}$C mixing model

We used IsoSource to calculate the ranges of possible contributions from five carbon sources to the mean FMC carbon of DOC, POC, DIC, dissolved $CH_4$, and ebullition $CO_2$ in the lithalsa and palsa thermokarst lakes, as well as DOC, POC, and DIC in the rivers. IsoSource is a software that generates every possible combination of source mixing proportions that sums to 100%, in 2% increments. The predicted mixture signature of every solution is compared to the observed mixed signature, and only the ones within the tolerance level are considered a feasible solution (Phillips and Greg, 2003). We used the standard deviation of the measurements of each carbon fraction (~0.04) as the tolerance value.

We performed the mixing model with five sources, using the mid-point FMC value of each source: (1) carbon from marine sediments deposited during the Tyrell sea transgression from around 8, 000 to 5, 000 yrs BP (FMC: 0.453); (2) "deep" carbon from peat deposition after the Tyrell sea retreat around 5, 000 yrs BP and until widespread permafrost formation around 500 yrs BP (FMC: 0.738), (3) carbon preserved in soils after permafrost development in the area during the Little Ice Age from around 500 yrs BP until thaw began around 100 yrs BP (FMC: 0.964), (4) carbon fixed after permafrost thaw and corresponding to the post-bomb period, calculated as the integrated annual average of atmospheric $^{14}CO_2$ from 1950–2012 by Elder et al. (2018) (FMC: 1.221); and (5) carbon from recent photosynthesis, from 2013 to 2018, which was also defined by Elder et al. (2018) (FMC: 1.031). No fossil carbon sources are known in this area, as there are no known deposits of fossil fuels or significant pre-Holocene sedimentary units.

## 3.6. Results

### 3.6.1. DOC and POC

DOC was consistently 100–2,800 $^{14}C$ years younger and 0.5–7.0 ‰ more $\delta^{13}C$ enriched than POC in all lakes and rivers and for all the seasons sampled (Figure 3.2a). The lower $\delta^{13}C$-

POC relative to DOC was much more pronounced in the lithalsa lakes. The $^{14}$C age difference between DOC and POC resulted in a larger estimated contribution of old carbon sources (i.e. “deep” and marine carbon) to POC relative to DOC by the mixing model (Figure 3.3). Where comparison was possible, the concentration of the particulate carbon, ranging 1–2 mg L$^{-1}$, was approximately one order of magnitude lower than the DOC concentrations, which ranged 7–32 mg L$^{-1}$.

DOC and POC from lakes and rivers associated with peatlands were older and contained a larger proportion of old carbon sources than lakes and rivers not associated with peatlands (Figures 3.2a and 3.3). In the non-peatland lakes and rivers, DOC was modern (FMC: ~1.07), with a relatively large proportion of carbon fixed during the bomb period (Figure 3.3), while $^{14}$C-POC ages ranged 100–800 yrs BP. In comparison, the $^{14}$C-DOC and $^{14}$C-POC from peatland lakes and rivers dated up to 1 millennium old (300–1,500 yrs BP) and up to 3 millennia old (900–3,100 yrs BP), respectively. DOC concentrations also varied between sites, with the palsa lakes having a higher average DOC concentration (21.0 ± 4.7 mg L$^{-1}$ in summer and 29.2 ± 3.8 mg L$^{-1}$ in winter) than the lithalsa lakes (8.7 ± 1.5 mg L$^{-1}$), non-peatland rivers (12.1 ± 3.8 mg L$^{-1}$), and the SAS river (8.1 ± 0.3 mg L$^{-1}$).

In winter, the palsa lakes $^{14}$C-DOC and $^{14}$C-POC ages, and DOC concentrations increased (Figure 3.2a and 3.2b). The results of the mixing model indicated a greater contribution of older carbon sources to DOC and POC in this season (Figure 3.3). This change was especially pronounced in POC, which was mostly sourced by marine carbon and to a lesser extent by “deep” carbon in the SAS2 lakes and SAS river.

### 3.6.2. Sedimentary Carbon

The concentration, $\delta^{13}C$, and $^{14}C$ ages of the surficial sedimentary carbon varied between the lithalsa and palsa lakes (Figure 3.2a). The collected sediment from the palsa lakes had a high carbon content that averaged 29.7 ± 6.2 % and $^{14}C$ ages that ranged 3 to 4 millennia (3,200–4,300 yrs BP), while in the lithalsa lakes the carbon content was low, averaging 2.4 ± 1.6 %, and yielded a $^{14}C$ age of 1,000 yrs BP.

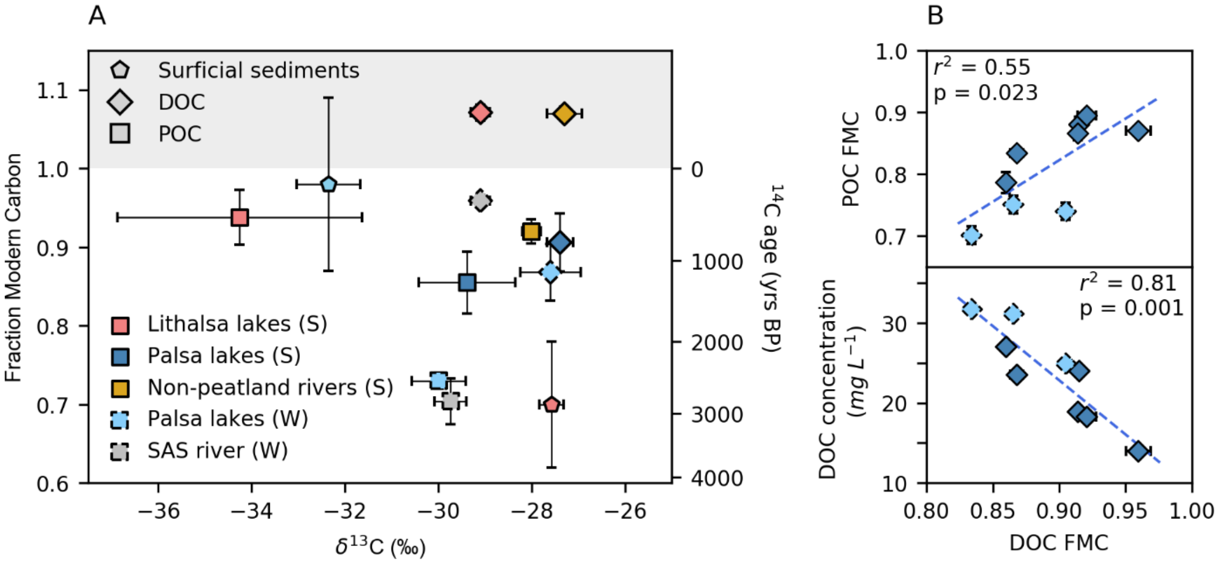

**Figure 3.2 Isotopic composition of DOC and POC.** a) $\delta^{13}C$ and $^{14}C$ content of DOC (diamonds), POC (squares), and sediment organic carbon (pentagons) by site in summer (S) and winter (W). The gray area represents modern carbon (fixed after CE 1950). b) In the SAS2 palsa lakes there were significant linear relationships ($p < 0.05$) between the 14C-DOC and 14C-POC and DOC concentration. DOC, dissolved organic carbon; POC, particulate organic carbon; SAS, Sasapimakwananisikw River.

### 3.6.3. $CH_4$

The $\delta^{13}C$-$CH_4$ and $^{14}C$-$CH_4$ ages differed between the lithalsa and palsa lakes and between the dissolved and ebullition pools (Figure 3.4a). In the lithalsa lakes, we found low dissolved $CH_4$ concentrations (sampled above the hypolimnion), ranging from less than 0.003 ppm to 0.21 ppm. When analysis was possible, $^{14}C$-$CH_4$ was primarily modern (FMC: 1.01 ± 0.04), implying a large proportion of carbon fixed during the bomb period (Figure 3.5), and $\delta^{13}C$-$CH_4$ was relatively enriched (-54.7 ± 0.1‰), which probably reflects extensive $CH_4$ oxidation in these lakes (Figure A1.2). On the other hand, dissolved $^{14}C$-$CH_4$ ages in the palsa lakes (sampled in the hypolimnion) ranged from modern to 600 yrs BP and did not significantly change between summer and winter (Figure 3.4a), implying predominant source contributions from recent carbon and centennial-aged permafrost carbon in both seasons (Figure 3.5). In summer, the concentration of dissolved $CH_4$ (7.7 ± 2.3 ppm) in these lakes showed a positive linear relationship with DOC (Figure 3.4c).

The concentration of ebullition $CH_4$ varied greatly between samples (0.4–30%), and even between replicates from the same site. Comparison of $^{14}C$ ages between ebullition and dissolved $CH_4$ revealed a much larger difference in the palsa lakes than in the lithalsa lakes (Figure 3.2a). Ebullition $^{14}C$-$CH_4$ in the lithalsa lakes was modern (FMC: 1.05) and similarly to dissolved $CH_4$, there was a large contribution of carbon fixed during the bomb period (Figure 3.5). In the palsa lakes, ebullition $CH_4$ was approximately one millennium old (1000–1800 yrs BP), and contained a much larger proportion of deep peat and marine carbon compared to dissolved $CH_4$ (Figure 3.5).

In addition to the source variability, the isotope separation factors $\varepsilon_c$ ($\varepsilon_c = \delta^{13}C_{CO2} - \delta^{13}C_{CH4}$) indicated variable $CH_4$ production pathways between the palsa and the lithalsa lakes (Figure A1.2). In the palsa lakes, ebullition and dissolved $CH_4$ showed $\varepsilon_c$ values spanning both hydrogenotrophic and acetotrophic ranges (47–57‰) in the summer, but the $\varepsilon_c$ value of dissolved $CH_4$ increased to

54 ‰ –60 ‰ in the winter, suggesting a shift of the methane production pathway towards increased hydrogenotrophic methanogenesis (Whiticar, 1999). In the lithalsa lakes, the highly depleted ebullition $\delta^{13}$C-$CH_4$ (~-71‰) suggested a higher production of $CH_4$ by hydrogenotrophic methanogenesis, or potentially the utilization of $^{13}$C depleted substrates to produce $CH_4$, as suggested by the low $\delta^{13}$C values of POC and sedimentary OC in these lakes.

### 3.6.4. Ebullition $CO_2$ and DIC

The $^{14}$C-DIC ages and source contributions varied across sites (Figure 3.4b and Figure 3.5). The SAS river yielded the oldest ages (1,000–1,100 yrs BP), with the largest contributions from deep carbon and permafrost carbon (Figure 3.5). In the palsa lakes, the summer $^{14}$C-DIC ranged from modern to 600 yrs BP (excluding one outlier), indicating that the main sources were recent carbon and centennial-aged permafrost carbon (Figure 3.5). In the winter, DIC in these lakes shifted to slightly older ages (400–800 yrs BP) (Figure 3.4), implying a larger contribution of older carbon sources in this season (Figure 3.5). The youngest DIC ages were found in the lithalsa lakes and non-peatland rivers (modern to 300 yrs BP), and like dissolved $CH_4$, DIC in these systems had a large contribution of bomb carbon and to a lesser extent recent carbon (Figure 3.5).

The DIC concentration and $\delta^{13}$C-DIC also varied across sites (Figure 3.4): palsa lakes had the highest DIC concentrations (19.0 ± 7.4 mg $L^{-1}$), which showed a linear relationship with DOC concentrations in summer (Figure 3.4c), and more positive $\delta^{13}$C-DIC (-6.5 ± 1.8‰). Lower DIC concentrations (5.6 ± 1.2 mg $L^{-1}$) and $\delta^{13}$C-DIC (-13.0 ± 0.2‰) were observed in the SAS river. The lithalsa lakes and non-peatland rivers showed the lowest DIC concentration (2.3 ± 1.4 mg $L^{-1}$) and more negative $\delta^{13}$C-DIC (-17.3 ± 2.3‰).

Compared to ebullition $CH_4$, the concentration of $CO_2$ in bubbles was lower and less variable (0.2–3%); and was below the $^{13}C$ and $^{14}C$ analytical limit in the samples from lithalsa lakes. In the palsa lakes, ebullition $^{14}C$-$CO_2$ (modern to 500 yrs BP) was younger than ebullition $^{14}C$-$CH_4$, but within the age range of $^{14}C$-DIC (Figure 3.4b). In addition, the mixing model showed a similar source contribution between ebullition $CO_2$ and DIC in these lakes, both containing a larger proportion of recent and bomb carbon compared to ebullition $CH_4$ (Figure 3.5).

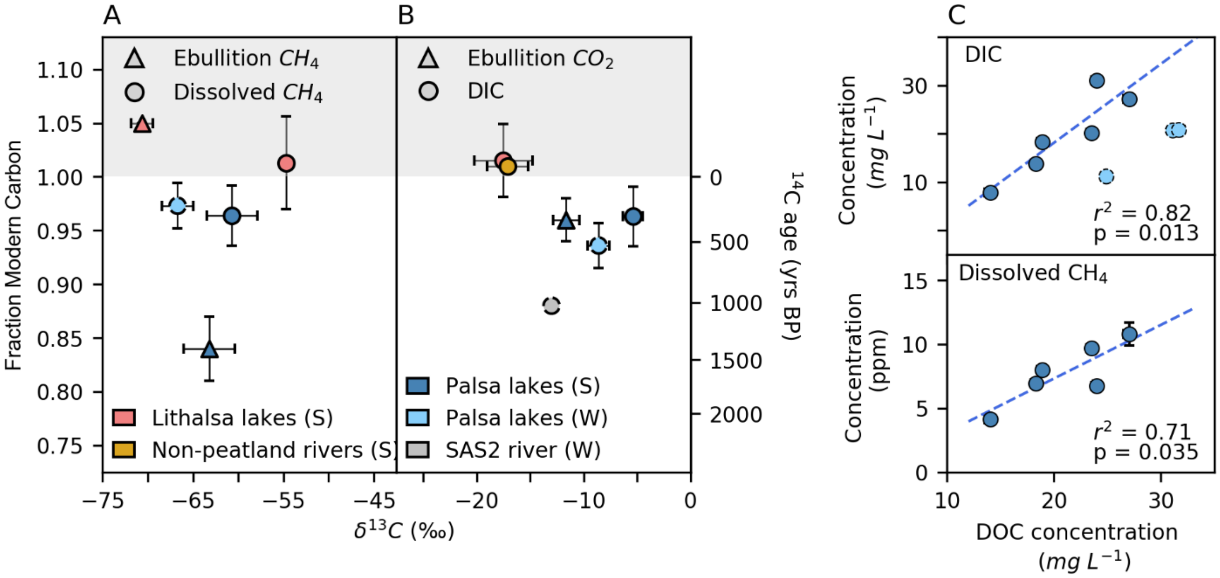

**Figure 3.3 Isotopic composition of $CH_4$, $CO_2$, and DIC.** $\delta^{13}C$ and $^{14}C$ content of a) dissolved and ebullition $CH_4$ and b) ebullition $CO_2$ and DIC by site. The gray area represents modern carbon (fixed after CE 1950). c) In the SAS2 palsa lakes, the DIC and dissolved $CH_4$ concentration increase linearly with DOC concentration ($p > 0.05$) in summer (S), but not in winter (W). $CH_4$, methane; DIC, dissolved inorganic carbon; DOC, dissolved organic carbon; SAS, Sasapimakwananisikw River.

### 3.7. Discussion

### 3.7.1. Difference in carbon sources between lake and river soil type

Soil type had a clear influence on the ages and source contributions of lake and river DOC. Centennial-aged permafrost carbon and modern carbon were the largest DOC sources in the SAS2 palsa lakes (Figure 3.3), emphasizing the influence of aquatic or terrestrial primary productivity and recent peat accumulation in the organic carbon export in these systems. In comparison, modern carbon strongly dominated DOC in the lithalsa lakes and non-peatland rivers (Figure 3.3), with a particularly large proportion of carbon fixed during the bomb period. This suggests that terrigenous carbon sources cycling on decadal timescales, such as shallow soil organic matter, likely predominated over carbon from autochthonous primary productivity, which would have a contemporary $^{14}C$ signature. These results are consistent with evidence from Arctic rivers, which shows that DOC does transport some pre-modern organic carbon, but it is dominantly derived from young carbon reservoirs (Dean et al., 2020; Guo et al., 2007; Raymond et al., 2007; Wild et al., 2019).

POC represented a small fraction of the total organic carbon in the lakes and rivers, but old carbon sources constituted a much larger portion of POC compared to DOC in all of our sites. Measurements of $^{14}C$-POC in other circum-Arctic rivers have shown that old carbon is transported mainly in the POC fraction, likely eroded or exported from permafrost soils (Guo et al., 2007; Lamoureux and Lafreniere, 2014; Wild et al., 2019), and as a consequence the POC ages in rivers is a function of regional or local soil age (Estop-Aragonés et al., 2020). The observed similarity between the POC ages in the non-peatland rivers and the KWK lithalsa lakes, and between the SAS2 palsa lakes and SAS river, could be related to the export of POC to the lakes and rivers from surrounding soils and the greater abundance of old carbon preserved in peat soils.

A notable feature of our data was that $\delta^{13}$C-POC was 2–3‰ lower than $\delta^{13}$C-DOC and surficial sedimentary carbon in lakes, and especially the lithalsa lakes, but not in the rivers. We speculate that particle-attached microbial communities are an important component of POC in lakes, causing the low $\delta^{13}$C-POC, as methanogenic and methanotrophic communities are highly abundant in the SAS2 and KWK lakes (Crevecoeur et al., 2015, 2016, 2017) and uptake $^{12}$C preferentially, resulting in their biomass being more isotopically depleted in $^{13}$C than the substrates (Fuchs et al., 1979; Summons et al., 1998). However, this particle-attached microbial biomass does not appear to be exported to the rivers we sampled.

The $^{14}$C age distribution of $CH_4$ and DIC was also influenced by the soil type. As with DOC and POC, $CH_4$ and DIC consistently exhibited younger $^{14}$C ages in the non-peatland lakes and rivers (Figure 4a). The strong bomb carbon input observed in non-peatland lake and river DOC (Figure 3) was also apparent in lithalsa lake $CH_4$, both in ebullition and dissolved fractions, and non-peatland lake and river DIC. These results suggest a strong influence of terrestrial soil carbon that is cycled on decadal timescales in the total $CH_4$ and $CO_2$ emissions of non-peatland systems. In contrast, the palsa lakes dissolved $CH_4$ and DIC contained inputs of centennial aged permafrost carbon, and the palsa lakes ebullition $CH_4$ and SAS river DIC contained inputs from even older carbon sources. The difference in $CH_4$ and DIC between the peatland and non-peatland lakes is broadly consistent with previous studies (Elder et al., 2018; Dean et al., 2020) that have found that the geological substrate and soil type exerts a strong influence on the age of carbon emitted from lacustrine $CH_4$ and $CO_2$ fluxes.

Overall, it is clear that in our study area the peatland lakes and rivers contain a much larger fraction of carbon from pre-modern reservoirs than the non-peatland aquatic systems. This difference may be partly a result of the more advanced stage of permafrost degradation in the KWK valley if permafrost carbon reservoirs have already been largely mobilized. This difference is also likely a function of the much larger reservoirs of old carbon in peat soils, and the fact that this carbon is decomposed more slowly than carbon in mineral soils, regardless of the presence of permafrost (Frolking et al., 2001). This result emphasizes the likely importance of peatlands as a landscape feature when considering the cycling and emission of old carbon in regions undergoing permafrost thaw (Hugelius et al., 2020).

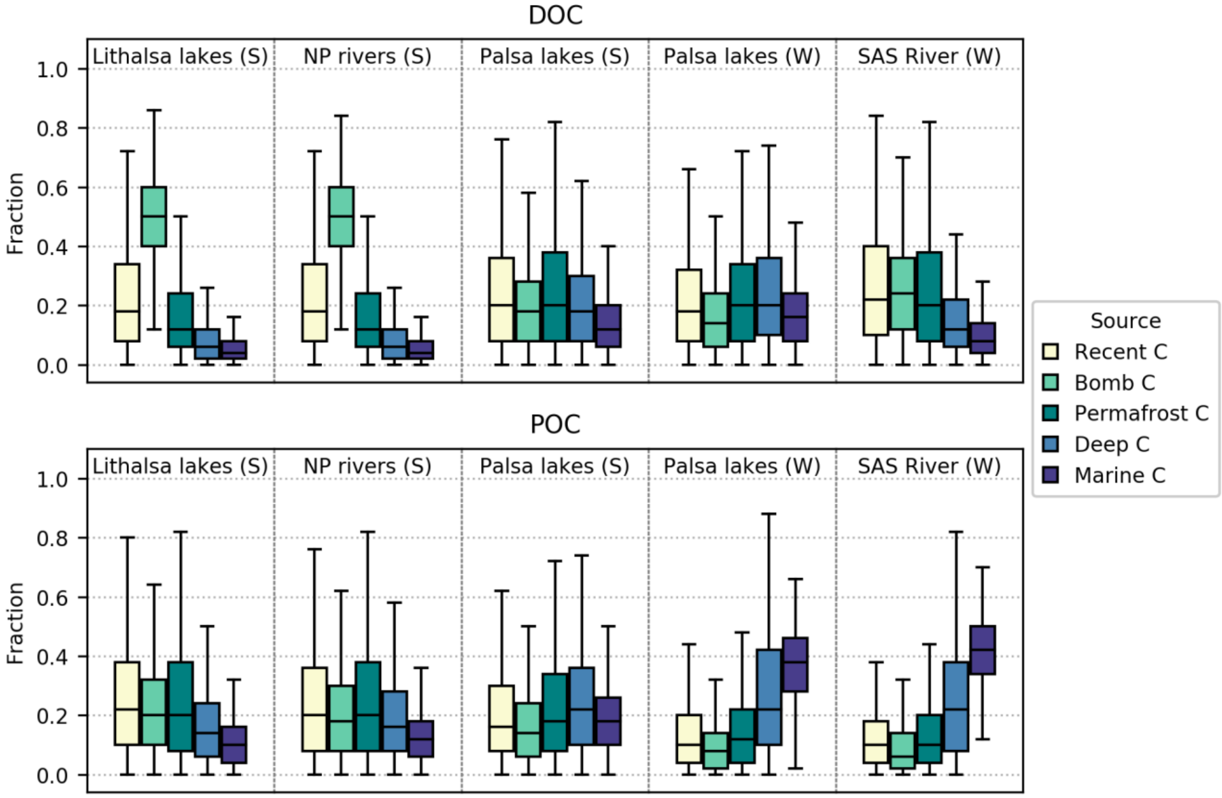

**Figure 3.4. Potential contributions from five carbon sources to the $^{14}$C content of DOC and POC by site in summer (S) and winter (W).** The boxplots show the median, the first quartile

(Q1) and third quartile (Q3). The range represents the range of the feasible solutions. DOC, dissolved organic carbon; POC, particulate organic carbon.

### 3.7.2 Sources of $CH_4$ and $CO_2$ in different emission pathways

Variations in the contributions of old organic carbon to $CH_4$ between the dissolved and ebullition pathways were only observed in the palsa lakes, where the ebullition $CH_4$ had a substantially larger contribution of older sources compared to dissolved $CH_4$ (Figure 3.5). Modern and permafrost-aged carbon were the primary sources of dissolved $CH_4$ and DIC in the palsa lakes, suggesting that the peatland or lacustrine primary productivity strongly influences $CH_4$ and $CO_2$ diffusive emissions in these lakes. The close relationship between DOC, and DIC and $CH_4$ summer concentrations suggests that DOC fuels both DIC and dissolved $CH_4$ microbial production either in the surrounding peatland, shallow sediments, or in the water column. This is also supported by the inference from carbon isotope separation values that dissolved $CH_4$ in summer is largely produced through the acetotrophic pathway (McCalley et al., 2014). The younger ages of $CH_4$ and DIC relative to DOC could be explained by reduced reactivity of older DOC carbon (Douglas et al., 2020), implying that dissolved $CH_4$ is produced from a more labile component of DOC with relatively young ages. We suggest that peat organic matter deposited before permafrost development (i.e. deposits older than 500 yrs BP) has undergone a greater degree of microbial decomposition before being frozen than carbon accumulated after ~500 yrs BP, resulting in these old carbon deposits being more recalcitrant to microbial communities.

By contrast, the ebullition $^{14}C$-$CH_4$ ages in the palsa lakes reflected the $^{14}C$ age of the organic carbon in the surficial sediment, probably due to the production of bubbles in the sediment pore waters. The high hydrostatic pressure and osmotic and capillary forces in the sediments slow the diffusion of methane and favor the accumulation of methane in bubbles (Stepanenko et al., 2011), which are released when the pore pressure exceeds a certain threshold. The relatively young age of ebullition $CH_4$ in the lithalsa lakes (Figure 3.4a) probably reflects the young overall age of sediments in these lakes (Figure 3.2a), whereas in the palsa lakes older $^{14}C$ ages in sediments are leading to the release of old carbon in ebullition $CH_4$. In turn, the differences in sediment age are likely a function of the difference in carbon sources to POC and DOC in these lakes. In both lakes sediment OC is similar in its $^{14}C$ age distribution to POC, and in the palsa lakes input of old carbon in the form of POC may be driving the observed contribution of old carbon reservoirs to ebullition $CH_4$. In general, our results from the SAS2 palsa ebullition $CH_4$ support previous reports of $^{14}C$-$CH_4$ ages in thermokarst lakes that have demonstrated the key role of bubbles for emitting old soil organic carbon to the atmosphere in the form of $CH_4$ and $CO_2$ (Bouchard et al., 2015; Elder et al., 2019; Walter et al., 2016).

Compared to ebullition $CH_4$, the contribution of older carbon sources to ebullition $CO_2$ of the palsa lakes was limited. The higher solubility of $CO_2$ in water and the incorporation of younger $CO_2$ during the formation and rise of the bubbles to the surface could explain why the ebullition $CO_2$ was younger and less concentrated than $CH_4$ but within the range of radiocarbon ages of DIC. Similar age discrepancies between ebullition $CH_4$ and $CO_2$ have been observed in some sites in Canada and Alaska (Bouchard et al., 2015; Elder et al., 2019; Matveev et al., 2016), although other thermokarst lakes in Eastern Canada show the opposite trend, with older $CO_2$ ebullition ages (Bouchard et al., 2015; Matveev et al., 2018). The mechanism for the reversed $^{14}C$ age differences between ebullition $CH_4$ and $CO_2$ in different lakes remains unclear. Even though our results showed that carbon fixed during the bomb period strongly dominated ebullition $CH_4$ in the lithalsa lakes, previous studies have measured millennial-old ebullition $CO_2$ from lithalsa lakes in sites undergoing thaw or recently thawed (Matveev et al., 2018), implying that there is potential for old carbon release specifically through $CO_2$ ebullition fluxes in lithalsa lakes.

Overall, for both the palsa and lithalsa lakes diffusive fluxes represent much larger $CH_4$ and $CO_2$ emissions than ebullition fluxes (Matveev et al., 2016, 2018). The substantial contribution of modern carbon sources to dissolved $CH_4$ and DIC in all lakes (Figure 3.5) suggest that these fluxes are largely fueled by recently fixed carbon probably from aquatic or terrestrial primary productivity, despite the presence of older organic carbon in both these aquatic systems. This could suggest that the increase of vegetation growth in permafrost free areas, which increases the input of labile DOC from plant exudates into aquatic environments, will strongly influence diffusive $CO_2$ and $CH_4$ emissions from thermokarst lakes of Nunavik in Northern Quebec. These results are similar to other studies highlighting that diffusive $CH_4$ and $CO_2$ fluxes from lakes incorporate large proportions of modern carbon (Cooper et al., 2017; Dean et al., 2020; Elder et al., 2019).

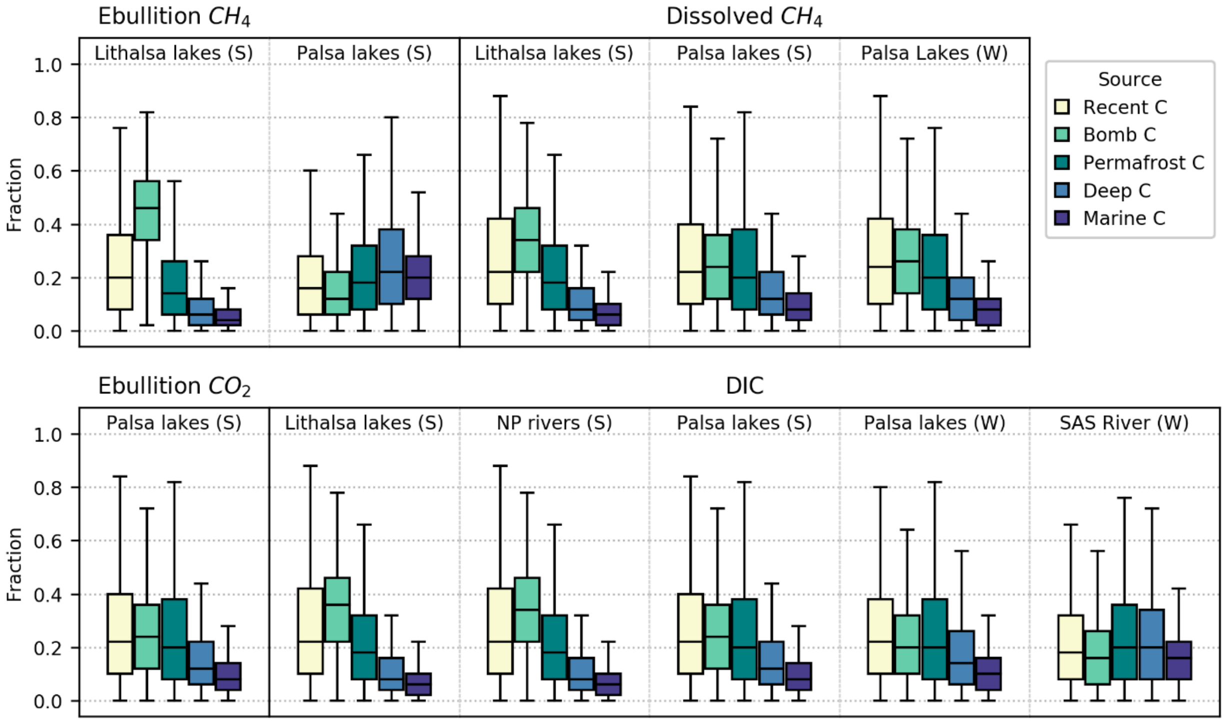

**Figure 3.5. Potential contributions from five carbon sources to the $^{14}$C content of ebullition $CH_4$ and $CO_2$, dissolved $CH_4$, and DIC by site in summer (S) and winter (W).** The boxplots show the median, the first quartile (Q1) and third quartile (Q3). The range represents the range of the feasible solutions. $CH_4$, methane; DIC, dissolved inorganic carbon.

### 3.7.3 Seasonal variations of carbon sources in the palsa lakes

The seasonal variation of $^{14}$C-DOC and $^{14}$C-POC in the palsa lakes indicated a larger contribution of older carbon sources in the ice-cover season. This increase was more pronounced in POC, which was dominated by old carbon sources in winter (Figure 3.3). Results from previous studies comparing the DOC or POC seasonal variation in aquatic systems have shown that progressively older DOC is exported from spring to winter, probably due to an increase in active layer depth (Dean et al., 2020; Wild et al., 2019). In the palsa lakes, the input of DOC from deeper and older peat layers that remained unfrozen for all or part of the ice cover season while the upper and younger peat layers were frozen could potentially explain the seasonal changes. This change in carbon input might be coupled with a slower rate of DOC decomposition at colder temperatures, which could explain the simultaneous increase of DOC concentrations and $^{14}$C ages in the ice-cover season. Moreover, changes in the redox conditions in these lakes could result in the remobilization of DOC and POC from the sediments, for example, through the dissolution of organic carbon complexed with iron under reducing conditions (Gonsior et al., 2013; Skoog and Arias-Esquivel, 2009). Previous studies looking at 16r RNA in the SAS2A lake showed there is an increased potential for reducing metabolisms in winter, including iron reducers (Vigneron et al., 2019).

Despite the higher abundance of older DOC and POC in the ice-cover season, the dissolved $^{14}$C-$CH_4$ age did not vary seasonally. In contrast, $^{14}$C-DIC was on average older in the ice-cover season. We hypothesized that the older DOC added to the water column in the ice cover season is more recalcitrant and less available to methanogens. Alternatively, it may contain limited quantities of substrates involved in methanogenesis (e.g. acetate) but larger quantities of substrates metabolized by other $CO_2$ producing metabolisms including fermentative bacteria. The apparent shift to a greater prevalence of hydrogenotrophic methanogenesis in the ice-cover, based on $\varepsilon_{C,}$ season may have also contributed to a lack of seasonal change in dissolved $^{14}$C-$CH_4$ ages, since DIC in the ice cover season has an average $^{14}$C age that is younger than that of DOC (Figure 3.4).

These results contrasted with results from a previous study comparing lake dissolved $^{14}$C-$CH_4$ and $^{14}$C-$CO_2$ ages in the ice-free and ice-cover season (Elder et al., 2019). This study found that in a Yedoma thermokarst lake in Alaska, dissolved $CH_4$ and $CO_2$ were both significantly older in the winter, at least in part due to the accumulation and dissolution of bubbles under the ice, which lowered the $^{14}C$ age of dissolved $CH_4$ (Elder et al., 2019). In the SAS2 palsa lakes, we did not observe evidence of ebullition in the winter. There were no visible openings in the ice or bubble accumulation in the surface that could have been released by the drilling of ice and missed by our sampling procedure. We argue that the ebullition $^{14}C$-$CH_4$ signal is probably not detectable in the winter dissolved $^{14}C$-$CH_4$ data, since ice-free season ebullition fluxes are one order of magnitude less than dissolved fluxes (Matveev et al., 2020). It is also plausible that the cooling of sediments in the winter results in a slower production of bubbles in these lakes (Wik et al., 2014).

Overall, our data point to intriguing seasonal differences in the source and age of carbon cycled in the palsa lakes. The mechanisms responsible for this variability are unclear, but it would be interesting to observe whether similar patterns occur in other permafrost environments. Regardless, this seasonal change in carbon cycling does not appear to have a strong effect on the source and age of carbon that is converted to GHG, and in particular $CH_4$. This, along with the general finding of a relatively young dissolved $^{14}C$ age, implies that the mobilization of old carbon reservoirs into aquatic environments does not necessarily lead to this carbon being released to the atmosphere. This is generally consistent with other studies implying a limited role of old carbon reservoirs in GHG emissions in some areas of permafrost thaw (Cooper et al., 2017; Dean et al., 2020; Elder et al., 2018).

### 3.8. Conclusions

We identified potential sources of DOC, POC, $CH_4$, and DIC in lakes and rivers near Northern Quebec's permafrost southern limit to evaluate if the increasing GHG emissions are fueled by permafrost carbon or other carbon reservoirs. We found that the soil type strongly influenced the age of the organic carbon and GHG present in the lakes and rivers, but in all sites POC contained a larger proportion of old carbon sources than DOC. The non-peatland lakes and rivers contained primarily modern DOC, DIC, and both dissolved and ebullition $CH_4$, in particular $^{14}C$ enriched carbon fixed during the bomb period.

The peatland-associated systems contained from modern to millennia-aged DOC and POC, likely including a significant contribution from permafrost carbon. In winter, both DOC and POC contained a larger proportion of old carbon sources, most likely deep peat carbon and marine sediments. Dissolved $CH_4$ and DIC were younger than DOC and POC and were sourced mainly by modern and centennial-aged permafrost-aged carbon in both summer and winter, implying that increased amounts of old organic carbon input to the lakes was not readily metabolized by methanogens. In contrast, the millennial-aged ebullition $CH_4$ in the palsa lakes and DIC in the SAS river indicated larger contribution of old carbon from deep peat and marine sediments. Whether these millennia aged DIC carbon in the SAS river will be transported to the atmosphere as $CO_2$ is not clear, as $CO_2$ fluxes from this river are not well constrained, and their magnitude relative to fluxes from the lakes remains unclear.

Overall, these results indicated that carbon fixed in the past few centuries is the primary source of diffusive $CH_4$ and $CO_2$ fluxes in all lakes and all seasons, which in this region greatly exceed ebullition fluxes that contain a greater proportion of millennial-aged carbon. Therefore, even though there is a clear presence of millennial-aged carbon in the landscape, and specifically within these aquatic ecosystems in the form of POC and sediments, this carbon is not strongly contributing to the large observed greenhouse gas fluxes. However, given the relatively recent timing of permafrost formation in this landscape, it is likely that destabilization of permafrost is contributing to greenhouse gas emissions, specifically in the peatland lakes.

### 3.9. Acknowledgements

This research was funded by the National Science and Engineering Research Council of Canada Discovery Grant Northern Research Supplement (NSERC DG 03902), the Trottier Institute for Science and Public Policy Fellowship, The Fonds de Recherche de Québec Nature et Technologie New Researcher Grant (NC-253022), the NERC Radiocarbon Facility NRCF010001 (allocation number 2128.1018), and the Concordia CUPFA PD Grant 2019. The authors thank Dr. Isabelle Laurion and Dr. Warwick Vincent for their scientific inputs on the study area; the Center d'études nordiques, Stephanie Arnold, Richard Petagumskum, Sydney Aruda, and Patrick Lacerte for their support in the field; the UQAM-GEOTOP Light Stable Isotope Geochemistry Laboratory, the University of Ottawa Lalonde Radiocarbon Laboratory, the University of Ottawa Ján Veizer Laboratory, Thi Bu Hao, and Mike Dalva for their sample analysis support; and Robert Bogue for his assistance with Python coding. Last, the authors acknowledge the Mexican National Council of Science and Technology (CONACYT) for partially sponsoring Regina Gonzalez Moguel PhD studies.

### 3.10. References

Arlen-Pouliot, Y., & Bhiry, N. (2005). Paleoecology of a palsa and a filled thermokarst pond in a permafrost peatland, subarctic Québec, Canada. The Holocene, 15(3), 408–419.

Bastviken, D., Cole, J., Pace, M., & Tranvik, L. (2004). Methane emissions from lakes: Dependence of lake characteristics, two regional assessments, and a global estimate. Global Biogeochemical Cycles, 18(4).

Bhiry, N., Delwaide, A., Allard, M., Bégin, Y., Filion, L., Lavoie, M., et al. (2011). Environmental change in the Great Whale River region, Hudson Bay: Five decades of multidisciplinary research by Center d'études nordiques (CEN). Écoscience, 18(3), 182-203.

Bhiry, N., & Robert, É. C. (2006). Reconstruction of changes in vegetation and trophic conditions of a palsa in a permafrost peatland, sub-arctic Québec, Canada. Écoscience, 13(1), 56–65.

Bouchard, F., Francus, P., Pienitz, R., & Laurion, I. (2011). Sedimentology and geochemistry of thermokarst ponds in discontinuous permafrost, subarctic Quebec, Canada. Journal of Geophysical Research – Biogeosciences, 116(G00M04).

Bouchard, F., Francus, P., Pienitz, R., Laurion, I., & Feyte, S. (2014). Subarctic Thermokarst Ponds: Investigating Recent Landscape Evolution and Sediment Dynamics in Thawed Permafrost of Northern Québec (Canada). Arctic Antarctic and Alpine Research, 46(1), 251–271.

Bouchard, F., Laurion, I., Prėskienis, V., Fortier, D., Xu, X., & Whiticar, M. J. (2015). Modern to millennium-old greenhouse gases emitted from ponds and lakes of the Eastern Canadian Arctic (Bylot Island, Nunavut). Biogeosciences, 12, 7279–7298.

Cooper, M. D. A., Estop-Aragonés, C., Fisher, J. P., Thierry, A., Garnett, M. H., Charman, D. J., et al. (2017). Limited contribution of permafrost carbon to methane release from thawing peatlands. Nature Climate Change, 7(7), 507–511.

Crann, C. A., Murseli, S., St-Jean, G., Zhao, X., Clark, I. D., & Kieser, W. E. (2017). First Status Report on Radiocarbon Sample Preparation Techniques at the A.E. Lalonde AMS Laboratory (Ottawa, Canada). Radiocarbon, 59(3), 695–704.

Crevecoeur, S., Vincent, W. F., Comte, J., & Lovejoy, C. (2015). Bacterial community structure across environmental gradients in permafrost thaw ponds: Methanotroph-rich ecosystems. Frontiers in Microbiology, 6, 192.

Crevecoeur, S., Vincent, W. F., Comte, J., Matveev, A., & Lovejoy, C. (2017). Diversity and potential activity of methanotrophs in high methane-emitting permafrost thaw ponds. PloS One, 12(11). https://doi.org/10.1371/journal.pone.0188223

Crevecoeur, S., Vincent, W. F., & Lovejoy, C. (2016). Environmental selection of planktonic methanogens in permafrost thaw ponds. Scientific Reports, 6(1), 1–10. https://doi.org/10.1038/srep31312

Dean, J. F., Meisel, O. H., Rosco, M. M., Marchesini, L. B., Garnett, M. H., Lenderink, H., & Röckmann, T. (2020). East Siberian Arctic inland waters emit mostly contemporary carbon. Nature Communications, 11(1), 1–10. https://doi.org/10.1038/s41467-020-16005-1

Dean, J. F., Van Der Velde, Y., Garnett, M. H., Dinsmore, K. J., Baxter, R., Lessels, J. S., & Billett, M. F. (2018). Abundant pre-industrial carbon detected in Canadian Arctic headwaters: Implications for the permafrost carbon feedback. Environmental Research Letters, 13(3). https://doi.org/10.1088/1748-9326/aaa1fe

Deshpande, B. N., MacIntyre, S., Matveev, A., & Vincent, W. F. (2015). Oxygen dynamics in permafrost thaw lakes: Anaerobic bioreactors in the Canadian subarctic. Limnology & Oceanography, 60(5), 1656–1670. https://doi.org/10.1002/lno.10126

Douglas, P. M. J., Gonzalez Moguel, R., Walter Anthony, K. M., Wik, M., Crill, P. M., Dawson, K. S., & Sessions, A. L. (2020). Clumped isotopes link older carbon substrates with slower rates of methanogenesis in northern lakes. Geophysical Research Letters, 47(6), 1–10. https://doi.org/10.1029/2019gl086756

Elder, C. D., Schweiger, M., Lam, B., Crook, E. D., Xu, X., Walker, J., et al. (2019). Seasonal sources of whole-lake CH4 and CO2 emissions from interior Alaskan thermokarst lakes. Journal of Geophysical Research: Biogeosciences, 124(5), 1209–1229. https://doi.org/10.1029/2018jg004735. https://doi.org/10.1029/2018JG004735

Elder, C. D., Xu, X., Walker, J., Schnell, J. L., Hinkel, K. M., Townsend-Small, A., & Czimczik, C. I. (2018). Greenhouse gas emissions from diverse Arctic Alaskan lakes are dominated by young carbon. Nature Climate Change, 8, 166–171. https://doi.org/10.1038/s41558-017-0066-9

Estop-Aragonés, C., Olefeldt, D., Abbott, B. W., Chanton, J. P., Czimczik, C. I., Dean, J. F., et al. (2020). Assessing the potential for mobilization of old soil carbon after permafrost thaw: A synthesis of 14C measurements from the northern permafrost region. Global Biogeochemical Cycles, 34, e2020GB006672. https://doi.org/10.1029/2020GB006672

Fillion, M.-È., Bhiry, N., & Touazi, M. (2014). Differential Development of Two Palsa Fields in a Peatland Located Near Whapmagoostui-Kuujjuarapik, Northern Québec, Canada. Arctic Antarctic and Alpine Research,46(1),40–54. https://doi.org/10.1657/1938-4246-46.1.40

Frolking, S., Roulet, N. T., Moore, T. R., Richard, P. J. H., Lavoie, M., & Muller, S. D. (2001). Modeling northern peatland decomposition and peat accumulation. Ecosystems, 4(5), 479–498. https://doi.org/10.1007/s10021-001-0105-1

Fuchs, G., Thauer, R., Ziegler, H., & Stichler, W. (1979). Carbon isotope fractionation by Methanobacterium thermoautotrophicum. Archives of Microbiology, 120(2), 135–139. https://doi.org/10.1007/bf00409099

Garnett, M. H., Gulliver, P., & Billett, M. F. (2016). A rapid method to collect methane from peatland streams for radiocarbon analysis. Ecohydrology, 9(1), 113–121. https://doi.org/10.1002/eco.1617

Garnett, M. H., Hardie, S. M. L., & Murray, C. (2012). Radiocarbon analysis of methane emitted from the surface of a raised peat bog. Soil Biology and Biochemistry, 50, 158–163. https://doi.org/10.1016/j.soilbio.2012.03.018

Gonsior, M., Schmitt-Kopplin, P., & Bastviken, D. (2013). Depth-dependent molecular composition and photo-reactivity of dissolved organic matter in a boreal lake under winter and summer conditions. Biogeosciences, 10(11), 6945–6956. https://doi.org/10.5194/bg-10-6945-2013

Guo, L., & Macdonald, R. W. (2006). Seasonal fluxes and age of particulate organic carbon exported from Arctic catchments impacted by localized permafrost slope disturbances. Global Biogeochemical Cycles, 20(2). https://doi.org/10.1029/2005gb002593

Guo, L., Ping, C. L., & Macdonald, R. W. (2007). Mobilization pathways of organic carbon from permafrost to arctic rivers in a changing climate. Geophysical Research Letters, 34(13), 1–5. https://doi.org/10.1029/2007gl030689

Hillaire-Marcel, C. (1976). La déglaciation et le relèvement isostatique sur la côte est de la baie d'Hudson. Cahiers de Géographie du Québec, 20(50), 185–220.

Hugelius, G., Loisel, J., Chadburn, S., Jackson, R. B., Jones, M., MacDonald, G., et al. (2020). Large stocks of peatland carbon and nitrogen are vulnerable to permafrost thaw. Proceedings of the National Academy of Sciences of the United States of America, 117(34), 20438–20446. https://doi.org/10.1073/pnas.1916387117

Kling, G. W., Kipphut, G. W., & Miller, M. C. (1991). Arctic lakes and streams as gas conduits to the atmosphere: Implications for tundra carbon budgets. Science, 251(4991), 298–301. https://doi.org/10.1126/science.251.4991.298

Laberge, M.-J., & Payette, S. (1995). Long-Term Monitoring of Permafrost Change in a Palsa Peatland in Northern Quebec, Canada: 1983–1993. Arctic and Alpine Research, 27(2), 167–171. https://doi.org/10.2307/1551898

Lalonde, K., Middlestead, P., & Gélinas, Y. (2014). Automation of13C/12C ratio measurement for freshwater and seawater DOC using high temperature combustion. Limnology & Oceanography, 12(12), 816–829. https://doi.org/10.4319/lom.2014.12.816

Lamoureux, S. F., & Lafreniere, M. J. (2014). Seasonal fluxes and age of particulate organic carbon exported from Arctic catchments impacted by localized permafrost slope disturbances. Environmental Research Letters, 9(4), 045002. https://doi.org/10.1088/1748-9326/9/4/045002

Laurion, I., Vincent, W. F., MacIntyre, S., Retamal, L., Dupont, C., Francus, P., & Pienitz, R. (2010). Variability in greenhouse gas emissions from permafrost thaw ponds. Limnology & Oceanography, 55(1), 115–133. https://doi.org/10.4319/lo.2010.55.1.0115

Mann, P. J., Eglinton, T. I., McIntyre, C. P., Zimov, N., Davydova, A., Vonk, J. E., & Spencer, R. G. M. (2015). Utilization of ancient permafrost carbon in headwaters of Arctic fluvial networks. Nature Communications, 6, 7856. https://doi.org/10.1038/ncomms8856

Matveev, A., Laurion, I., Deshpande, B. N., Bhiry, N., & Vincent, W. F. (2016). High methane emissions from thermokarst lakes in subarctic peatlands. Limnology & Oceanography, 61(S1), S150–S164. https://doi.org/10.1002/lno.10311

Matveev, A., Laurion, I., Deshpande, B. N., & Vincent, W. F. (2020). Concentrations of dissolved methane, carbon dioxide and oxygen in thermokarst lakes and ponds in palsa peatlands, northern Québec, Canada, v. 1.100000 (2012-2017). Nordicana D48. https://doi.org/10.5885/45588CE-5A12A84DFAAF4D36

Matveev, A., Laurion, I., & Vincent, W. F. (2018). Methane and carbon dioxide emissions from thermokarst lakes on mineral soils. Arctic Science, 4(4), 584–604. https://doi.org/10.1139/as-2017-0047

Matveev, A., Laurion, I., & Vincent, W. F. (2019). Winter Accumulation of Methane and its Variable Timing of Release from Thermokarst Lakes in Subarctic Peatlands. Journal of Geophysical Research: Biogeosciences, 124(11), 3521–3535. https://doi.org/10.1029/2019jg005078

Mayorga, E., Aufdenkampe, A. K., Masiello, C. A., Krusche, A. V., Hedges, J. I., Quay, P. D., et al. (2005). Young organic matter as a source of carbon dioxide outgassing from Amazonian rivers. Nature, 436(7050), 538–541. https://doi.org/10.1038/nature03880

McCalley, C. K., Woodcroft, B. J., Hodgkins, S. B., Wehr, R. A., Kim, E. H., Mondav, R., & Saleska, S. R. (2014). Methane dynamics regulated by microbial community response to permafrost thaw. Nature, 514(7253), 478–481. https://doi.org/10.1038/nature13798

Murseli, S., Middlestead, P., St-Jean, G., Zhao, X., Jean, C., Crann, C. A., et al. (2019). The preparation of water (DIC, DOC) and gas (CO2, CH4) samples for radiocarbon analysis at AEL-AMS, Ottawa, Canada. Radiocarbon, 61(5), 1563–1571. https://doi.org/10.1017/rdc.2019.14

Olefeldt, D., Goswami, S., Grosse, G., Hayes, D., Hugelius, G., Kuhry, P., & Turetsky, M. R. (2016). Circumpolar distribution and carbon storage of thermokarst landscapes. Nature Communications, 7(1), 13043. https://doi.org/10.1038/ncomms13043

Pack, M. A., Xu, X., Lupascu, M., Kessler, J. D., & Czimczik, C. I. (2015). A rapid method for preparing low volume CH4 and CO2 gas samples for 14 C AMS analysis. Organic Geochemistry, 78, 89–98. https://doi.org/10.1016/j.orggeochem.2014.10.010

Phillips, D. L., & Gregg, J. W. (2003). Source partitioning using stable isotopes: Coping with too many sources. Oecologia, 136(2), 261–269. https://doi.org/10.1007/s00442-003-1218-3

Prėskeinis, V., Laurion, I., Bouchard, F., Douglas, P. M., Billett, M. F., Fortier, D., & Xu, X. (2021). Seasonal patterns in greenhouse gas emissions from lakes and ponds in a High Arctic polygonal landscape. Limnology & Oceanography, 66(S1), S117–S141. https://doi.org/10.1002/lno.11660

Raymond, P. A., McClelland, J. W., Holmes, R. M., Zhulidov, A. V., Mull, K., Peterson, B. J., & Gurtovaya, T. Y. (2007). Flux and age of dissolved organic carbon exported to the Arctic Ocean: A carbon isotopic study of the five largest arctic rivers. Global Biogeochemical Cycles, 21(4). https://doi.org/10.1029/2007gb002934

Schuur, E. A. G., McGuire, A. D., Schädel, C., Grosse, G., Harden, J. W., Hayes, D. J., et al. (2015). Climate change and the permafrost carbon feedback. Nature, 520(7546), 171–179. https://doi.org/10.1038/nature14338

Skoog, A. C., & Arias-Esquivel, V. A. (2009). The effect of induced anoxia and reoxygenation on benthic fluxes of organic carbon, phosphate, iron, and manganese. The Science of the Total Environment, 407(23), 6085–6092. https://doi.org/10.1016/j.scitotenv.2009.08.030

Smith, S. L., Romanovsky, V. E., Lewkowicz, A. G., Burn, C. R., Allard, M., Clow, G.D., et al. (2010). Thermal state of permafrost in North America: A contribution to the international polar year. Permafrost and Periglacial Processes, 21(2), 117–135.

Spencer, R. G. M., Mann, P. J., Dittmar, T., Eglinton, T. I., McIntyre, C., Holmes, R. M., et al. (2015). Detecting the signature of permafrost thaw in Arctic rivers. Geophysical Research Letters, 42, 2830–2835. https://doi.org/10.1002/2015GL063498

Stepanenko, V. M., Machul'Skaya, E. E., Glagolev, M. V., & Lykossov, V. N. (2011). Numerical modeling of methane emissions from lakes in the permafrost zone. Izvestiya – Atmospheric and Oceanic Physics, 47(2), 252–264. https://doi.org/10.1134/s0001433811020113

Summons, R. E., Franzmann, P. D., & Nichols, P. D. (1998). Carbon isotopic fractionation associated with methylotrophic methanogenesis. Organic Geochemistry, 28(7–8), 465–475. https://doi.org/10.1016/s0146-6380(98)00011-4

Tank, S. E., Vonk, J. E., Walvoord, M. A., McClelland, J. W., Laurion, I., & Abbott, B. W. (2020). Landscape matters: Predicting the biogeochemical effects of permafrost thaw on aquatic networks with a state factor approach. Permafrost and Periglacial Processes, 31(3), 358–370. https://doi.org/10.1002/ppp.2057

Vallée, S., & Payette, S. (2007). Collapse of permafrost mounds along a subarctic river over the last 100 years (northern Quebec). Geomorphology, 90(1–2), 162–170. https://doi.org/10.1016/j.geomorph.2007.01.019

Vigneron, A., Lovejoy, C., Cruaud, P., Kalenitchenko, D., Culley, A., & Vincent, W. F. (2019). Contrasting winter versus summer microbial communities and metabolic functions in a permafrost thaw lake. Frontiers in Microbiology, 10, 1656.

Vincent, W. F., Lemay, M., & Allard, M. (2017). Arctic permafrost landscapes in transition: Toward an integrated Earth system approach. Arctic Science, 3(2), 39–64.

Walter Anthony, K., Daanen, R., Anthony, P., Schneider Von Deimling, T., Ping, C.-L., Chanton, J. P., & Grosse, G. (2016). Methane emissions proportional to permafrost carbon thawed in Arctic lakes since the 1950s. Nature Geoscience, 9(9), 679–682.

Walter, K. M., Zimov, S. A., Chanton, J. P., Verbyla, D., & Chapin, F. S. (2006). Methane bubbling from Siberian thaw lakes as a positive feedback to climate warming. Nature, 443(7107), 71–75.

Wang, J.-J., Lafrenière, M. J., Lamoureux, S. F., Simpson, A. J., Gélinas, Y., & Simpson, M. J. (2018). Differences in riverine and pond water dissolved organic matter composition and sources in Canadian high arctic watersheds affected by active layer detachments. Environmental Science & Technology, 52(3), 1062–1071.

Wang, Z., & Roulet, N. (2017). Comparison of plant litter and peat decomposition changes with permafrost thaw in a subarctic peatland. Plant and Soil, 417, 197–216.

Whiticar, M. J. (1999). Carbon and hydrogen isotope systematics of bacterial formation and oxidation of methane. Chemical Geology, 161(1), 291–314.

Wik, M., Thornton, B. F., Bastviken, D., MacIntyre, S., Varner, R. K., & Crill, P. M. (2014). Energy input is primary controller of methane bubbling in subarctic lakes. Geophysical Research Letters, 41(2), 555–560.

Wild, B., Andersson, A., Bröder, L., Vonk, J., Hugelius, G., McClelland, J. W., et al. (2019). Rivers across the Siberian Arctic unearth the patterns of carbon release from thawing permafrost. Proceedings of the National Academy of Sciences of the United States of America, 116(21), 10280–10285.

Zhang, J., Quay, P. D., & Wilbur, D. O. (1995). Carbon isotope fractionation during gas water exchange and dissolution of CO2. Geochimica et Cosmochimica Acta, 59(1), 107–114.

Zimov, S. A., Voropaev, Y. V., Semiletov, I. P., Davidov, S. P., Prosiannikov, S. F., Chapin, F. S., III, & Tyler, S. (1997). North Siberian lakes: A methane source fueled by pleistocene carbon. Science, 277(5327), 800–802.

# 4. The production rates and radiocarbon content of $CH_4$ from incubations of thermokarst lake sediments vary with temperature and landscape position.

Authors: Regina Gonzalez Moguel[1], Nagissa Mahmoudi[1], Peter M.J. Douglas[1]

1. Earth and Planetary Sciences Department, McGill University

## 4.1. Context within the thesis

We determined in the previous chapter that old carbon reservoirs, including permafrost-aged organic carbon, and contemporary carbon pools are significant sources of $CH_4$ and other carbon fractions in the studied lakes. While these results show a detailed “snapshot” of the current state of the carbon cycle in the lakes, they lead to the question of how the relative contributions from these carbon pools will change in the future. For instance, parameters such as temperature and substrate quality, both strong controls $CH_4$ production in lakes, are predicted to respond to climate change in the near future. One way to address this question is to use a laboratory approach, in which key parameters such as temperature can be manipulated and therefore changes in the $CH_4$ production from the sediments can be directly measured. Radiocarbon measurements in $CH_4$ can, again, directly inform us on what the sources of $CH_4$ are under these different experimental conditions, while additional tracers such as $\delta^{13}C$ in $CH_4$ and C:N ratios in sediments can help us explain mechanistically the variation we observed in $CH_4$ production. In this chapter, which is currently being prepared for submission to *Biogeosciences* or *Global biogeochemical cycles*, we used laboratory experiments to assess how the $CH_4$ production rates and the utilization of the different carbon sources (i.e., permafrost-aged carbon and contemporary organic carbon) changes with increased temperatures, as well as between sediments of different lakes.

## 4.2. Abstract

Thermokarst lakes are predicted to constitute major feedbacks to climate change through increases in $CH_4$ emissions at higher temperatures. The magnitude of this feedback is unclear, partly because we do not fully understand how the production of $CH_4$ from contemporary to millennial carbon pools in lake sediments will respond to global warming and permafrost thaw. We incubated thermokarst lake surficial sediments anaerobically at increasing temperatures to evaluate how $CH_4$ production rates and the radiocarbon content of $CH_4$ vary with temperature and landscape position relative to a permafrost thaw gradient. With these measurements we generated the first dataset of radiocarbon values of $CH_4$ produced by the incubation lake sediments under a warming scenario. We found that $CH_4$ production rates increased with warming and were higher in a permafrost-free bog lake compared to lakes closer to the permafrost thaw front. The radiocarbon values were closely linked to the $CH_4$ production rates, suggesting that slower $CH_4$ production at lower temperatures is associated with metabolism of older carbon pools, and vice versa. Radiocarbon values from the same ponds spanned a wide range, implying that methanogens utilize highly different carbon pools depending on environmental conditions. These findings suggest that the reactivity of carbon pools of different ages might be an important mediator in the metabolic response of $CH_4$ production to global warming.

## 4.3. Introduction

Lakes in high latitudes have a critical role on the release of the greenhouse gas methane ($CH_4$) from the northern permafrost region, acting as conduits for the decomposition of destabilized soil organic carbon (Walter Anthony , et al., 2016; Wik, Varner, Walter Anthony, MacIntyre, & Batsviken , 2016). Net $CH_4$ emissions from lakes, currently estimated to range from

7 to 25 Tg $CH_4$ $yr^{-1}$, are regulated by the balance between the anaerobic $CH_4$ production in lake sediments by methanogenic microbial communities and the consumption of $CH_4$ by methanotrophic microbial communities in the sediments and water column (Bridgham, Cadillo-Quiroz, Keller, & Zhuang, 2013; Wik, Varner, Walter Anthony, MacIntyre, & Batsviken , 2016). This balance is also influenced by the transport mechanism of $CH_4$ in the lake, as the rapid transport of $CH_4$ (e.g., by ebullition) can decrease how much $CH_4$ is oxidized (Bastviken, Cole, Pace, & Tranvik, 2004). Emissions of $CH_4$ from high latitude lakes are expected to increase due to an increase in global temperatures and from increased carbon and nutrient inputs resulting from permafrost thaw, but the magnitude of this increase is highly uncertain (Tan & Zhuang, 2015; Walter Anthony , et al., 2018; Hugelius, et al., 2020). Due to the large global warming potential of $CH_4$, it is essential to understand how $CH_4$ emissions will respond to climate change and to predict to what extent will lake systems accelerate climate change.

The production of $CH_4$ in lake sediments is a microbial process largely controlled by temperature and substrate availability, both which are expected to respond to climate change (Dean, et al., 2018). As high latitudes are predicted to warm by 2.6 to 6.4 °C by 2100 (IPCC, 2013), the production rates of $CH_4$ from lake sediments will most likely increase (Gudasz, et al., 2010; Marotta, et al., 2014). However, the magnitude of temperature response will likely be mediated by the composition of the organic substrates (Duc , Crill, & Bastviken , 2010; Lupascu, Wadham, Hornibook, & Pancost, 2012; Treat, et al., 2015; Sepulveda-Jauregui, et al., 2018). In permafrost ecosystems, large amounts of old organic matter contained in permafrost soils can become available to microbial communities in lake sediments through erosion and slumping, river and groundwater transport, or through the deepening of active layers (Lamoureux & Lafrenière, 2014;

Vonk, et al., 2015; Walter Anthony , et al., 2018). The reactivity of this organic matter will likely depend on factors such as the soil composition and the extent of degradation prior to thaw (Treat, et al., 2014; Elder, et al., 2018; Estop-Aragonés, et al., 2020). Furthermore, changes in vegetation and nutrient availability due to global warming in permafrost-free soils will most likely change the composition of the organic matter supplied to lakes, influencing the microbial community composition, and affecting $CH_4$ production (Hodgkins, Tfaily, McCalley, & Chanton , 2014; McCalley, et al., 2014).

Since $CH_4$ production is a key component of $CH_4$ emissions from lakes, there is an urgent need to examine how the changes in substrate composition driven by permafrost thaw will influence the response of $CH_4$ production in sediment lakes to temperature increases caused by global warming. Radiocarbon measurements of $CH_4$ can provide evidence of the utilization of older organic carbon pools previously stabilized in permafrost soils and sediments and can therefore inform how these carbon pools influence $CH_4$ production (Estop-Aragonés, et al., 2020). Recent studies assessing the contribution of soil organic carbon pools to $CH_4$ emissions through radiocarbon measurements have found that thermokarst lakes frequently emit permafrost-aged organic carbon through ebullition $CH_4$ fluxes (Bouchard, et al., 2015; Walter Anthony , et al., 2016; Elder, et al., 2018; Preskenis, et al., 2021). At the same time, there is growing evidence of primarily contemporary carbon being incorporated to dissolved $CH_4$ in lakes (Elder, et al., 2018; Preskenis, et al., 2021; Gonzalez Moguel, et al., 2021; Elder, et al., 2019). Although these findings provide information about how contemporary to millennial organic carbon is processed in thermokarst lakes and distributed to $CH_4$ fluxes, there is a lack data that constrains how the use of these substrates change with global warming. In this sense, coupling radiocarbon measurements to laboratory experiments could help assess how increased temperatures will affect the age of substrate used for $CH_4$ production.

We incubated surficial lake sediments from five thermokarst lakes at three temperatures, 4 °C, 12 °C, and 22 °C under anaerobic conditions. The lakes are located in two Canadian sporadic permafrost subarctic valleys, one of them a peatland and the other a valley in mineral soil, that have undergone an extensive loss of permafrost in the last five decades (Bhiry, et al., 2011; Bouchard, Francus, Pienitz, Laurion, & Feyte, 2014). Numerous thermokarst lakes have been formed from the collapse of permafrost mounds in the region and are currently significant sources of modern to millennial $CH_4$ and $CO_2$ to the atmosphere (Matveev, Laurion, Deshpande, Bhiry, & Vincent, 2016). Previous studies analyzing $^{14}C$ ages showed the presence of soil organic carbon (SOC) in all the sampled lakes in dissolved and particulate carbon; and showed that SOC is also released to the atmosphere especially through the formation and release of $CH_4$ bubbles from the sediment (Gonzalez Moguel, et al., 2021).

We addressed two research goals. First, we calculated the rates of $CH_4$ production from the lakes sediment incubations to evaluate the response of $CH_4$ production to warming and landscape position. We hypothesized that $CH_4$ production would increase with warming given the influence of temperature in microbial metabolisms (Zhu, et al., 2020), and hypothesized that lakes in permafrost-free areas would result in higher $CH_4$ production rates, as permafrost thaw might cause the increase of labile compounds in soils (Hodgkins, Tfaily, McCalley, & Chanton , 2014). Second, we measured the radiocarbon content of the produced $CH_4$ with the goal of assessing how the relative contribution of older substrates to $CH_4$ would change with increasing temperatures and different landscape positions. We hypothesized that warming would change the carbon pools utilized for methanogenesis as previous radiocarbon measurements of $CO_2$ produced in the aerobic incubations of soils have shown that microbes respond to warming by metabolizing substrates of different ages (Vaughn & Torn, 2019). To support our interpretation, we measured $CO_2$ production rates of the incubations and their radiocarbon values, and analyzed the sediment organic carbon content, nitrogen content, and C:N ratios with the aim of linking the $CH_4$ production rates to the sediments reactivity.

## 4.4. Methods

### 4.4.1. Study Site and sample collection

The study sites are located in two valleys adjacent to the southeastern coast of the Hudson Bay near Kuujjuarapik-Whapmagoostui in Nunavik, Quebec, Canada. The region was glaciated for most of the Pleistocene, but after the Laurentide Ice Sheet retreated the Tyrell Sea submerged the area, leading to marine clay deposition over the Precambrian bedrock (Hillaire-Marcel, 1976). When the area emerged due to isostatic uplift after approximately 6000 to 5700 years Before Present (calibrated), extensive peatlands were deposited and permafrost developed in some areas, producing features such as permafrost mounds (Arlen-Pouliot & Bhiry, 2005). Nowadays, the permafrost in the region is in an advanced state of degradation and the thawing of permafrost mounds has resulted in the extensive formation of shallow thermokarst ponds and a marked increase in vegetation cover (Bouchard, Francus, Pienitz, Laurion, & Feyte, 2014). Currently, the climate in the area is classified as subarctic and the two valleys lie in the sporadic permafrost zone of the Taiga Shield ecozone (Bhiry, et al., 2011). The snow-free season spans from May to September, that is when lakes are not ice-covered and emit $CH_4$ and $CO_2$ to the atmosphere through diffusion and ebullition (Matveev, Laurion, Deshpande, Bhiry, & Vincent, 2016).

We sampled six sites in summer of 2019 and 2021 (Figure 4.1). The first site is a lake with underlying mineral sediment (KWK1 or mineral lake) located in a valley south of the Kwakwatanikapistikw River (KWK valley; 55° 19’ 50.6” N; 77° 30’ 15.9” W). Nowadays the permafrost in the valley has almost disappeared and the landscape is characterized by the presence of thermokarst lakes that were formed by the collapse of mineral permafrost over marine deposits, and the areas surrounding the ponds are colonized by shrubs (*Salix* spp., *Alnus crispa*, *Myrica gale*), mosses (*Sphaghnum* spp.), and herbaceous plants such as sedges (*Carex* spp) (Bouchard, Francus, Pienitz, Laurion, & Feyte, 2014). The other five sampled sites are located in a peatland adjacent to the Sasapimakwananisikw river (SAS2 peatland; 55° 13’ 36.7’’ N; 77° 41’ 44.1’’ W). The permafrost that is left in the peatland exists in the palsas, while permafrost-free soil contains bogs populated by peat moss (*Sphaghnum* spp.) and sedges (*Carex* spp.), and thermokarst lakes (Vallee & Payette, 2007; Vincent, Lemay, & Allard, 2017). Here, we sampled surface soil from an intact palsa (palsa site), and sediments from a lake forming from a palsa collapse (SAS2X or palsa lake), a lake close to the palsa (SAS2C or near-palsa lake), a lake close to the bog (SAS2A or near-bog lake), and a lake within in the bog (SAS2B or bog lake).

We collected approximately 5–10 cm of surface sediments from the center of the five lakes using an Eckman dredge, as previous studies assessing potential $CH_4$ production rates from thermokarst lake sediments have associated the highest $CH_4$ productions to the surface sediments (Heslop, et al., 2015; Lofton, Whalen, & Hershey, 2015; Praetzel, et al., 2020). The sediments were stored in sealed 0.5 L Nalgene bottles (in 2019), or Whirlpak bags (in 2021) at 4 °C until the incubations.

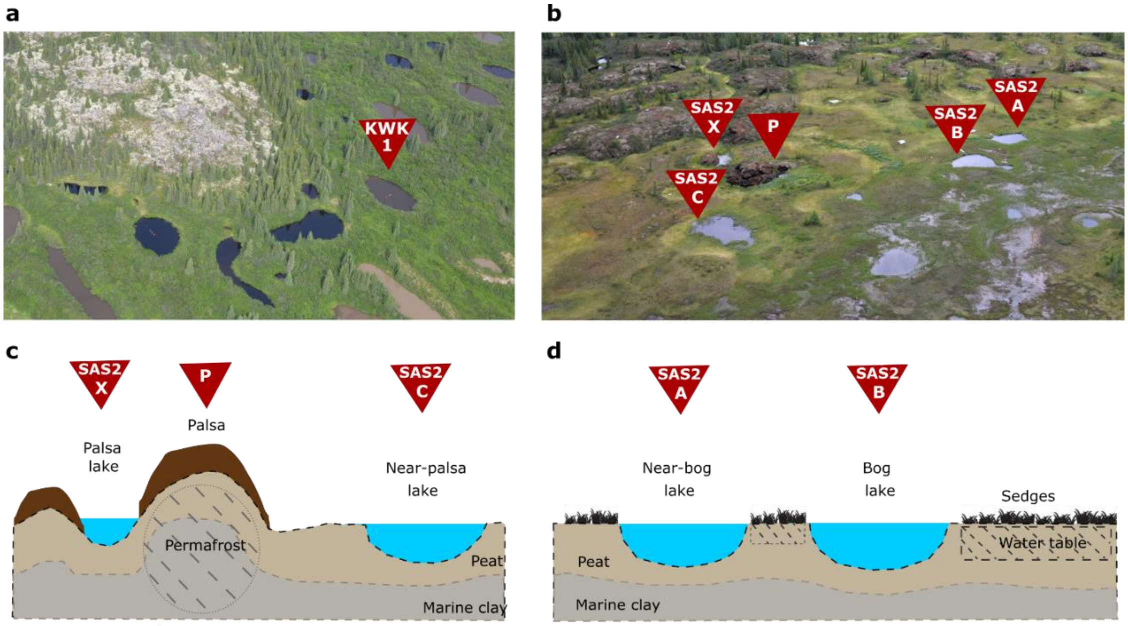

**Figure 4.1 Illustration of the sampling sites.** We sampled six sites: a) a lake with underlying mineral sediment (KWK1 or mineral lake); b, c) surface soil from an intact palsa (P or palsa site); b,c) a lake forming from a palsa collapse (SAS2X or palsa lake); b,c) a lake close to the palsa (SAS2C or near-palsa lake); b,d) a lake close to the bog (SAS2A or near-bog lake); b,d) and a lake in the bog (SAS2B or bog lake). The illustration of the five peatland sites is not to scale.

### 4.4.2. Sediment incubations

We prepared sediment “slurries” by adding approximately 10 grams (wet weight) of homogenized sediment from each site and 20 mL of media to 100 mL amber serum bottles in an anaerobic chamber (99.4% Nitrogen). The media consisted of an autoclaved solution of approximately 70 mM of salts (NaCl, $NH_4Cl$, $KH_2PO_4$, and $Na_2HPO_4$) at a pH of 5.9. After preparing the slurry, the serum vials were sealed with butyl rubber stoppers and flushed with pure Nitrogen for one to three minutes to remove any remaining gases such as oxygen from the sediment. The sediment slurries were prepared in duplicates or triplicates and incubated at 4 °C, 12 °C, and 22 °C. For each site and temperature, we added a control consisting of an autoclaved slurry. The purpose of this was to kill the microbial community in the sediment and verify that there was no inorganic $CH_4$ production in the sediment. Additionally, we added two controls consisting of 20 mL of media and an empty serum bottle at each temperature to verify there was no sources of $CH_4$ other than the sediment in the bottles. The headspace $CH_4$ concentration of each bottle was measured at discrete intervals, ranging from every three days the first weeks of incubation, to once or twice a month when $CH_4$ production slowed down. To measure the headspace $CH_4$ concentration, we used a Thermo Trace 1310 gas chromatograph (GC) with a flame ionization detector (FID). Four reference standards of 250 ppmv, 1000 ppmv, 1 %, and 5 % were analyzed to calibrate these measurements.

We assembled three incubations in sequence, and incubations were stopped when the headspace had enough $CH_4$ to measure radiocarbon, which is around 1 mg of carbon. The first incubation consisted of slurries of the sediment collected in Nalgene bottles in 2019 from the bog lake (SAS2B), near palsa lake (SAS2C), and mineral lake (KWK1). The incubation lasted 105 days and the maximum $CH_4$ production rates were reached around day 10. The second incubation was assembled eight months after the first incubation from the same sediment collected in 2019, with the addition of a slurry of the near-bog lake (SAS2A). This means that the sediment used for the second incubation was stored approximately 11 months before the experiment began. The experiment lasted 219 days and the maximum $CH_4$ production rates were reached around day 10 in the mineral lake and near-palsa lake and around day 40 in the bog lake and near-bog lake. After 70 days, the headspace $CH_4$ concentration in the second incubation decreased in some of the samples, suggesting anaerobic $CH_4$ consumption was occurring.

In the third incubation we prepared slurries of the sites palsa, palsa lake (SAS2X), near-palsa lake (SAS2C), and near-bog lake (SAS2A) using sediment collected in Whirlpak bags in 2021. The incubation lasted 260 days, but the production of $CH_4$ started after 58 days in the palsa lake and the near bog lake at 22 °C, and after approximately 140 days in the near palsa lake at 22 °C and in the palsa lake at 12 °C. There was no production in any palsa replicate, in replicates at 4 °C, and from the replicates at 12 °C only the palsa lake produced $CH_4$. Lastly, we did not observe any $CH_4$ production in any of the autoclaved controls in the three incubations.

### 4.4.3. Methane production rates

We calculated the rate of $CH_4$ production in each replicate using Equation 1, where $C_{CH4}$ is the concentration of $CH_4$ in the headspace (fractional), $V$ (mL) is the volume of headspace, $P$ (atm) is the headspace pressure, $R$ (L atm mol$^{-1}$ K$^{-1}$) is the ideal gas constant, $T$ (K) the temperature, $t$ (days) the incubation time, and $gdw$ (g) is the dry weigh of the sediment.

$$\boldsymbol{r_{CH4}}(\mu \boldsymbol{mol\ CH4\ g^{-1}\ day^{-1}}) = \frac{\boldsymbol{C_{CH4} * V_H(mL) * P\ (atm) * 1000}}{\boldsymbol{R\ (L\ atm\ mol^{-1}\ K^{-1}) * T(K) * t(days) * gdw(g)}} \qquad \text{Equation 1}$$

We reported the maximum $CH_4$ production rates, which corresponded to 10 days in incubation 1 and the palsa lake and mineral lake sites in incubation 2; 40 days in the near-bog lake and bog lake in incubation 2; and 80 days from when $CH_4$ production started in incubation 3. We also report net long-term incubation rates of both $CH_4$ and $CO_2$, which correspond to the whole timespan of the incubation: 105 days for incubation 1; 219 days for incubation 2; and 202 days for the sites palsa lake and near bog lake, and 66 days for the near palsa lake in incubation 3 subtracting the time-lag prior to methane formation. To estimate the temperature sensitivity of the $CH_4$ production rates by site and incubation we used the activation energy $E_a$ (J mol$^{-1}$) from the

Arrhenius equation (Equation 2), where $K$ is the rate of $CH_4$ production, $A$ is the Arrhenius constant, $R$ (J $K^{-1}$ $mol^{-1}$) is the ideal gas constant, and $T$ (K) is the experimental temperature.

$$\mathbf{ln}(\boldsymbol{K}) = \frac{-\boldsymbol{E_a}}{\boldsymbol{RT}} + \mathbf{ln}(\boldsymbol{A}) \qquad \text{Equation 2}$$

#### 4.4.4. Isotope and geochemical analyses

At the time the incubations were prepared, an aliquot of the sediment was homogenized, weighed, freeze-dried, and analyzed for total carbon, organic carbon, and nitrogen, $\delta^{13}C$, and $\delta^{15}N$ in the GEOTOP Light Stable Isotope Geochemistry Laboratory (Montreal, Canada). Here, samples were weighed in tin cups and analyzed alongside two internal reference standards with a Micromass model Isoprime 100 Isotope Ratio Mass Spectrometer coupled to an Elementar Vario MicroCube elemental analyzer in continuous flow mode. A third reference material was analyzed to assess the uncertainty of the normalization. The $\delta^{13}C$ results were normalized to the NBS19-LSVEC scale and expressed in delta units against VPDB. Analytical uncertainty (2σ) was <±0.2‰.

When experiments were finalized, the headspace gas was collected and stored in a serum vial sealed with a butyl rubber cap and sent to the W.M. Keck Carbon Cycle Accelerator Mass Spectrometer facility at UC Irvine for analysis. There, $CO_2$ and $CH_4$ were extracted in three steps (Pack, Xu, Lupascu, Kessler, & Czimczik, 2015). First, $CO_2$ in the sample was separated cryogenically using liquid nitrogen in a vacuum line. Second, carbon monoxide (CO) was removed by oxidizing it into $CO_2$ at 290 °C and then using the liquid nitrogen trap to collect it. Last, $CH_4$ was oxidized to $CO_2$ at 975 °C and collected. An aliquot of the $CH_4$-derived $CO_2$ was analyzed for $\delta^{13}C$ using a Gas Bench coupled to a Finnigan Delta Plus Isotope Ratio Mass Spectrometer. Both the $CO_2$ and oxidized $CH_4$ were reduced to graphite using the sealed-tube Zinc reduction method

(Xu, et al., 2007) and the $^{14}C$ to $^{12}C$ ratio of the graphite was measured in the Accelerator Mass Spectrometer or AMS (Beverly, et al., 2010). Radiocarbon values of $CO_2$ and $CH_4$ were reported in FMC, $\Delta^{14}C$, and conventional radiocarbon age (Stuiver & Polach, 1977). The measured sample ratio is normalized to a $\delta^{13}C$ value of -25‰ to correct for the mass-dependent fractionation of $^{14}C$ using the $\delta^{13}C$ measured by the AMS.

## 4.5. Results

### 4.5.1. Incubation $CH_4$ production rates

The $CH_4$ production rates ranged from 0 to 1.7 μmol $CH_4$ $gdw^{-1}$ $d^{-1}$ and varied with temperature, and between sites and incubations (Figures 4.2a and 4.3a). The first two incubations reached the maximum $CH_4$ production rates between day 10 and day 40, and followed the same $CH_4$ production patterns between sites, with the highest production rates from the bog lake, followed by the near-palsa lake, the near-bog lake, and lastly the mineral lake. However, the $CH_4$ production rates in the second experiment were consistently lower and responded less strongly to warming compared to the first experiment. The $CH_4$ production rates from the third incubation were the lowest of the three incubations, and there was no production at 4 °C and at 12 °C, except in the palsa lake. Production rates of $CH_4$ in this incubation were highest rates in the near bog lake, followed by near palsa lake, and lastly the palsa lake. Averaging for all temperatures and incubation, the maximum $CH_4$ production rates were zero in the palsa, 0.03 ± 0.02 μmol $CH_4$ $gdw^{-1}$ $d^{-1}$ in the palsa lake, 0.16 ± 0.06 μmol $CH_4$ $gdw^{-1}$ $d^{-1}$ in the near-palsa lake, 0.12 ± 0.08 μmol $CH_4$ $gdw^{-1}$ $d^{-1}$ in the near-bog lake, 0.85 ± 0.56 μmol $CH_4$ $gdw^{-1}$ $d^{-1}$ in the bog lake, and 0.08 ± 0.04 μmol $CH_4$ $gdw^{-1}$ $d^{-1}$ in the mineral lake.

The $CH_4$ production rates increased with temperature in all the experiments, increasing from 1.2 to 3 times with each temperature step (Figure 4.2a). We assessed the temperature sensitivity of the $CH_4$ production rates by fitting the data of each experiment to the Arrhenius equation with the goal of determining if landscape position affected the response of $CH_4$ production rates to warming. A high Arrhenius activation energy indicates a higher temperature sensitivity and therefore a larger increase in $CH_4$ production with temperature. The activation energies ranged between 20 and 50 KJ $mol^{-1}$ and varied with time and incubation, but we did not observe clear differences between sites.

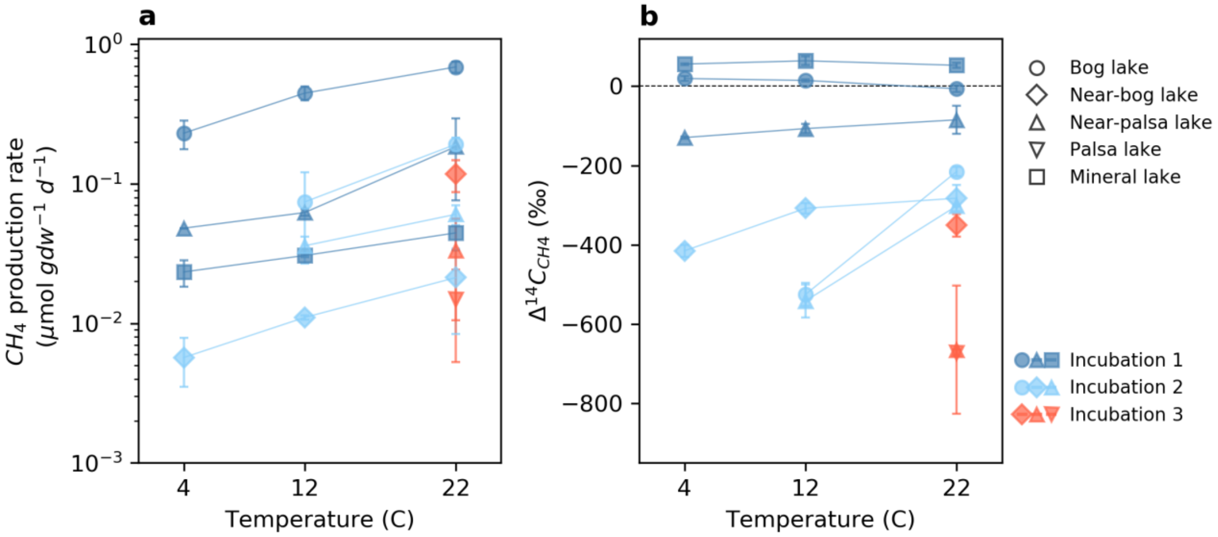

**Figure 4.2 Effect of temperature in the incubation $CH_4$ production rates and $\Delta^{14}C_{CH4}$ values.** a) Long-term $CH_4$ production rates, corresponding to 106 days in the first incubation, 219 days in the second incubation, and 266 days in the third incubation, increased with warming. b) $\Delta^{14}C_{CH4}$, measured at the end of the incubations, increased with temperature in experiments were $\Delta^{14}C_{CH4}$ was negative**.**

### 4.5.2. Geochemical characteristics of the sediment

We analyzed the organic carbon content, inorganic carbon content, nitrogen (N) content, and carbon to nitrogen ratios (C: N) of the sediments before incubation with the aim of linking the organic carbon availability in sediments to $CH_4$ production rates. A high organic matter content is frequently used as an indicator of a larger quantity of substrate available to microbial communities compared to lower organic matter contents (Heslop, et al., 2015; Treat, et al., 2015). We found that the organic carbon content was highest in the palsa site and palsa lake, followed by the near-palsa lake and near-bog lake, and was lowest in the bog lake and mineral lake (Figure 4.3b). High C:N ratios can indicate a low organic matter reactivity because the decomposition of organic matter removes reactive N-containing compounds while structural compounds containing carbon are left behind (Melillo , et al., 1989). Low C:N ratios can indicate high reactivity due to the presence of easily degradable N compounds, although at high decomposition stages C:N ratios decrease again as carbon is lost and the N that is left is incorporated into stable chemical structures such as aromatic rings (Schadel, et al., 2014). The C:N ratios were highest in the palsa site and palsa lake, followed by the near-palsa lake and the near-bog lake, and were lowest in the bog lake and mineral lake (Figure 4.3b).

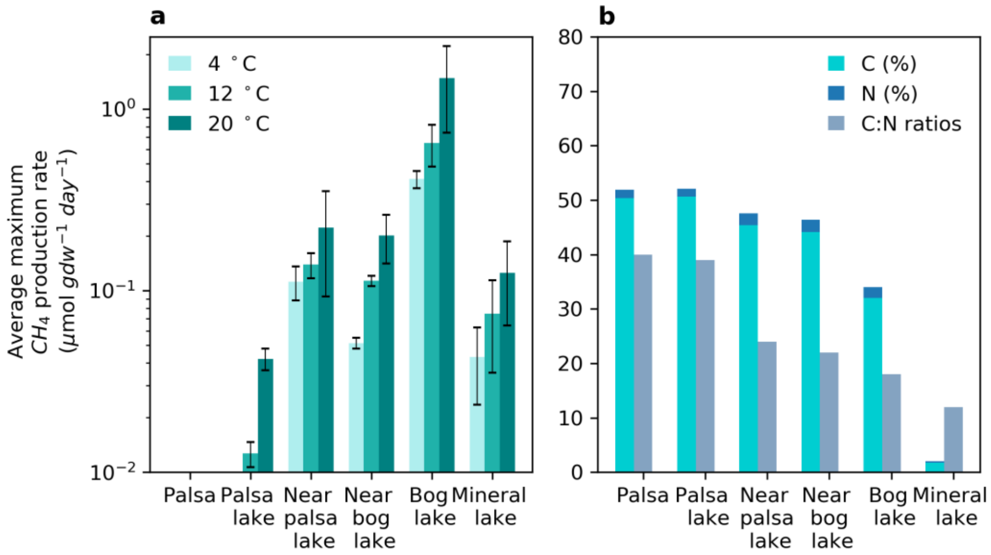

**Figure 4.3 Effect of landscape position in the incubation maximum $CH_4$ production rates and sediment characteristics.** a) The maximum incubation $CH_4$ production rates increased with temperature and varied by site. Bars represent the averaged maximum $CH_4$ production rates for each site and temperature. b) The organic carbon content (OC), nitrogen content (N), and carbon to nitrogen ratios (C: N) by site.

### 4.5.3. Long-term incubation $\Delta^{14}C_{CH4}$ and $\delta^{13}C_{CH4}$

$\Delta^{14}C_{CH4}$ from the first incubation ranged from -130 to 70 ‰, corresponding to radiocarbon ages from contemporary to 1,000 years BP (Figure 4.2b). A positive $\Delta^{14}C_{CH4}$ indicates a larger amount of contemporary carbon (post-1950) while more negative $\Delta^{14}C_{CH4}$ indicates a larger contribution of carbon from centennial or millennial aged pools. In the second incubation, $\Delta^{14}C_{CH4}$ decreased along with $CH_4$ production rates, shifting towards a slower production of $CH_4$ from older carbon pools. $\Delta^{14}C_{CH4}$ from the third incubation yielded $\Delta^{14}C_{CH4}$ values from -350 to -670 ‰, the lowest from the three incubations and substantially lower than bulk sediment OC $\Delta^{14}C$

values. When considered all together, the incubation $CH_4$ production rates in peatland sites were significantly correlated to $\Delta^{14}C_{CH4}$ ($r = 0.64$; $p = 0.008$).

The incubation $\Delta^{14}C_{CH4}$ values responded to the increasing temperatures in most sites. In incubations where the $\Delta^{14}C_{CH4}$ value was negative, indicating that a substantial amount of old carbon pools are being used to produced $CH_4$, $\Delta^{14}C_{CH4}$ became more positive with warming (Figure 4.2b). In incubations where the $\Delta^{14}C_{CH4}$ was positive, indicating that $CH_4$ is produced mainly from a contemporary carbon pool, $\Delta^{14}C_{CH4}$ did not vary significantly as a function of temperature.

The $\Delta^{14}C_{CH4}$ values from the first incubation were in the same range as in-situ dissolved and ebullition $\Delta^{14}C_{CH4}$ measured in a previous study (Gonzalez Moguel, et al., 2021; Figure 4.4b). Here, ebullition $\Delta^{14}C_{CH4}$ values ranged from 40 to -210 ‰, or contemporary to 2,000 years BP; and dissolved $\Delta^{14}C_{CH4}$ values ranged -8 to -78 ‰, or contemporary to 600 years BP (Gonzalez Moguel, et al., 2021). While these field measurements showed a correlation between the concentration of $CH_4$ in the bubbles and ebullition $\Delta^{14}C_{CH4}$ ($r = 0.88$; $p = 0.004$), there was no correlation between dissolved $CH_4$ concentrations and $\Delta^{14}C_{CH4}$ (Figure 4.4b).

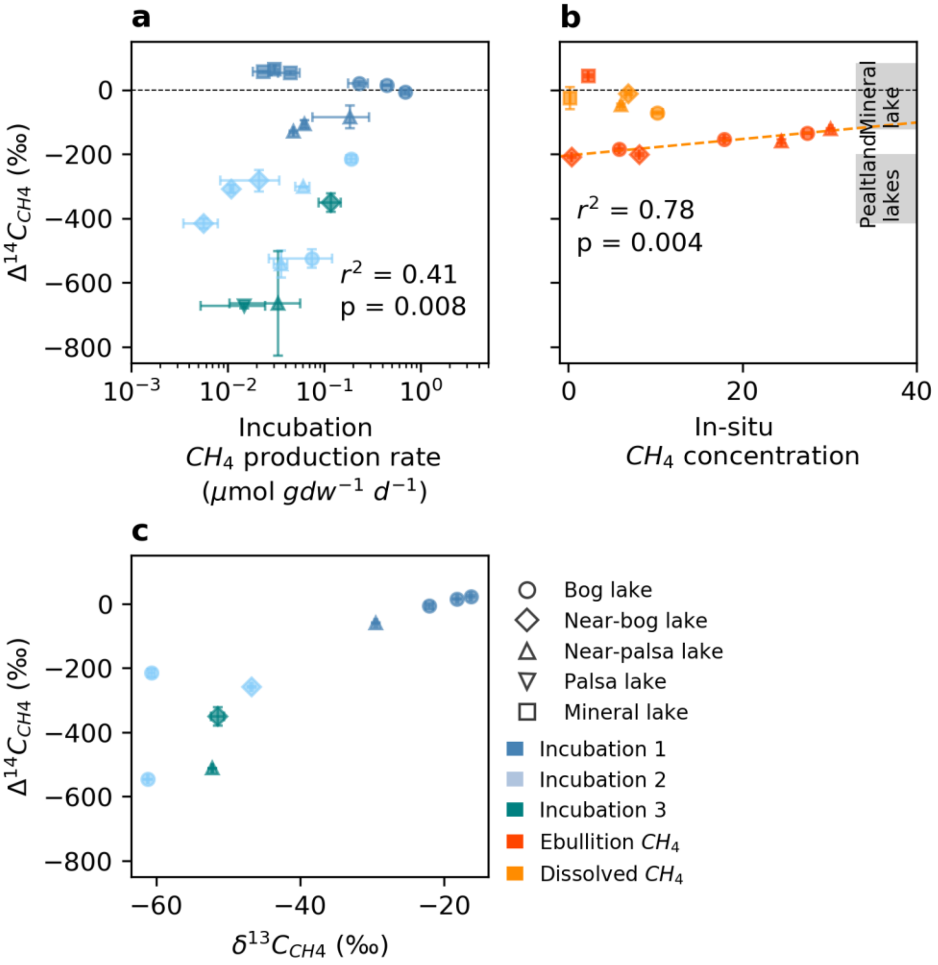

**Figure 4.4 Long-term incubation $CH_4$ production rates and $\Delta^{14}C_{CH4}$ for the three incubations compared to in-situ $\Delta^{14}C_{CH4}$ of ebullition $CH_4$ and dissolved $CH_4$.** a) The long-term incubation $CH_4$ production rates, shown in a logarithmic scale, were significantly correlated to $\Delta^{14}C_{CH4}$ in the peatland sites (r = 0.64; p = 0.008). b) Field $\Delta^{14}C_{CH4}$ values of dissolved and ebullition $CH_4$ published in Gonzalez Moguel et al. (2021) and corresponding to the sites bog lake, near-bog lake, near-palsa lake, and mineral lake. The x-axis is the $CH_4$ concentration in gas or water, which is in units of % in the case of ebullition $CH_4$ and ppm in the case of dissolved $CH_4$. Ebullition $CH_4$ showed a significant correlation between $CH_4$ concentration and $\Delta^{14}C_{CH4}$ in the

peatland lakes ($r = 0.88$; $p = 0.004$). The range of $\Delta^{14}C$ bulk sediment values for the peatland lakes and mineral lake are showed as a gray rectangle. c) Incubation $\delta^{13}C_{CH4}$ plotted against $\Delta^{14}C_{CH4}$.

### 4.5.4. Long-term $CO_2$ production rates and $\Delta^{14}C_{CO2}$

We measured headspace $CO_2$ concentration at the end of each incubation, calculated a long-term $CO_2$ production using the recovered $CO_2$ mass, and measured $\Delta^{14}C_{CO2}$. $CO_2$ production rates ranged 0.1 to 0.8 μmol $CO_2$ $gdw^{-1}$ $day^{-1}$ and were consistently higher than $CH_4$ production rates in all sites except the bog-lake (Figure 4.5e). In contrast to $CH_4$ production, we did not observe clear patterns in $CO_2$ production rates between incubations and sites. The $CO_2$ production rates responded to warming, increasing specifically when temperature was increased from 12 to 22 °C, but not from 4 to 12 °C (Figure 4.5a). $\Delta^{14}C_{CO2}$ values ranged from 0 to −600 ‰ and followed closely the $\Delta^{14}C_{CH4}$ values but were slightly more negative, indicating somewhat older carbon reservoirs being metabolized (Figure 4.5f). Like $\Delta^{14}C_{CH4}$, $\Delta^{14}C_{CO2}$ were highest in the first incubation and decreased in later incubations. Unlike $\Delta^{14}C_{CH4}$, there did not appear to be a systematic difference in $\Delta^{14}C_{CO2}$ between sites. $\Delta^{14}C_{CO2}$ responded to temperature in most sites, becoming more positive with warming (Figure 4.5b). In contrast to $\Delta^{14}C_{CH4}$, $\Delta^{14}C_{CO2}$ did not seem to be correlated to $CO_2$ production (Figure 4.5c), but it was correlated strongly to $\delta^{13}C_{CO2}$ ($r = 0.90$, $p < 0.001$; Figure 4.5d).

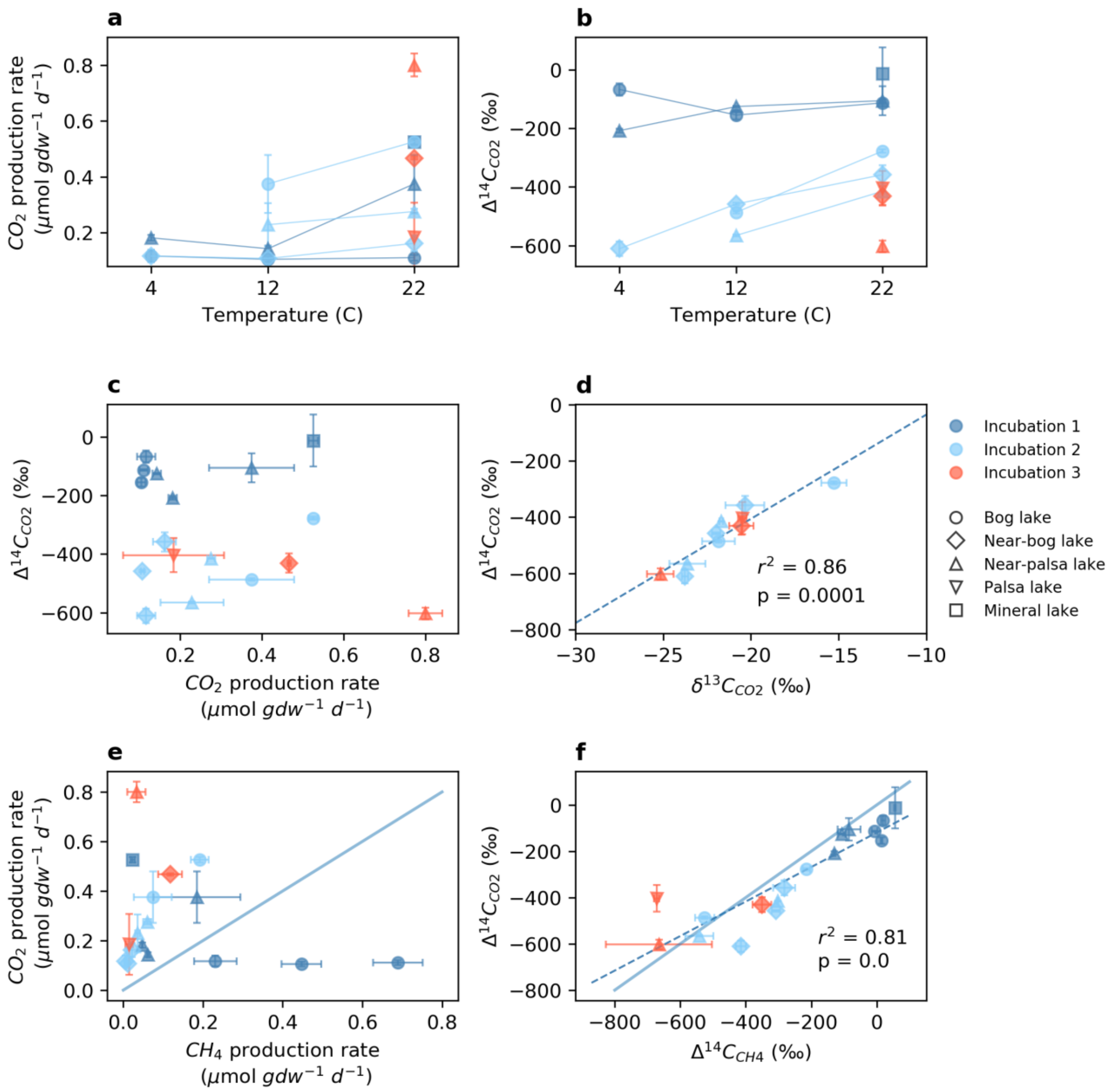

**Figure 4.5. Long term incubation $CO_2$ and $\Delta^{14}C_{CO2}$.** a) Long-term $CO_2$ production rate responded to warming when increasing the temperature from 12 °C to 22 °C. b) $\Delta^{14}C_{CO2}$ responded to warming in the second incubation. c) Long-term $CO_2$ production rate compared to $\Delta^{14}C_{CO2}$. d) $\delta^{13}C_{CO2}$ was correlated with $\Delta^{14}C_{CO2}$ ($r = 0.90$, $p < 0.001$). e) Long-term $CH_4$ production rates

compared to $CO_2$ production rates with 1 to 1 line for reference. f) $\Delta^{14}C_{CH2}$ values were correlated to $\Delta^{14}C_{CO2}$ values ($r = 0.92$, $p < 0.001$). The continuous lines in panels e and f represent a 1:1 line.

## 4.6. Discussion

### 4.6.1. Variations in the radiocarbon values of the incubation $CH_4$

Our results showed a large variability in the $CH_4$ production rates and $\Delta^{14}C_{CH4}$ values across incubations. The changes in $CH_4$ production rates and $\Delta^{14}C_{CH4}$ from the first to the second incubation might suggest that the availability of reactive substrates derived from modern carbon pools decreased between these incubations, either by the depletion of these substrates in the sampled sediment during refrigerated storage or by the substrate uptake by competing microbial communities that might have become active in the second experiment due to the longer storage time prior to starting the experiment. For example, the consumption of $CH_4$, higher $CO_2$ production rates, and the presence of sulfate in the second incubation imply that anaerobic methanotrophs became active after the first experiment. In the third incubation, the low $CH_4$ production rates, low $\Delta^{14}C_{CH4}$, and observed lag-times point towards the inhibition of the microbial communities in the sediment, probably by exposure to oxygen during the sampling of sediment in the field. Despite this variability, our results constitute one of the first datasets presenting the $\Delta^{14}C_{CH4}$ of thermokarst lake sediments under warming and therefore they constitute the first insight into how methanogenic communities might respond to warming in thermokarst lakes.

Taken altogether, the results showed that incubation $CH_4$ production rates were linked to $\Delta^{14}C_{CH4}$ values in the peatland lakes (Figure 4.3a), which is consistent with previous findings that the rate of $CH_4$ production is slower when methanogens metabolize older carbon substrates

(Douglas, et al., 2020). They also showed that this linkage is found in field observations, specifically in $CH_4$ released through bubbles. While we were not able to observe a clear relationship between dissolved $CH_4$ concentrations and $\Delta^{14}C_{CH4}$, we speculate this is because the concentration of $CH_4$ in the water column is affected by processes other than $CH_4$ production, including $CH_4$ oxidation and the frequency of water column mixing. Within incubations, we observed that the near-palsa lake and palsa lake yielded the lowest $\Delta^{14}C_{CH4}$ values for any given temperature, which would suggest that there is a larger contribution of older organic components to $CH_4$ production in these sites. However, these patterns were not reflected the in in-situ data, where we did not observe consistent differences between the near-palsa lake, near-bog lake, and bog lake (Figure 4.3b).

### 4.6.2. Effect of landscape position on $CH_4$ production rates and $\Delta^{14}C_{CH4}$

The patterns of $CH_4$ production rates, organic carbon content, and C:N ratios between the different sites suggest that the position in the landscape influences the production rates of $CH_4$ through the availability of reactive organic carbon. In areas where the collapse of palsas have formed bogs, the development of vegetation (i.e., sedges) can increase the availability of easily degradable substrates through the exudation of simple organic compounds and the thawing of permafrost can result in the increase in the methanogenic community diversity (Hodgkins, Tfaily, McCalley, & Chanton , 2014). These labile substrates might be transported from the bog to the bog lake and to a less extent to the near-bog lake, enhancing organic matter decomposition and $CH_4$ production. Contrastingly, sites where the palsa is still actively eroding, such as the palsa lake and to a lesser extent palsa site, might contain a large amount of peat organic material. Since the peatlands in the region underwent extensive decomposition before the development of permafrost (Arlen-Pouliot & Bhiry, 2005), it is likely that the peat organic matter is less reactive and therefore $CH_4$ production and decomposition rates in the palsa lake and near-palsa lake might be relatively low. Along with the low organic carbon reactivity, the lack of $CH_4$ production from the palsa site might have been due to the absence of an active methanogenic community soil, as dry and oxic conditions are not favorable for methanogens. Despite the different potential sources in the different lakes, we found that the near bog lake and the near palsa lake sediments had similar C:N ratios and similar incubation $CH_4$ production rates, probably indicating that the reactivity of the combined sources in both lakes was similar.

In the mineral lake, a lower quantity of organic substrates combined with the retention of organic matter in the sediment mineral horizons through sorption could make the substrates difficult to access to microorganisms, therefore resulting in the relatively low $CH_4$ production rates observed in this lake (Kalbitz, Shwesig, Rethemeyer, & Matzner, 2005).

These results were broadly in agreement with in-situ measurements of permafrost peatland soil $CH_4$ emissions, where $CH_4$ fluxes were largest in wet, permafrost-free, sedge-covered areas compared to the palsas and permafrost covered soil (Olefeldt, Turetsky, Crill, & McGuire, 2013; Hodgkins, Tfaily, McCalley, & Chanton , 2014). Contrastingly, they were less consistent with patterns of in-situ $CH_4$ concentrations measured in the sampled lakes. Previous measurements of dissolved $CH_4$ in 2018 and 2019 showed that the bog lake had the highest $CH_4$ concentrations while the near-palsa lake had the lowest $CH_4$ concentration (Gonzalez Moguel, et al., 2021). However, results from years previous to 2018 observed the opposite trend (Matveev, Laurion, Deshpande, Bhiry, & Vincent, 2016). This could suggest that similarly to other northern lakes,

$CH_4$ fluxes from the lake to the atmosphere are not always coupled to the rate of $CH_4$ production in the sediments (DelSontro, Boutet, St-Pierre, del Giorgio, & Prairie, 2016; Douglas, et al., 2020). They could, instead, be influenced by other factors such as varying rates of $CH_4$ oxidation, varying sediment organic matter concentration and composition, and dissolved $CH_4$ originating from sources other than the sediment OC, such as $CH_4$ produced in the bog and transported to the lake and $CH_4$ produced from DOC in the water column.

### 4.6.3. Effect of temperature on $CH_4$ production rates and $\Delta^{14}C_{CH4}$

The responses in $CH_4$ production rates and $\Delta^{14}C_{CH4}$ to temperature suggested that as temperatures increase, the methanogen community increasingly use contemporary carbon pools to produce $CH_4$ at a faster rate. Three hypotheses could explain these findings. First, higher temperatures might favor a methanogen community structure that is better suited for degrading contemporary carbon. Second, at lower temperatures non-methanogenic microbial metabolisms involved in the degradation of organic matter could outcompete methanogens and utilize the more reactive contemporary substrates, which means methanogens are only able to access older and less reactive carbon. Third, warming might stimulate certain fermentative metabolisms to a greater extent than other metabolisms, resulting in a higher concentration of contemporary substrates that could be available to methanogens.

While there are no studies assessing how the utilization of substrates of different radiocarbon ages influence the methanogenic community structure in lake sediments, previous studies have shown that temperature affects methanogenesis not only through changes in methanogen metabolism but also by changing the broader microbial community structure or metabolic interactions (Zhu, et al., 2020; Glissman, Chin, Casper, & Conrad, 2004; Lavergne, et al., 2021). For example, warming has been found to shift the methanogenic community towards a larger contribution of hydrogenotrophic methanogens compared to acetrotrophic methanogens (Glissman et al., 2004; Treat et al., 2015; Zhu et al., 2020; Lavergne et al., 2021). It is likely that these changes are a result of high temperatures stimulating the fermentative metabolisms that produce $H_2$, and of the methanogenic community being shaped based on the availability this substrate (Glissman et al., 2004). In addition to the change in community structure, there is certain evidence that the diversity and relative abundance of methanogenic community compared to non methanogenic community increased with warming in incubation studies of Arctic peat (Høj, Olsen, & Torsvik, 2008). Overall, our results contrasted with previous soil incubations measuring how warming affects $\Delta^{14}C_{CO2}$ in oxic respiration, where $\Delta^{14}C_{CO2}$ values decreased with warming, indicating that there was a change towards older carbon pools by microbial communities (Vaughn and Torn 2019).

We did not observe variations in temperature sensitivity between sites. The kinetics of enzymatic reactions postulate that complex substrates require more energy to break down and as a result, less reactive organic matter should have higher activation energies and higher temperature sensitivities than reactive substrates (Davidson & Janssens, 2006). Previous incubation studies measuring aerobic soil respiration from fractionated soils have been in agreement with Arrhenius kinetics, showing an increased temperature sensitivity in less reactive carbon pools, while incubation studies that did not isolate soil pools have not observed a change in temperature sensitivity between carbon pools (Fang, Smith , Moncrieff, & Smith, 2005; Craine, Fierer, & McLauchlan , 2010; Vaughn & Torn, 2019). We speculate that these differences might arise because in non fractionated soils and sediments, $CH_4$ is produced from carbon pools with differing temperature sensitivities, and as temperatures change, the combination of carbon pools also changes.

## 4.7. Conclusions

Northern ecosystems store large amounts of carbon that can be exposed to microbial decomposition as high latitude regions are warming faster than the rest of the world. Predicting how microbial $CH_4$ production, a crucial component of carbon decomposition and $CH_4$ emissions, responds to warming is important to predict feedbacks to climate change. Our results suggested that the reactivity of the organic carbon used to produce $CH_4$ in lake sediments could depend on the landscape position and could influence production rates of $CH_4$. We infer from our results that, in the studied peatland lakes, the reactivity of organic carbon is probably linked to the age of the organic carbon substrate, and older substrates might result in slower rates of $CH_4$ production. Our data supported the hypothesis that $CH_4$ production rates not only respond to warming by producing $CH_4$ at a faster rate, but the combination of carbon pools utilized by microbial organisms as a substrate for $CH_4$ production will respond to warming. More research is required to verify the direction of this response, as our results differed from a previous study showing that in terrestrial soils, microbes have utilized older carbon pools at increased temperatures. Lastly, our results show that $CH_4$ production will most likely be sensitive to both environmental warming but also to landscape changes induced by permafrost thaw that change the composition of substrates available to microbial communities.

## 4.8. Acknowledgements

In the lab: Kathryn Rico, Lauren Rosenthal, Thi Bu Hao, Xiaomei Xu and the UC Irvine's KCCAMS team, and the UQAM-GEOTOP Light Stable Isotope Geochemistry Laboratory Team.

For the 2021 field campaign: Melanie Burnett, Martial Leroy, Audrey Laberge-Carignan, Valérie Langlois, Raoul-Marie Couture, and the Centre d'Etudes Nordiques team. For the 2018 and 2019 field campaigns: Benjamin Keenan, Alex Matveev, Adrian Bass, Martin Pilote, Stephanie Arnold, Richard Petagumskum, Sydney Aruda, Patrick Lacerte, Isabelle Laurion, and Warwick Vincent.

This research was funded by National Science and Engineering Research Council of Canada Discovery Grant Northern Research Supplement (NSERC DG 03902), the Trottier Institute for Science and Public Policy Fellowship, the Fonds de Recherche de Québec Nature et Technologie New Researcher Grant (NC-253022), the McGill Wares Science Prospector Fund, the Mexican National Council of Science and Technology (CONACYT), and the Fonds de Recherche de Québec Nature et Technologie Merit Scholarship program for foreign students.

## 4.9. References

Arlen-Pouliot , Y., & Bhiry, N. (2005). Paleoecology of a palsa and filled thermokarst pond in a permafrost peatland, subarctic Quebec, Canada. The Holocene, 15(3), 408-419.

Bastviken, D., Cole, J., Pace, M., & Tranvik, L. (2004). Methane emissions from lakes: Dependence on lake characteristics, two regional assessments, and a global estimate. Global biogeochemical cycles, 18.

Beverly, R., Beaumont, W., Tauz, D., Ormsby, K., von Reden, K., Santos, G., & Southon, J. (2010). The keck carbon cycle AMS laboratory, University of California, Irvine: Status report. Radiocarbon, 52(2), 301-309.

Bhiry, N., Delwaide, A., Allard, M., Begin, Y., Filion, L., Lavoie, M., . . . Vincent, W. (2011). Environmental change in the Great Whale River region, Hudson Bay: Five decades of multidisciplinary research by Centre d'études nordiques (CEN). Ecoscience, 18(3), 182-203.

Bouchard, F., Francus, P., Pienitz, R., Laurion, I., & Feyte, S. (2014). Subarctic thermokarst ponds: Investigating recent landscape evolution and sediment dynamics in thawed permafrost of northern Québec (Canada). Arctic, Antarctic, and Alpine Research, 46(1), 251-271.

Bouchard, F., Laurion, I., Preskienis, V., Fortier, D., Xu, X., & Whiticar, M. (2015). Modern to millennium-old greenhouse gases emitted from ponds and lakes of the Eastern Canadian Arctic. Biogeosciences, 7279-7298.

Bridgham, S., Cadillo-Quiroz, H., Keller, J., & Zhuang, Q. (2013). Methane emissions from wetlands: biogeochemical, microbial, and modeling perspectives from local to global scales. Global Change Biology, 19, 1325-1346.

Craine, J., Fierer, N., & McLauchlan , K. (2010). Widespread coupling between the rate and temperature sensitivity of organic matter decay. Nature Geoscience, 3, 854-857.

Davidson , E., & Janssens, I. (2006). Temperature sensitivity of soil carbon decomposition and feedbacks to climate change. Nature, 440, 165-173.

Dean, J., Middelburg, J., Rockmann, T., Aerts, R., Blauw, L., Egger, M., . . . Dolman, A. (2018). Methane feedbacks to the global climate system in a warmer world. Reviews of geophysics, 56, 207-250.

DelSontro, T., Boutet, L., St-Pierre, A., del Giorgio, P., & Prairie, Y. (2016). Methane ebullition and diffusion from northern ponds and lakes regulated by the interaction between temperature and system productivity. Limnology and oceanography, 61(S1), S62-S77.

Douglas, P., Gonzalez Moguel, R., Walter Anthony, K., Wik, M., Crill Patrick M., Dawson , K., . . . Sessions, A. (2020). Clumped isotopes link older carbon substrates with slower rates of methanogenesis in northern lakes. Geophysical research letters, 47(6).

Duc , N., Crill, P., & Bastviken , D. (2010). Implications of temperature and sediment characteristics on methane formation and oxidation in lake sediments. Biogeochemistry, 100(1), 185-196.

Elder, C., Schweiger, M., Lam, B., Xu, X., Walker, J., Walter Anthony, K., & Czimczik, C. (2019). Seasonal sources of whole-lake CH4 and CO2 emissions from interior Alaska thermokarst lakes. JGR Biogeosciences, 124, 1209-1229.

Elder, C., Xu, X., Walker, J., Schnell, J., Hinkel, K., Townsend-Small, A., . . . Czimczik, C. (2018). Greenhouse gas emissions from diverse Arctic Alaskan lakes are dominated by young carbon. Nature climate change, 8, 166-171.

Estop-Aragonés, C., Olefeldt, D., Abbott, B., Chanton, J., Czimczik, C., Dean , J., . . . Walter Anthony, K. (2020). Assessing the potential for mobilization of old soil carbon after permafrost thaw: a synthesis of 14C measurements from the northern permafrost region. Global biogeochemical cycles(34).

Fang, C., Smith , P., Moncrieff, J., & Smith, J. (2005). Similar response of labile and resistant soil organic matter pools to changes in temperature. Nature, 433, 57-59.

Glissman, K., Chin, K., Casper, P., & Conrad, R. (2004). Methanogenic pathway and archeal community structure in the sediment of Eutrophic Lake Dagow: Effect of temperature. Microbial ecology, 48, 389-399.

Gonzalez Moguel, R., Bass, A., Garnett, M., Pilote, M., Keenan, B., Matveev, A., & Douglas, P. (2021). Radiocarbon data reveal contrasting sources for carbon fractions in thermokarst lakes and rivers of Eastern Canada (Nunavi, Quebec). Journal of geophysical research: biogeosciences. doi: https://doi.org/10.1029/2020JG005938

Gudasz, C., Bastviken, D., Steger, K., Premke, K., Sobek, S., & Tranvik, L. (2010). Temperature-controlled organic carbon mineralization in lake sediments. Nature, 466(7305), 478-481.

Heslop, J., Walter Anthony, K., Sepulveda-Jauregui, A., Martinez-Cruz, K., Bondurant, A., Grosse, G., & Jones, M. (2015). Thermokarst lake methanogenesis along a complete talik profile. Biogeosciences, 12(14), 4317-4331.

Hillaire-Marcel, C. (1976). La déglaciation et le relèvement isostatique sur la côte est de la baie d'Hudson. Cahiers de géographie du Québec, 20(50), 185-220. doi:https://doi.org/10.7202/021319ar

Hodgkins, S., Tfaily, M. M., McCalley, C., & Chanton , J. (2014). Changes in peat chemistry associated with permafrost thaw increase greenhouse gas production. Proceedings of the national academy of sciences, 111(16), 5819-5824.

Høj, L., Olsen, R. A., & Torsvik, V. L. (2008). Effects of temperature on the diversity and community structure of known methanogenic groups and other archaea in high Arctic peat. *The ISME journal*, *2*(1), 37-48.

Hugelius, G., Loisel, J., Chadburn, S., Jackson, R., Jones, M., MacDonald, G., . . . Yu, Z. (2020). Large stocks of peatland carbon and nitrogen are vulnerable to permafrost thaw. Proceedings of the National Academy of Sciences, 117(34), 20438-20446.

IPCC. (2013). Contribution of working group I to the fifth assessment report of the intergovernmental panel on climate change. In T. Stocker, D. Qin, G. Plattner, M. Tignor, S. Allen, J. Boschung, . . . P. Midgley (Eds.), Climate Change 2013: The Physical Science Basis. (p. 1535). Cambridge and New York: Cambridge University Press.

Kalbitz, K., Shwesig, D., Rethemeyer, J., & Matzner, E. (2005). Stabilization of dissolved organic matter by sorption to the mineral soil. Soil biology and biogeochemistry, 37(7), 1319-1331.

Lamoureux, S., & Lafrenière, M. (2014). Lamoureux, S. F., & Lafrenière, M. J. (2014). Seasonal fluxes and age of particulate organic carbon exported from Arctic catchments impacted by localized permafrost slope disturbances. Environmental research letters, 9(4), 045002.

Lavergne, C., Aguilar-Munoz, P., Calle, N., Thalasso, F., Astorga-Espana, M., Sepulveda-Jauregui, A., . . . Cabrol, L. (2021). Temperature differently affected methanogenic pathways and microbial communities in sub-Antarctic freshwater ecosystems. Environment international, 154, 106575.

Lofton, D., Whalen, S., & Hershey, A. (2015). Vertical sediment distribution of methanogenic pathways in two shallow Arctic Alaskan lakes. Polar Biology, 38(6), 815-827.

Lupascu, M., Wadham, J., Hornibook, E., & Pancost, R. (2012). Temperature sensitivity or methane production in the permafrost active layer at Stordalen, Sweden: a comparison with non-permafrost northern wetlands. Arctic, Antarctic, and Alpine Research, 44(4), 469-482.

Marotta, H., Pinho, L., Gudasz, C., Bastviken, D., Tranvik, L., & Enrich-Prast, A. (2014). Greenhouse gas production in low-latitude lake sediments responds strongly to warming. Nature Climate Change, 4(6), 467-470.

Matveev, A., Laurion, I., Deshpande, B., Bhiry, N., & Vincent, W. (2016). High methane emissions from thermokarst lakes in subarctic peatlands. Limnology and oceanography, 61(S1), S150-S164.

McCalley, C., Hodgkins, S., Wher, R., Kim, E.-H., Mondav, R., Crill , P., . . . Saleska , S. (2014). Methane dynamics regulated by microbial community response to permafrost thaw. Nature, 514, 478-481.

Melillo , J., Aber, J., Linkins, A., Ricca, A., Fry, B., & Nadelhoffer, K. (1989). Carbon and nitrogen dynamics along the decay continuum: plant litter to soil organic matter. Plant and soil, 115(2), 189-198.

Olefeldt, D., Turetsky, M., Crill, P., & McGuire, D. (2013). Environmental and physical controls on northern terrestrial methane emissions across permafrost zones. Global change biology, 19, 589.

Pack, M., Xu, X., Lupascu, M., Kessler, J., & Czimczik, C. (2015). A rapid method for preparing low volume CH4 and CO2 gas samples for 14C AMS analysis. Organic geochemistry, 78, 89-98.

Praetzel, L., Plenter, N., Schilling, S., Schmiedeskamp, M., Broll, G., & Knorr, K. (2020). Organic matter and sediment properties determine in-lake variability of sediment CO 2 and CH 4 production and emissions of a small and shallow lake. Biogeosciences, 17(20), 5057-5078.

Preskenis, V., Laurion, I., Bouchard, F., Douglas, P., Billet, M., Fortier, D., & Xu, X. (2021). Seasonal patterns in greenhouse gas emissions from lakes and ponds in a High Arctic polygonal landscape. Limnology and Oceanography, 66, S117-S141.

Schädel, C., Schuur, E. A. G., Bracho, R., Elberling, B., Knoblauch, C., Lee, H., … Turetsky, M. R. (2014). Circumpolar assessment of permafrost C quality and its vulnerability over time using long-term incubation data. *Global Change Biology*, *20*(2), 641–652. https://doi.org/10.1111/GCB.12417

Sepulveda-Jauregui, A., Hoyos-Santillan, J., Martinez-Cruz, K., Walter Anthony, L., Casper, P., Belmonte-Izquierdo, Y., & Thalasso, F. (2018). Eutrophication exacerbates the impact of climate warming on lake methane emission. Science of the Total Environment, 636, 411-419.

Stuiver, M., & Polach, H. (1977). Discussion reporting of 14C data. Radiocarbon, 19(3), 355-363.

Tan, Z., & Zhuang, Q. (2015). Arctic lakes are continuous methane sources to the atmopshere under warming conditions. Environmental research letters, 10(5), 054016.

Treat, C., Natali, S., Ernakovich, J., Colleen, I., Lupascu, M., McGuire, A., . . . Waldrop, M. (2015). A pan-Arctic synthesis of CH4 and CO2 production from anoxic soil incubations. Global change biology, 21, 2787-2803.

Treat, C., Wollheim, W., Varner, R., Grandy, A., Talbot, J., & Frolking, S. (2014). Temperature and peat type control CO 2 and CH 4 production in Alaskan permafrost peats. Global change biology, 20(8), 2674-2686.

Vallee, S., & Payette, S. (2007). Collapse of permafrost mounds along a subarctic river over the last 100 years (northern Quebec). Geomorphology, 90(1-2), 162-170.

Vaughn, L., & Torn, M. (2019). 14C evidence that millennial and fast-cycling soil carbon are equally sensitive to warming. nature climate change, 9, 467-471.

Vincent, W., Lemay, M., & Allard, M. (2017). Arctic permafrost landscapes in transition: towards an integrated Earth system approach. Arctic Science, 3(2), 39-64.

Vonk, J., Tank, S., Bowden, W., Laurion, I., Vincent, W., Alekseychik, P., . . . Wickland, K. (2015). Reviews and syntheses: Effects of permafrost thaw on Arctic aquatic ecosystems. Biogeosciences, 12(23), 7129-7167.

Walter Anthony , K., Daanen, R., Anthony, P., Schneider von Demling , T., Ping, C., Chanton, J., & Grosse , G. (2016). Methane emissions proportional to permafrost carbon thawed in Arctic lakes since the 1950s. Nature geoscience, 9, 679-682.

Walter Anthony , K., Schneider von Deimling, T., Nitze, I., Frolking , S., Emond, A., Daanen, R., . . . Grosse , G. (2018). 21st-century modeled permafrost carbon emissions accelerated by abrupt thaw beneath lakes. Nature communications, 9(1), 1-11.

Wik, M., Varner, R., Walter Anthony, K., MacIntyre, S., & Batsviken , D. (2016). Climate-sensitive northern lakes and ponds are critical components of methane release. nature geoscience, 0, 99-105.

Xu, X., Trumbore, S., Zheng, S., Southon, J., McDuffee, K., Luttgen, M., & Liu, J. (2007). Modifying a sealed tube zinc reduction method for preparation of AMS graphite targets: Reducing background and attaining high precision. Nuclear instruments and Methods in physics research Section B: Beam Interactions with Materials and Atoms, 259(1), 320-329.

Zhu, Y., Purdy, K., Eyie, O., Shen , L., Harpenslager, S., Yvon-Durocher, G., . . . Trimmer, M. (2020). Disproportionate increase in freshwater methane emissions induced by experimental warming. Nature Climate Change, 10(7), 685-690.

# 5. Using carbon-13 and carbon-14 measurements for source attribution of atmospheric methane in the Athabasca Oil Sands Region

Authors and affiliations: Regina Gonzalez Moguel[1], Felix Vogel[2], Sébastien Ars[2], Hinrich Schaefer[3], Jocelyn C. Turnbull[4,5], Peter M.J. Douglas[1]

1. Earth and Planetary Sciences Department, McGill University; GEOTOP research center
2. Environment and Climate Change Canada
3. National Institute for Water and Atmospheric Research of New Zealand
4. GNS Science, New Zealand
5. CIRES, University of Colorado at Boulder, USA

## 5.1. Context within the thesis

We explored in previous chapters how climate-driven natural processes such as permafrost thaw affect the carbon cycle in lakes situated in Canadian wetlands through the study of $CH_4$ sources. In addition to these processes, anthropogenic disturbances can greatly impact the carbon cycle and therefore $CH_4$ emissions at vulnerable high latitude ecosystems. In Canada, extensive disturbance of wetland ecosystems can be attributed to a myriad of activities that include the building of roads, dumps, buildings, mines, and dams. Examples of such disturbed wetlands are in the Athabasca region, which due to its extensive oil deposits, known as the oil sands, has been transformed and developed in order to extract bitumen through mining. Currently, the oil sands surface mines in the Athabasca region have become a significant source of greenhouse gases, including atmospheric $CH_4$, at a national level. Two sources are estimated to be especially large emitters of methane: the tailings ponds where residues of bitumen mines are stored, and the surface of the mines, which release $CH_4$ when the rocks are crushed to extract the bitumen. Despite the extensive coverage of $CH_4$-emitting mines in the region, there has been a limited number of studies aiming to determine the relative contribution of anthropogenic and natural sources in the region. As $\delta^{13}C$ and $\Delta^{14}C$ can be used as tracers of atmospheric $CH_4$, we aimed to use these two isotopes simultaneously in this chapter, published in *Atmospheric Chemistry and Physics* in 2021, to evaluate the proportion of atmospheric $CH_4$ originating from anthropogenic sources (surface mines and tailings ponds) and the proportion of $CH_4$ originating from natural sources (wetlands).

### 5.2. Abstract

The rapidly expanding and energy intensive production from the Canadian oil sands, one of the largest oil reserves globally, accounts for almost 12% of Canada's greenhouse gas emissions according to inventories. Developing approaches for evaluating reported methane ($CH_4$) emission is crucial for developing effective mitigation policies, but only one study has characterized $CH_4$ sources in the Athabasca Oil Sands Region (AOSR). We tested the use of $^{14}C$ and $^{13}C$ carbon isotope measurements in ambient $CH_4$ from the AOSR to estimate source contributions from key regional $CH_4$ sources: (1) tailings ponds, (2) surface mines and processing facilities, and (3) wetlands. The isotopic signatures of ambient $CH_4$ indicate that the $CH_4$ enrichments measured at the site were mainly influenced by fossil $CH_4$ emissions from surface mining and processing facilities (56 ± 18 %), followed by fossil $CH_4$ emissions from tailings ponds (34 ± 18 %), and to a lesser extent by modern $CH_4$ emissions from wetlands (10 ± < 1 %). Our results confirm the importance of tailings ponds in regional $CH_4$ emissions and show that this method can successfully distinguish wetland $CH_4$ emissions. In the future, the isotopic characterization of $CH_4$ sources, and measurements from different seasons and wind directions are needed to provide a better source attribution in the AOSR.

## 5.3. Introduction

Methane ($CH_4$) is an important greenhouse gas that has 32 times the global warming potential (mass basis) of carbon dioxide ($CO_2$) on a 100-year timescale, and which contributes to the production of ozone, water vapor (in the stratosphere), and $CO_2$ in the atmosphere (Myhre et al., 2013; Etminan et al., 2016). Global $CH_4$ concentration in the atmosphere has almost tripled compared to pre-industrial values (Rubino et al., 2019), largely due to increased anthropogenic activities that include fossil fuel production and use and agriculture (Jackson et al., 2020; Turner et al., 2019). Since most fossil fuel emissions originate from coal, oil, and natural gas exploitation, transportation, and use (Jackson et al., 2020; Saunois et al., 2020), mitigating $CH_4$ emissions from these activities is necessary to fulfill governmental $CH_4$ emissions reduction goals. Furthermore, a fast $CH_4$ mitigation from the oil and gas sector is projected to have a key role in slowing the rate of global warming over the next few decades (Ocko et al., 2021).

Canada contains approximately 10% of the world's crude oil proven reserves, with 82% of these reserves located in the Athabasca Oil Sands Region (AOSR) in Alberta (Alberta Energy Regulator, 2015). Oil sand deposits, composed of a mixture of sand grains, water, bitumen, and clay minerals (Mossop, 1980; Takamura, 1982), are extracted through two methods. Shallow deposits (< 75 m) are recovered through surface mining and the bitumen is subsequently separated from sands with alkaline warm water, concentrated, upgraded, and refined (Larter and Head, 2014). Residual water, solids, and diluents used to separate the bitumen are then stored in tailings, which depending on their age and composition emit volatile organic compounds (VOCs), reduced sulfur compounds, $CO_2$, and $CH_4$ (Small et al., 2015). In contrast, the recovery of deeper deposits requires the use of in situ techniques that involve lowering the viscosity of bitumen by injecting steam into the reservoir to extract it (Bergerson et al., 2012). Although only around 20% of the oil sands deposits are recoverable using surface mining (Alberta Energy Regulator, 2015), surface mining accounts for 45–65 % of the annual crude oil production from oil sands (Holly et al., 2016). Each of these methods have greenhouse gas (GHG) emissions associated with them, and it is estimated that the oil sands account for 12% of Canada's total GHG emissions (Government of Canada, 2018). In the AOSR, an aircraft-based study attributed $CH_4$ emissions to three main sources: microbial methanogenesis in tailings ponds (45% of total $CH_4$ emissions), disturbance of mine-faces in open pit mines (50% of total $CH_4$ emissions), and facilities activities such as venting, cogeneration, and natural gas leakage (5% of total emissions) (Baray et al., 2018).

Methane emissions from the oil sands are reported annually to Environment and Climate Change Canada (ECCC) through the Greenhouse Gas Reporting Program (GHGRP), based on inventories of facilities that emit more than $10^7$ kg $CO_2$-eq $yr^{-1}$ (Government of Canada, 2018). The GHGRP and other inventory approaches have varying degrees of accuracy and are vulnerable to uncertainty in the "emission factors" used to calculate the GHG emission rates. Top-down approaches are used to verify inventory-based GHG emission estimates, and aircraft-based top-down estimates in the AOSR have shown that inventories underestimate GHG emissions (Liggio et al., 2019), with an aircraft-based estimate reporting 48% higher $CH_4$ emissions than in the inventories (Baray et al., 2018). However, these aircraft measurements were limited to a short period of time (summer 2013), and there have not been other studies confirming and updating these findings. Given these limitations, additional measurements of $CH_4$ and source specific tracers are needed to reconcile differences amongst methods, to generate data at different times of the year, and to generate long-term data for monitoring the evolution of AOSR emissions.

We can use $^{13}C$ and $^{14}C$ carbon isotopes to determine the sources of $CH_4$ emissions because different $CH_4$ sources have distinct isotopic compositions (Sherwood et al., 2017; Whalen et al., 1989). $\delta^{13}C$ denotes the ratio of $^{13}C$ relative to $^{12}C$ compared to the PDB standard and reported in parts per thousand. The $\delta^{13}C$ of $CH_4$ depends strongly on how $CH_4$ is produced: by microbial activity (-61.7 ± 6.2 ‰), by the thermal breakdown of organic molecules (-44.8 ± 10.7 ‰), and by incomplete combustion (-26.2 ± 15 ‰) (Sherwood et al., 2017). $\Delta^{14}C$ reports the ratio of $^{14}C$ relative to $^{12}C$ compared to a decay-corrected standard and normalized to a $\delta^{13}C$ of -25 ‰ to account for fractionation (Stuiver and Polach, 1977). Fossil fuels, including $CH_4$ in natural gas, as well as $CH_4$ produced from fossil fuel precursors lack $^{14}C$ and have a $\Delta^{14}C$ value of -1000 ‰. In contrast, $CH_4$ produced from other substrates has a $\Delta^{14}C$ signal close to the contemporary atmospheric $\Delta^{14}CO_2$ value (Whalen et al., 1989), which was approximately -5 ‰ in 2019 in the northern hemisphere, estimated to trends reported by Hammer and Levin (2017). $CH_4$ produced from contemporary substrates do not approximate the atmospheric $\Delta^{14}CH_4$ value (estimated to be 340 ‰ from the available data), which is determined by the ratio of modern biogenic to fossil methane emissions, as well as the $^{14}C$-enrichment due to global nuclear power plant $^{14}CH_4$ emissions (Lassey et al., 2007). The implication is that in the AOSR, $\delta^{13}C$ can be used to separate thermogenic $CH_4$ from surface mine emissions, and microbial $CH_4$ from tailings ponds, local wetlands, and landfill emissions, while $\Delta^{14}C$ can further separate the fossil microbial $CH_4$ from tailings ponds from the modern microbial $CH_4$ from landfills and wetlands.

Previous studies have shown that $\delta^{13}C$ can be successfully used for regional $CH_4$ source attribution in urban, natural, and fossil fuel industrial settings (Eisma et al., 1994; Lowry et al., 2001; Fisher et al., 2011; Townsend-Small et al., 2012; Lopez et al., 2017; Maazallahi et al., 2020), and current instruments allow for relatively cheap and precise $\delta^{13}C$ determinations in small atmospheric samples using gas-source mass spectrometers or cavity ringdown spectrometers. Conversely, $\Delta^{14}C$ measurements have been successful in $CO_2$ source attribution (Lopez et al., 2013; Zimnoch et al., 2012; Turnbull et al., 2015; Miller et al., 2020), but less successful in $CH_4$ source attribution (Eisma et al., 1994; Townsend-Small et al., 2012). Additionally, $\Delta^{14}C$ measurements are rarely used as analyzing $^{14}C$ requires larger samples than $^{13}C$ analysis, a more demanding extraction of methane from air, and more expensive measurements using accelerator mass spectrometry. Furthermore, $\Delta^{14}C$ regional source attribution can become complicated in places such as continental Europe where there is a large influence of nuclear power plants with poorly constrained $^{14}CH_4$ emissions (Eisma et al., 1994). Improvements in the atmospheric methane collection and processing are currently being developed, which could increase the use of $^{14}CH_4$ measurements in the near future (Zazzeri et al., 2021), and at the same time there have been improvements in constraining the influence of nuclear power in $\Delta^{14}CH_4$ measurements (Graven et al., 2019).

In this study, our main goal is to test the use of combined $\Delta^{14}C$ and $\delta^{13}C$ measurements in ambient $CH_4$ to estimate contributions from the largest $CH_4$ sources in the AOSR region including wetlands, surface mines, and tailings ponds. We expect to provide a new and practical proof-of-concept method for the long-term monitoring of key $CH_4$ emissions in regions with multiple $CH_4$ sources like the AOSR, which is crucial to developing effective $CH_4$ mitigation policies and, in the specific case study, to fulfill Canada’s goal of reducing $CH_4$ emissions from the oil and gas sector by 40–45 % below 2012 levels by 2025 (Government of Canada, 2016).

## 5.4. Methods

### 5.4.1. Sampling campaign

The sampling campaign took place between 16 and 23 August 2019 at the Environment Canada atmospheric monitoring site Fort McKay South (FMS), adjacent to the Wood Buffalo Environmental Association Air Monitoring Station 13 (AMS13). The monitoring station is located in the AOSR (57°08'57.54" N, 111°38'32.66" W), surrounded to the east and west by boreal forest and wetland complexes and to the north and south by oil sands mining and processing facilities (Figure 5.1). Air pollution levels at the site depend on the wind direction, and the principal wind directions in Fort McKay are northerly and southerly (Bari and Kindzierski, 2015).

To the north, facilities include the Canadian Natural Resources Limited (CNRL) Horizon Processing Plant and Mine, and Muskeg River and Jackpine Mines; the Fort Hills Oil Sands Mine; Syncrude Aurora North Mine Site; and the Imperial Oil Kearl Processing Plant and Mine (Government of Canada, 2017). $CH_4$ emissions from CNRL Horizon facilities, Muskeg River and Jackpine Mines, and the Syncrude Aurora North Mine have been primarily attributed to open pit mining ($5200 \pm 1200$ kg $h^{-1}$), but significant $CH_4$ emissions originating from the CNRL Horizon main plant facility ($1000 \pm 300$ kg $h^{-1}$) have also been detected (Baray et al., 2018). To the south, the main facilities are Syncrude Canada Mildred Lake and Suncor Energy Inc. Oil Sands (Government of Canada, 2017). $CH_4$ emissions from these two facilities have been mainly attributed to tailings ponds ($8800 \pm 1100$ kg $h^{-1}$) followed by open mining ($4600 \pm 600$ kg $h^{-1}$) (Baray et al., 2018).

We collected air samples in 70 L cylinder tanks by filling the tank for around 10 min to a pressure of 13.8 MPa using a Bauer PE-100 compressor with a magnesium perchlorate water trap.

We aimed to sample $CH_4$ peaks coming from different wind directions. Before the field campaign, the new Bauer PE-100 compressor was tested at the ECCC laboratories and compared to an existing oil-free RIX compressor system, used to fill reference gases ('laboratory standards') for ECCC. The difference in methane dry air mole fraction in the cylinders when using the Bauer PE-100 and RIX compressor was found to be within 10 ppb when consecutively filling tanks using ambient air. During the sampling campaign, we flushed the cylinders two times by filling the tank with air until it reached 13.8 MPa and subsequently purging the air by opening the tank valve before collecting the air sample.

We performed continuous measurements of methane ($CH_4$), carbon dioxide ($CO_2$), and carbon monoxide (CO) dry air mole fractions for the whole sampling campaign using a Picarro G2401 gas analyzer, which has a five-minute average precision of 1.5 ppb for CO, 20 ppb for $CO_2$, and 0.5 ppb for $CH_4$. Results were reported as 1-hour averages of the dry air mole fractions. The intake lines of all the instruments were attached at the rooftop of the air monitoring station, approximately 3 meters above ground level (m.a.g.l.).

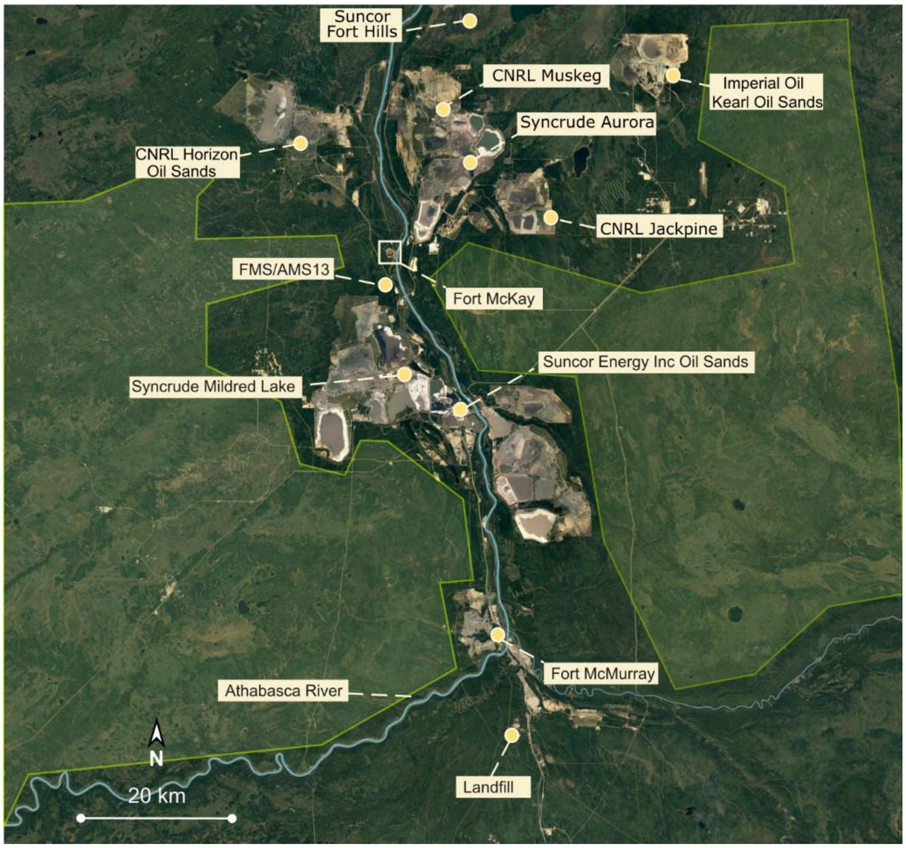

**Figure 5.1. Satellite view of the Athabasca oil sands region (satellite image: Google Landsat/Copernicus).** The map shows the location of oil sands mining and processing facilities and the FMS/AMS13 site from which samples described in this paper were collected (57◦08′57.54″ N, 111◦38′32.66″ W). The light green polygons show the approximate area of the forest–wetland complexes in the region (based on data from Golder Associates Ltd., 2002).

### 5.4.2. $CH_4$ isotopic analyses

Methane was extracted from the gas samples at the National Institute of Water and Atmospheric Research (NIWA) in Wellington, New Zealand, following the methods described in Lowe et al. (1991), with updates as described in the following. In summary, a mass flow controller set at 1 L min$^{-1}$ was connected to the tanks. Air was drawn from the tanks using a 170 L min$^{-1}$

rotary pump and pumped through two cryogenic traps to remove $CO_2$, $H_2O$, $N_2O$, and other specific hydrocarbons. Each of these cryogenic traps is made of four 350 mm long loops passing in and out of liquid nitrogen. The loops are made of 12mm ID Pyrex tubing and are kept at pressures lower than 10 kPa. After these first two traps, the sample passed through a third trap containing a *Sofnocat* reagent (containing platinum and palladium on a tin oxide support) which acts as a catalyst in the conversion of CO to $CO_2$. This $CO_2$ was subsequently removed using two additional cryogenic traps. Next, $CH_4$ was combusted at 750 °C to $CO_2$ and $H_2O$ using an alumina-supported platinum catalyst. The resulting $CO_2$ was collected and purified in three additional cryogenic traps. Last, $H_2O$ was removed using alcohol dry ice traps at -80 °C and $CO_2$ was vacuum distilled into glass vials or break seals for mass spectrometry. Separate extractions were carried out for each $^{13}C$ and $^{14}C$ analysis, processing 26 L of air for $^{13}C$ and 230–290 L for $^{14}C$ (depending on $CH_4$ content of the sample).

Analysis of $^{13}C$ was performed on a Thermo MAT-253 isotope ratio mass spectrometer (IRMS) in dual inlet mode. Samples were analyzed against a pure $CO_2$ working reference gas derived from a $^{13}C$ depleted barium carbonate standard (NZCH). The standard deviation for a $\delta^{13}C$ determination is 0.02 ‰. The results were reported relative to PDB-$CO_2$. For $^{14}C$ analysis, the methane-derived $CO_2$ was reduced to graphite using $H_2$ and an iron catalyst at 550 °C (Turnbull et al., 2015a) and measured for $^{14}C$ content by accelerator mass spectrometry (Zondervan et al., 2015). The results were reported as fraction modern carbon and $\Delta^{14}C$ age corrected to date of sample collection following internationally agreed conventions (Stuiver and Polach, 1977, Donahue et al., 1990, Reimer et al., 2004). The measurement precision for this dataset is 2.2 to 2.6 ‰ in $\Delta^{14}C$.

### 5.4.3. Back-trajectory modelling using HYSPLIT-5

We generated hourly 12-hour backward trajectories for the duration of the sampling campaign using HYSPLIT-5. HYSPLIT is a model for computing atmospheric transport and dispersion of air masses developed by NOAA's Air Resources Laboratory, and a more complete description of the system can be found in Stein et al. (2015). In this model, a back-trajectory is calculated from a particle that represents a gas being moved by the mean wind field. To calculate the concentration of the trace gas (air concentrations), a number of particles are released from the receptor and dispersion equations are applied to the upwind trajectory calculation. Then, the mass of the computed particles is added and divided by the volume of their horizontal and vertical distribution. We configured the model to start 3 m above ground level from the location of the FMS site and to use meteorological parameters from the NAM 12 km (hybrid sigma pressure US 2010-Present) database.

### 5.4.4. Estimating source contributions using keeling plots

The Keeling plot approach is based on the conservation of mass in the lower planetary boundary layer (Keeling, 1958, 1961). It assumes that the atmospheric $CH_4$ is the result of a simple mixing between two components, background $CH_4$ and the sum of all $CH_4$ sources, and that the isotope ratio of the two components does not change substantially over time, as in this study. As a result, the intercept of a linear regression between 1/ [$CH_4$] and $\delta^{13}CH_4$ or $\Delta^{14}CH_4$ from atmospheric samples is interpreted as the mean isotopic signature of the $CH_4$ sources (Equations. 3 and 4). Here, we calculated the slope and intercept of the linear regression and their uncertainties after York et al. (2004).

$$\Delta^{14}C_{air} = \frac{C_{background}(\Delta^{14}C_{background} - \Delta^{14}C_{source})}{C_{air}} + \Delta^{14}C_{source} \quad \textbf{Equation 3}$$

$$\delta^{13}C_{air} = \frac{C_{background}(\delta^{13}C_{background} - \delta^{13}C_{source})}{C_{air}} + \delta^{13}C_{source} \quad \textbf{Equation 4}$$

Because the source isotopic signature represents the weighted sum of all the $CH_4$ sources, a mixing model can be used to determine the individual $CH_4$ source contributions from the mean $CH_4$ source isotopic signature if the individual source isotope signatures are known. We used MixSIAR, a Bayesian isotope mixing model framework implemented as an open-source R package (see Stock et al., 2018), to estimate the contribution of potential $CH_4$ sources to the 'mixture mean' (mean source signature in air samples). The base of the MixSIAR framework is a mixing model in which the tracer value of the mixture (e.g., $\delta^{13}C$) is the sum of the mean tracer value of each source component multiplied by its proportional contribution to the mixture (*p*) as in Equation 5. The assumptions for this model are that all the sources are known, tracers are conserved through the mixing process, tracer values do not vary over time, the tracer values differ between sources, and that the sum of the proportional contributions (*p*) is 1 (Stock et al. 2018).

$$\delta^{13}C^{mixture} = \sum_k \delta^{13}C_k^{source} p_k \quad \textbf{Equation 5}$$

To account for source uncertainty, MixSIAR incorporates error structures using the summary statistics of the source isotopic values (mean, variance, and sample size) and source parameters are fitted as in Ward et al. (2010). The mixing system can then be solved analytically for multiple tracers simultaneously if the number of sources does not exceed the number of tracers plus one. In this case, we used two tracers, $\delta^{13}C$ and $\Delta^{14}C$, and three sources. The source isotopic values used in the mixing model were derived from the literature and are described in the following section.

## 5.5. Results and discussion

### 5.5.1. Isotopic signature of $CH_4$ sources in the AOSR

To estimate the proportion of $CH_4$ emitted from different potential sources, the isotopic signatures of these potential sources must be known. However, specifying the $\delta^{13}CH_4$ from these sources can be especially challenging because $\delta^{13}CH_4$ signatures can have wide ranges and vary locally (Sherwood et al., 2017), and there are no studies isotopically characterizing $CH_4$ from different sources in the AOSR. Based on the previous aircraft source attribution study (Baray et al., 2018), we identified two main $CH_4$ source categories: $CH_4$ emissions related to the mining and processing of bitumen (e.g., leaking and venting), and tailings ponds $CH_4$ emissions. Furthermore, we added wetlands as a third source of regional $CH_4$ emissions as they are estimated to cover approximately 60% of the Athabasca Oil Sands Region (Rooney et al., 2012) and the wetland $CH_4$ emissions in the province of Alberta have been estimated to be roughly half of the total anthropogenic emissions (Baray et al., 2021).

Thermogenic $CH_4$ associated with Alberta's Lower cretaceous oils varies between -42 and -48‰ (Jha, Gray and Strausz, 1979; Tilley et al., 2007), but the prevalence of anaerobic biodegradation in shallow subsurface petroleum reservoirs changes the $\delta^{13}CH_4$ composition of heavily degraded oils to between -45 to -55 ‰, in particular by hydrogenotrophic $CH_4$ production (Head, Jones, Larter, 2003; Jones et al., 2008). This biogenically over-printed thermogenic $CH_4$ is present in the mined material of the AOSR, which is potentially released when oil sands are mined, but also during transport, ore preparation, and extraction of bitumen (Johnson et al., 2016). Thus, we used this $\delta^{13}C$ range to represent $CH_4$ emissions derived from the bitumen mining and processing (Table 5.1).

Residual water generated from the surface mining process is stored in tailings ponds where aerobic and anaerobic degradation are mainly fueled by certain naphtha components in the diluents, in specific short-chain n-alkanes ($C_6$ to $C_{10}$), BTEX compounds (i.e., toluene and xylenes), and long-chain n-alkanes ($C_{14}$ to $C_{18}$) (Siddique et al., 2006, 2007, 2011, 2012). Radiocarbon measurements of tailings ponds components, including total organic carbon (TOC), total lipid extract (TLE), and phospholipid fatty acids (PLFAs) have yielded $\Delta^{14}C$ signatures of approximately -995 ‰ (Ahad and Pakdel, 2013). We infer that $CH_4$ is most likely produced from these substrates and therefore has the same $\Delta^{14}C$ signature (Table 5.1). The chemical composition of the tailings ponds – determined by mineralogy of the oil sands, extraction techniques and additives used, and age of the ponds– influences the microbial communities involved in the substrate degradation (Small et al., 2015), which are likely dominated by syntrophic communities as well as both acetoclastic methanogens, previously associated to short n-alkane degradation, and hydrogenotrophic methanogens, associated to the metabolism of long-chain alkanes and BTEX (Penner and Fought, 2010; Shahimin et al., 2016; Siddique et al., 2012; Zhou et al., 2012). Measurements of the dissolved $\delta^{13}CH_4$ from the hypolimnion of Base Mine Lake, a dimictic end pit lake, range between -60 and -65 ‰ and to our knowledge are the only available $\delta^{13}CH_4$ measurements associated to oil sands lakes (Goad 2017). However, variations in the microbial community composition between ponds results in variations in the rate of $CH_4$ production (Small et al., 2015), and might also result in differences in the $\delta^{13}CH_4$ due to different fractionation in acetoclastic and hydrogenotrophic methanogenesis (Whiticar 1999; Whiticar, Faber, and Schoell, 1986). Moreover, the Base Mine Lake $\delta^{13}CH_4$ value should be regarded as a minimum, because methanotrophic communities are active in the surface of the tailings ponds, most likely shifting the $\delta^{13}CH_4$ towards more positive values during partial oxidation of methane before emission to the atmosphere (Saidi-Mehrabad et al., 2013).

Boreal wetland $CH_4$ emissions are estimated to have a mean $\delta^{13}C$ value -67.8 ‰, based on atmospheric measurements (Ganesan et al., 2018). In terms of $\Delta^{14}C$, wetland $CH_4$ emissions are most likely predominantly modern and close to the atmospheric $\Delta^{14}CO_2$ value, even in wetlands associated to permafrost collapse (Cooper et al., 2017; Estop-Aragonés et al., 2020). Because the residence time of carbon released as $CH_4$ in wetlands is likely decadal (Whalen et al., 1989; Chanton et al., 1995), we used a $\Delta^{14}C$ signature ranging from approximately 40 ‰, corresponding to the atmospheric $\Delta^{14}CO_2$ value in the Northern Hemisphere in 2010 (Hammer and Levin, 2017) to approximately -10 ‰, which is the lower limit when using that same dataset to extrapolate for the atmospheric $\Delta^{14}CO_2$ value in 2019 (Table 5.1).

Additional $CH_4$ potential regional sources that were not included in this analysis to avoid having an undetermined mixing model were forest fires and landfills, both of which would emit $CH_4$ with a modern $\Delta^{14}CO_2$ signature. Three major wildfire events occurred in 2019 in Alberta: the Battle complex (Peace River area), Chuckegg Creek wildfire (High Level area), and the McMillan complex (Slave Lake area). The three events started in May and were declared under control the 26 June, 1 July, and the 18 August, respectively (MNP LLP 2020), with the third event briefly overlapping with some of the sampling dates (16 to 18 of August). However, the event was

290 km Southwest of the sampling site, while the air in the sampling site originated from the Northwest (see section 3.2), and therefore it is unlikely that this was a significant source of $CH_4$ in the air samples. In the case of the landfill, some back trajectories show air masses coming from the general Fort McMurray direction, where the municipal landfill is (Figure 5.1). We speculated that between these two sources, wetlands are the most prominent $CH_4$ source because at a provincial level (Alberta), $CH_4$ wetland emissions are estimated to be 2.5 to $3.5 * 10^9$ kg $a^{-1}$ while solid waste disposal accounts for $5.2 * 10^4$ kg $a^{-1}$ (Baray et al., 2021; Environment Climate Change Canada, 2018). If we were to add a landfill component, assuming a $\delta^{13}C$ value of -55 ‰ for landfills (Lopez et al., 2017), the revised estimation would result in a slightly larger contribution of microbial fossil $CH_4$ relative to thermogenic $CH_4$. For example, if 10% of the microbial modern emissions were derived from landfills and 90% from wetlands, our model estimate of the contribution from tailings ponds increases by 2%.

**Table 5.1. Estimated values of $\delta^{13}CH_4$ and $\Delta^{14}CH_4$ for the three source categories used in the source attribution.**

| Source Category | Potential Sources | Estimated $\delta^{13}C$ | Estimated $\Delta^{14}C$ |
|---|---|---|---|
| Thermogenic Fossil | Surface mining, extraction and upgrade, venting, leaking | -45 to -55 ‰[a] | -1000 ‰ |
| Microbial Fossil | Tailings ponds | -60 to -65 ‰[b] | -995 to -1000 ‰[d] |
| Microbial Modern | Canadian boreal wetlands | - 65 to -68 ‰[c] | -10 to 40 ‰[e] |

(a) $\delta^{13}CH_4$ associated to heavily degraded oils from Head et al. (2003)

(b) Hypolimnetic $\delta^{13}CH_4$ values from Base Mine Lake from Goad (2017)

(c) Canadian boreal wetlands $\delta^{13}CH_4$ from Ganesan et al. (2018)

(d) Tailing pond substrate signature from Ahad and Pakdel (2013)

(e) Range of atmospheric $\Delta^{14}CO_2$ values from 2010 to 2019 extrapolated from Hammer and Levin (2017)

### 5.5.2. Isotopic signature of ambient $CH_4$

Analyses of the 12-hour back trajectories for the 7-day sampling campaign showed that air masses arriving at the FMS station during this time period primarily originated from two general directions (Figure 5.2b): from the northwest between 16 to 19 August, and from the southwest and southeast between 20 to 23 August. The $CH_4$ mole fraction time series for this time period indicated that most $CH_4$ enrichments were associated to trajectories originating from the west and south, in particular from air masses that transit over the Syncrude Mildred Lake facilities and CNRL Horizon oil sands facilities (Figure 5.2).

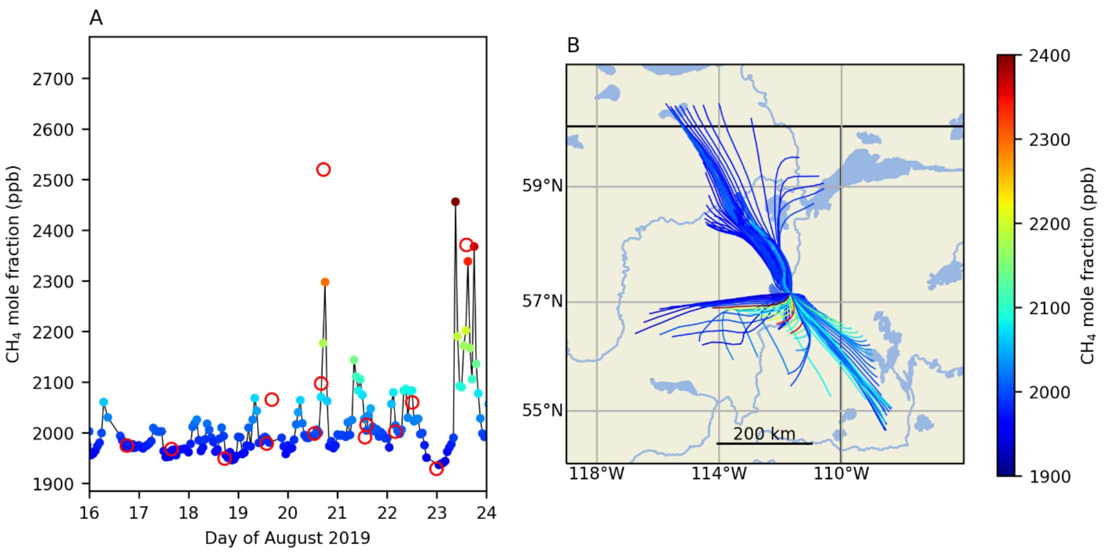

**Figure 5.2. HYSPLIT back trajectories for the duration of sampling campaign.** a) Hourly $CH_4$ dry air mole fraction measurements at the FMS13 station (Fort McKay South), with the $CH_4$ mole fraction of the collected air samples in red circles. b) HYSPLIT 12 h back-trajectories associated with hourly measurements, with the colour scale representing $CH_4$ dry air mole fractions in both panels.

The $CH_4$ mole fraction [$CH_4$], $\delta^{13}CH_4$, and $\Delta^{14}CH_4$ of the air samples are shown in Table 5.2. There were significant correlations between 1/[$CH_4$] and $\Delta^{14}CH_4$ ($r^2$ = 0.99; black lines in Figure 5.3a), between 1/[$CH_4$] and $\delta^{13}CH_4$ ($r^2$ = 0.84; black lines in Figure 5.3b), and between $\Delta^{14}CH_4$ and $\delta^{13}CH_4$ ($r^2$ = 0.8; black lines in Figure 5.3c) in the air samples associated to back-trajectories originating from the South and Southwest, corresponding to 20 to 23 August. The intercept of the $\Delta^{14}C$ Keeling plot for these samples showed a source signature of -898 ± 9 ‰ (Figure 5.3a), while the intercept of the $\delta^{13}C$ Keeling plot yielded a source value of -56 ± 0.8 ‰ (Figure 5.3b).

There were also significant correlations between all variables in the samples associated to back-trajectories originating from the north, corresponding to 16 to 19 August (red lines in Figure 5.3). However, there were only five data points, and four of them had very similar values which could artificially strengthen the correlation. When building the $\Delta^{14}C$ and a $\delta^{13}CH_4$ Keeling plot with these five samples, the intercepts yielded source values of $\Delta^{14}C \approx$ -1000 ‰ and $\delta^{13}C$ = -35.1 ± 4.5 ‰, which points to a thermogenic source of $CH_4$ originating in the northern mines.

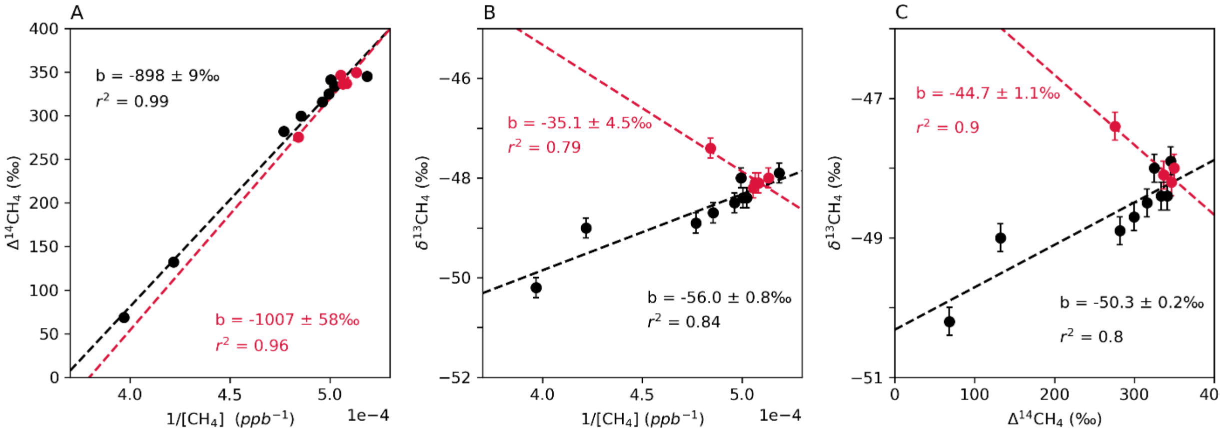

**Figure 5.3. Keeling plots of atmospheric samples.** Keeling plots of a) $CH_4$ and $\Delta^{14}CH_4$, b) $CH_4$ and $\delta^{13}CH_4$, and c) plot of $\delta^{13}CH_4$ and $\Delta^{14}CH_4$ in air samples collected from 20 to 23 August (south) in black (n = 9) and from 16 to 20 August (north) in red (n = 5). In a) and b), the intercept of the Keeling plot b indicates the isotopic signature of the $CH_4$ source. In panel c), the intercept b is interpreted as the $\delta^{13}C$ value of fossil $CH_4$.

**Table 5.2 Methane mole fraction, $\delta^{13}CH_4$, and $\Delta^{14}CH_4$ of air samples collected in the Athabasca Oil Sands Region in August 2019.** Note that local time of sampling (Mountain Time, MDT) is six hours behind UTC universal time.

| Sample | Date and time (UTC) | $[CH_4]$ (ppb) | $\delta^{13}CH_4$ (‰) | $\Delta^{14}CH_4$ (‰) | Wind direction |
|---|---|---|---|---|---|
| 1 | 16/08/2019 18:14 | 1974.5 ± 1.3 | -48.1 ± 0.02 | 336.4 ± 2.6 | N |
| 2 | 17/08/2019 15:46 | 1967.5 ± 0.7 | -48.1 ± 0.02 | 337.0 ± 2.6 | N |
| 3 | 18/08/2019 17:28 | 1948.8 ± 0.6 | -48.0 ± 0.02 | 349.8 ± 2.6 | N |
| 4 | 19/08/2019 13:46 | 1978.4 ± 1.3 | -48.2 ± 0.02 | 346.4 ± 2.6 | N |
| 5 | 19/08/2019 16:16 | 2065.3 ± 1 | -47.4 ± 0.02 | 275.7 ± 2.5 | N |
| 6 | 20/08/2019 12:50 | 1998.2 ± 1.3 | -48.4 ± 0.02 | 341.2 ± 2.6 | SE |
| 7 | 20/08/2019 16:05 | 2097.1 ± 1.3 | -48.9 ± 0.02 | 281.9 ± 2.5 | SE |
| 8 | 20/08/2019 17:14 | 2520.0 ± 1.2 | -50.2 ± 0.02 | 68.5 ± 2.2 | SE |
| 9 | 21/08/2019 13:17 | 1990.9 ± 1.6 | -48.4 ± 0.02 | 333.7 ± 2.6 | S/SE |
| 10 | 21/08/2019 14:00 | 2015.2 ± 0.5 | -48.5 ± 0.02 | 315.8 ± 2.6 | S/SE |
| 11 | 21/08/2019 3:55 | 2002.0 ± 1 | -48.0 ± 0.02 | 325.1 ± 2.6 | S/SE |
| 12 | 22/08/2019 12:04 | 2059.7 ± 0.7 | -48.7 ± 0.02 | 299.5 ± 2.6 | S |
| 13 | 22/08/2019 23:49 | 1928.6 ± 0.5 | -47.9 ± 0.02 | 345.4 ± 2.6 | W |
| 14 | 23/08/2019 14:19 | 2370.9 ± 1.6 | -49.0 ± 0.02 | 132.3 ± 2.4 | S |

### 5.5.3. Source contributions

The approximate contributions from each source category to samples associated with back-trajectories originating from the south were calculated with MixSIAR and are shown in Figure 5.4. The microbial and thermogenic fossil enrichment observed in the $CH_4$ air samples (~90 %), indicate that most of the $CH_4$ enrichment observed at the site was influenced by $CH_4$ emissions from the oil sands mines and processing facilities. Specifically, the contribution from thermogenic

$CH_4$ was estimated to be 56 ± 18 % while the contribution from fossil microbial $CH_4$ from tailings ponds contribution was estimated to 34 ± 18 %, with a large uncertainty associated with both estimates (Figure 5.4b). The results also indicate an influence of approximately 10 ± < 1% from microbial modern sources (Figure 5.4b), most likely from wetlands. If most of the microbial modern enrichment is derived from wetlands, it is likely that the contribution from this source is near the annual maximum, as $CH_4$ wetland emissions typically peak in the summer (Baray et al., 2021).

Analyses of the back-trajectories indicated that the air masses from which these sample were collected originated from the south, and therefore the samples are likely predominantly influenced by the Syncrude and Suncor facilities and tailings ponds (Figure 5.1). This would explain the substantial enrichment of fossil microbial $CH_4$ in our samples, as measurements of $CH_4$ emissions have shown that the largest $CH_4$ emitting tailings management areas are Syncrude's Mildred Lake Settling Basin and the Base Mine Lake (Small et al., 2015; You et al., 2021). In comparison to the oil sands facilities in the south (Syncrude Mildred Lake and Suncor), the facilities to the North of the air monitoring site have been shown to have much larger $CH_4$ contributions from surface mining and natural gas leaking and venting (Baray et al., 2018), as tailings ponds emissions are minimal (below 0.1 kg $m^{-2}$ $a^{-1}$) (Small et al., 2015). This was reflected in the few air samples originating from the north that show a $\delta^{13}CH_4$ of -35 ‰ and a $\Delta^{14}CH_4$ of -1000 ‰, which is consistent with the isotopic signature of thermogenic $CH_4$ (Figure 5.3b).

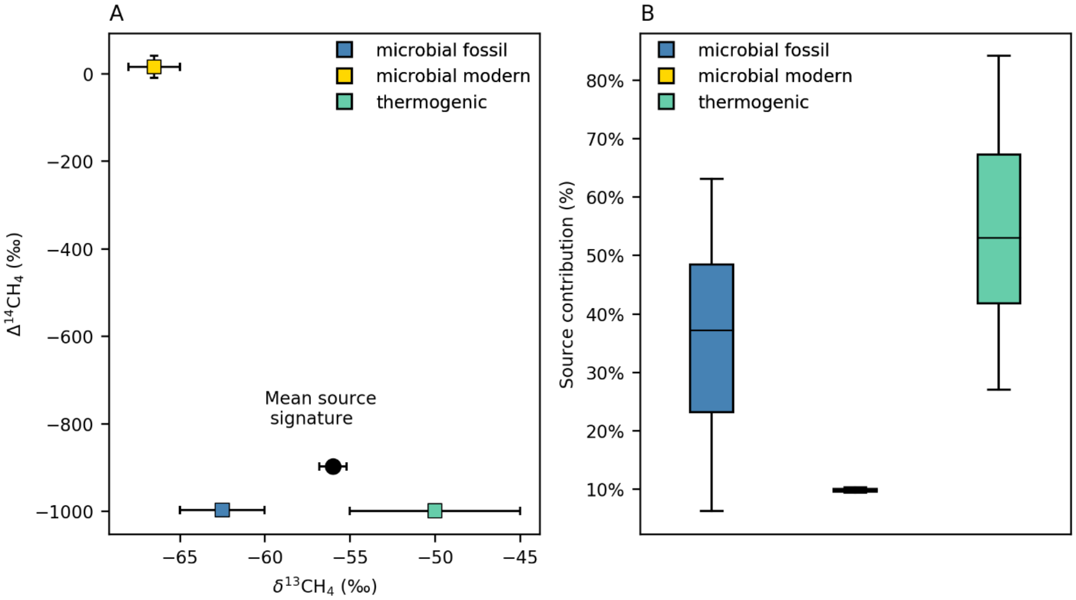

**Figure 5.4. Source contributions estimations from the southern samples.** a) $\delta^{13}C$ and $\Delta^{14}C$ signatures of potential $CH_4$ sources used to estimate source contribution using MixSIAR and mean $\delta^{13}CH4$ and $\Delta^{14}CH_4$ source signatures of the samples associated with south trajectories derived from Keeling plots. b) Boxplot of the estimated source contributions from microbial fossil $CH_4$ (tailings ponds), thermogenic $CH_4$ (surface mines and processing facilities), and microbial modern $CH_4$ (wetlands) for these samples. The line inside the boxes represents the median, boxes indicate the 25th and 75th percentiles, and whiskers show the 5th and 95th percentiles.

Compared to the only previous $CH_4$ source attribution study available (Baray et al., 2018), our results implied a lower contribution from tailings ponds and a larger contribution from surface mines and processing facilities. Baray et al. (2018) estimated that 65 % of $CH_4$ emissions from the Syncrude Mildred Lake and Suncor mines and facilities originated from tailings ponds and 34 % from surface mines, but there have not been studies updating these estimates since this study was performed in summer 2013. We suggest that differences between studies can be attributed to changes in bitumen production in the different sites from 2013 and from the large uncertainties in our estimates. The uncertainty in our estimates is mainly due to the uncertainty in the $\delta^{13}CH_4$ signatures of $CH_4$ sources. For example, a change of 5 ‰ towards more positive values in the tailings ponds $\delta^{13}CH_4$ signature due to microbial oxidation of $CH_4$ in the epilimnion, would increase the calculated contribution from tailings ponds to 52 ± 23 % and decrease the thermogenic contribution to 38 ± 23 %. This example illustrates the need to reduce the uncertainty in the source isotopic signatures with an extensive $\delta^{13}C$ characterization of $CH_4$ sources in the AOSR, in particular from tailings ponds and surface mines. Furthermore, the use of additional tracers such as methane/ethane ($C_2H_6/CH_4$) ratios and $\delta^2H$ in $CH_4$ could help constraining emissions from source categories since biogenic and thermogenic processes yield distinctive $CH_4/C_2H_6$ ratios and $\delta^2H$ in $CH_4$ (Townsend-Small et al., 2016; Lopez et al., 2017; Douglas et al., 2021).

While an exhaustive $\delta^{13}C$ characterization of $CH_4$ sources is needed to improve source estimates using carbon isotopes, the clear correlations in our air samples show that this method is useful for estimating $CH_4$ source contributions in regions with multiple $CH_4$ sources like the AOSR. Moreover, the collection of air in cylinders is less costly and easier to do on a regular basis compared to techniques such as aircraft measurements and therefore is well suited for monitoring how source emissions change with time (seasonally and annually). The use of an instrument for continuous $\delta^{13}CH_4$ measurement such as a Picarro G2201-I Isotope Analyzer could make this process even easier and more evenly distributed through the year.

## 5.6. Summary and conclusions

We conducted a sampling campaign in the Athabasca Oil Sands Region in summer 2019 with the objective of evaluating the potential of using combined $\Delta^{14}C$ and $\delta^{13}C$ measurements in ambient $CH_4$ for source attribution. While tracers such as $\delta^{13}C$, $\delta D$, and $C_2H_6/CH_4$ can separate thermogenic from microbially produced $CH_4$, the use of $\Delta^{14}C$ indicates if $CH_4$ is produced from a fossil source regardless of the pathway of $CH_4$ formation. We demonstrated the use combined $\Delta^{14}C$ and $\delta^{13}C$ measurements for separating emissions from three sources: mines and processing facilities, tailings ponds, and regional wetlands. Our results confirm the importance of tailings ponds in regional $CH_4$ emissions (Baray et al., 2018), which we estimated to be approximately 34 % of all the emissions in the region. Furthermore, the addition of $\Delta^{14}C$ in the measurements allowed us to separate wetland $CH_4$ emissions, which are a major provincial source of $CH_4$ (Baray et al., 2021) and therefore have the potential to interfere in the accuracy of top down $CH_4$ estimates. In general, this method showed to be a suitable tool for $CH_4$ source attribution in the AOSR and potentially other oil producing regions as there are clear correlations between between $\delta^{13}C$ and $\Delta^{14}C$, isotopic measurements are cheap relative to other approaches such as aircraft measurements, and the instrumentation set-up allows for continuous year-round measurements.

Although this study is one of the first to provide a conclusive source attribution using combined $\Delta^{14}C$ and $\delta^{13}C$ measurements in ambient $CH_4$, there are still large uncertainties associated with this method, mainly due to the lack of $\delta^{13}C$ data from key $CH_4$ sources. These uncertainties can be addressed with a characterization of $\delta^{13}C$ and $\Delta^{14}C$ in the main $CH_4$ sources and using additional tracers such as methane-ethane ratios and $\delta^{2}H$ signatures. Moreover, future work should focus in adding measurements at different times of the year and in consecutive years, as seasonal and annual variations in $CH_4$ emissions are currently not well constrained. At a seasonal scale, temperature changes in the winter probable reduce microbial methanogenesis, decreasing tailings ponds and wetlands emissions, and snow cover in open mining areas could affect $CH_4$ emissions. At an annual scale, changes in mine and processing facilities operations, the development of in-situ mining over surface mining, and changes in the age-dependent tailings pond emission profile could also result in $CH_4$ emission variations. Consequently, implementing isotopic measurements for long term $CH_4$ emission monitoring is essential to have a complete understanding of $CH_4$ emissions in the AOSR and for developing effective mitigation policies.

## 5.7. Acknowledgements and financial support.

We thank Lauriant Giroux for the compressor testing and support in the field. We thank Tony Bromley, Sally Gray, Rowena Moss, and Ross Martin for sample processing and GC and IRMS analyses. We thank the Rafter Radiocarbon Lab team for $^{14}C$ analyses and Ralf Staebler and Doug Worthy for the ECCC internal review of the manuscript. This project was supported by the Trottier Institute for Science and Public Policy and by NIWA funding under the Climate and Atmosphere Research Programme CAAC2104 (2021/21 SCI).

## 5.8. References

Ahad, J. M. E. and Pakdel, H.: Direct evaluation of in situ biodegradation in Athabasca oil sands tailings ponds using natural abundance radiocarbon, Environ. Sci. Technol., 47, 10214–10222, https://doi.org/10.1021/es402302z, 2013.

Alberta Energy Regulator: ST98-2015: Alberta's Energy Reserves 2014 and Supply/Demand, Alberta Energy Regulator, available at: https://static.aer.ca/prd/documents/sts/ST98/ST98-2015.pdf (last access: 19 January 2022), 2015.

Baray, S., Darlington, A., Gordon, M., Hayden, K. L., Leithead, A., Li, S.-M., Liu, P. S. K., Mittermeier, R. L., Moussa, S. G., O'Brien, J., Staebler, R., Wolde, M., Worthy, D., and McLaren, R.: Quantification of methane sources in the Athabasca Oil Sands Region of Alberta by aircraft mass balance, Atmos. Chem. Phys., 18, 7361–7378, https://doi.org/10.5194/acp-18-7361-2018, 2018.

Baray, S., Jacob, D. J., Maasakkers, J. D., Sheng, J.-X., Sulprizio, M. P., Jones, D. B. A., Bloom, A. A., and McLaren, R.: Estimating 2010–2015 anthropogenic and natural methane emissions in Canada using ECCC surface and GOSAT satellite observations, Atmos. Chem. Phys., 21, 18101–18121, https://doi.org/10.5194/acp-21-18101-2021, 2021.

Bari, M. and Kindzierski, W. B.: Fifteen-year trends in criteria air pollutants in oil sands communities of Alberta, Canada, Environ. Int., 74, 200–208, https://doi.org/10.1016/J.ENVINT.2014.10.009, 2015.

Bergerson, J. A., Kofoworola, O., Charpentier, A. D., Sleep, S., and MacLean, H. L.: Life Cycle Greenhouse Gas Emissions of Current Oil Sands Technologies: Surface Mining and In Situ Applications, Environ. Sci. Technol., 46, 7865–7874, https://doi.org/10.1021/ES300718H, 2012.

Chanton, J. P., Bauer, J. E., Glaser, P. A., Siegel, D. I., Kelley, C. A., Tyler, S. C., Romanowicz, E. H., and Lazrus, A.: Radiocarbon evidence for the substrates supporting methane formation within northern Minnesota peatlands, Geochim. Cosmochim. Ac., 59, 3663–3668, 1995.

Cooper, M. D. A., Estop-Aragonés, C., Fisher, J. P., Thierry, A., Garnett, M. H., Charman, D. J., Murton, J. B., Phoenix, G. K., Treharne, R., Kokelj, S. V., Wolfe, S. A., Lewkowicz, A. G., Williams, M., and Hartley, I. P.: Limited contribution of permafrost carbon to methane release from thawing peatlands, Nat. Clim. Change, 7, 507–511, https://doi.org/10.1038/nclimate3328, 2017.

Donahue, D. J., Linick, T. W., and Jull, A. J. T.: Isotope-Ratio and Background Corrections for Accelerator Mass Spectrometry Radiocarbon Measurements, Radiocarbon, 32, 135–142, https://doi.org/10.1017/S0033822200040121, 1990.

Douglas, P. M. J., Stratigopoulos, E., Park, S., and Phan, D.: Geographic variability in freshwater methane hydrogen isotope ratios and its implications for global isotopic source signatures, Biogeosciences, 18, 3505–3527, https://doi.org/10.5194/bg-18-3505-2021, 2021.

Eisma, R., van der Borg, K., de Jong, A. F. M., Kieskamp, W. M., and Veltkamp, A. C.: Measurements of the $^{14}$C content of atmospheric methane in The Netherlands to determine the regional emissions of $^{14}CH_4$, Nucl. Instrum. Meth. B, 92, 410–412, https://doi.org/10.1016/0168-583X(94)96044-5, 1994.

Estop-Aragonés, C., Olefeldt, D., Abbott, B. W., Chanton, J. P., Czimczik, C. I., Dean, J. F., Egan, J. E., Gandois, L., Garnett, M. H., Hartley, I. P., Hoyt, A., Lupascu, M., Natali, S. M., O'Donnell, J. A., Raymond, P. A., Tanentzap, A. J., Tank, S. E., Schuur, E. A. G., Turetsky, M., and Anthony, K. W.: Assessing the Potential for Mobilization of Old Soil Carbon After

Permafrost Thaw: A Synthesis of $^{14}$C Measurements From the Northern Permafrost Region, Global Biogeochem. Cy., 34, 1–26, https://doi.org/10.1029/2020GB006672, 2020.

Etminan, M., Myhre, G., Highwood, E. J., and Shine, K. P.: Radiative forcing of carbon dioxide, methane, and nitrous oxide: A significant revision of the methane radiative forcing, Geophys. Res. Lett., 43, 12614–12623, https://doi.org/10.1002/2016GL071930, 2016.

Fisher, R. E., Sriskantharajah, S., Lowry, D., Lanoisellé, M., Fowler, C. M. R., James, R. H., Hermansen, O., Myhre, C. L., Stohl, A., Greinert, J., Nisbet-Jones, P. B. R., Mienert, J., and Nisbet, E. G.: Arctic methane sources: Isotopic evidence for atmospheric inputs, Geophys. Res. Lett., 38, L2180, https://doi.org/10.1029/2011GL049319, 2011.

Ganesan, A. L., Stell, A. C., Gedney, N., Comyn-Platt, E., Hayman, G., Rigby, M., Poulter, B., and Hornibrook, E. R. C.: Spatially Resolved Isotopic Source Signatures of Wetland Methane Emissions, Geophys. Res. Lett., 45, 3737–3745, https://doi.org/10.1002/2018GL077536, 2018.

Goad, C.: Methane biogeochemical cycling over seasonal and annual scales in an oil sands tailings end pit lake, MS thesis, McMaster University, McSphere Institutional Repository, available at: http://hdl.handle.net/11375/21956 (last access: January 2022), 2017.

Golder Associates Ltd.: Terrestrial vegetation and wetlands resources environmental setting report for the Suncor voyageur south project, 50–55, Sect. 3.1, Golder associates Ltd., available at: https://open.alberta.ca/dataset/ea88e773-42b6-4d92-ba28-40aa636996c7/resource/e11c9cdb-293a-4776-af7d-3d609db70aba/download/vegetation.pdf (last access: 19 January 2022), 2002.

Gonzalez Moguel, R., Douglas, P., Vogel, F., Ars, S., Schaefer, H., and Turnbull, J.: Fort McKay South $CH_4$ and $CO_2$ mole fractions August 2019, figshare [data set], https://doi.org/10.6084/m9.figshare.17217542.v1, 2021.

Government of Canada: Pan-Canadian Framework on clean Growth and Climate Change, Government of Canada, available at: http://publications.gc.ca/collections/collection_2017/eccc/En4-294-2016-eng.pdf (last access: 19 January 2022), 2016.

Government of Canada: National pollutant Release Inventory's (NPIR) Sector Overview Series, Government of Canada, available at: https://maps.canada.ca/journal/content-en.html?lang= en&appid=703d9327d99d445eb4c1e94a47c1933e&appidalt=6df630d9067240059ccc7cb33a68e188 (last access: May 2021), 2017.

Government of Canada: National Inventory Report 1990–2015: Greenhouse Gas Sources and Sinks in Canada, Canada's Submission to the United Nations Framework Convention on Climate Change, Part 1. Environment and Climate Change Canada, available at: http://publications.gc.ca/collections/collection_2020/eccc/En81-4-2018-1-eng.pdf (last access: 19 January 2022), 2018.

Graven, H., Hocking, T., and Zazzeri, G.: Detection of fossil and biogenic methane at regional scales using atmospheric radiocarbon, Earths Future, 7, 283–299 https://doi.org/10.1029/2018EF001064, 2019.

Hammer, S. and Levin, I.: Monthly mean atmospheric $D^{14}CO_2$ at Jungfraujoch and Schauinsland from 1986 to 2016, V2, heiDATA [data set], https://doi.org/10.11588/data/10100, 2017.

Head, I., Jones, D., and Larter, S.: Biological activity in the deep subsurface and the origin of heavy oil, Nature, 426, 344–352, https://doi.org/10.1038/nature02134, 2003.

Holly, C., Mader, M., Soni S., and Toor, J.: Alberta Energy: Oil sands production profile 2004-2014, Government of Alberta, available at: https://open.alberta.ca/dataset/cd892173-c37f-4c68-bf5d-f79ef7d49e72/resource/ebd6b451-dfda-4218-b855-1416d94306fd/download/initiativeospp.pdf (last access: January 2022), 2016.

Jackson, R. B., Saunois, M., Bousquet, P., Canadell, J. G., Poulter, B., Stavert, A. R., Bergamaschi, P., Niwa, Y., Segers, A., and Tsuruta, A.: Increasing anthropogenic methane emissions arise equally from agricultural and fossil fuel sources, Environ. Res. Lett., 15, 071002, https://doi.org/10.1088/1748-9326/ab9ed2, 2020.

Jha, K. N., Gray, J., and Strausz, O. P.: The isotopic composition of carbon in the Alberta oil sand, Geochim. Cosmochim. Ac., 43, 1571–1573, https://doi.org/10.1016/0016-7037(79)90150-9, 1979.

Johnson, M. R., Crosland, B. M., McEwen, J. D., Hager, D. B., Armitage, J. R., Karimi-Golpayegani, M., and Picard, D. J.: Estimating fugitive methane emissions from oil sands mining using extractive core samples, Atmos. Environ., 144, 111–123, https://doi.org/10.1016/J.ATMOSENV.2016.08.073, 2016.

Jones, D. M., Head, I. M., Gray, N. D., Adams, J. J., Rowan, A. K., Aitken, C. M., Bennett, B., Huang, H., Brown, A., Bowler, B. F. J., Oldenburg, T., Erdmann, M., and Larter, S. R.: Crude-oil biodegradation via methanogenesis in subsurface petroleum reservoirs, Nature, 451, 176–180, https://doi.org/10.1038/nature06484, 2008.

Keeling, C. D.: The concentration and isotopic abundances of atmospheric carbon dioxide in rural areas, Geochim. Cosmochim. Ac., 13, 322–334, https://doi.org/10.1016/0016-7037(58)90033-4, 1958.

Keeling, C. D.: The concentration and isotopic abundance of carbon dioxide in rural and marine air, Geochim. Cosmochim. Acta, 24, 277–298, 1961.

Larter, S. R. and Head, I. M.: Oil sands and heavy oil: Origin and exploitation, Elements, 10, 277–283, https://doi.org/10.2113/gselements.10.4.277, 2014.

Lassey, K. R., Lowe, D. C., and Smith, A. M.: The atmospheric cycling of radiomethane and the “fossil fraction” of the methane source, Atmos. Chem. Phys., 7, 2141–2149, https://doi.org/10.5194/acp-7-2141-2007, 2007.

Liggio, J., Li, S.-M., Staebler, R. M., Hayden, K., Darlington, A., Mittermeier, R. L., O'Brien, J., McLaren, R., Wolde, M., Worthy, D., and Vogel, F.: Measured Canadian oil sands $CO_2$ emissions are higher than estimates made using internationally recommended methods, Nat. Commun., 101, 1–9, https://doi.org/10.1038/s41467-019-09714-9, 2019.

Lopez, M., Schmidt, M., Delmotte, M., Colomb, A., Gros, V., Janssen, C., Lehman, S. J., Mondelain, D., Perrussel, O., Ramonet, M., Xueref-Remy, I., and Bousquet, P.: CO, $NO_x$ and $^{13}CO_2$ as tracers for fossil fuel $CO_2$: results from a pilot study in Paris during winter 2010, Atmos. Chem. Phys., 13, 7343–7358, https://doi.org/10.5194/acp-13-7343-2013, 2013.

Lopez, M., Sherwood, O. A., Dlugokencky, E. J., Kessler, R., Giroux, L., and Worthy, D. E. J.: Isotopic signatures of anthropogenic $CH_4$ sources in Alberta, Canada, Atmos. Environ., 164, 280–288, https://doi.org/10.1016/j.atmosenv.2017.06.021, 2017.

Lowe, D. C., Brenninkmeijer, C. A. M., Tyler, S. C., and Dlugkencky, E. J.: Determination of the isotopic composition of atmospheric methane and its application in the Antarctic, J. Geophys. Res.-Atmos., 96, 15455–15467, https://doi.org/10.1029/91JD01119, 1991.

Lowry, D., Holmes, C. W., Rata, N. D., O'Brien, P., and Nisbet, E. G.: London methane emissions: Use of diurnal changes in concentration and $\delta^{13}C$ to identify urban sources and verify inventories, J. Geophys. Res.-Atmos., 106, 7427–7448, https://doi.org/10.1029/2000JD900601, 2001.

Maazallahi, H., Fernandez, J. M., Menoud, M., Zavala-Araiza, D., Weller, Z. D., Schwietzke, S., von Fischer, J. C., Denier van der Gon, H., and Röckmann, T.: Methane mapping, emission quantification, and attribution in two European cities: Utrecht (NL) and Hamburg (DE), Atmos. Chem. Phys., 20, 14717–14740, https://doi.org/10.5194/acp-20-14717-2020, 2020.

Miller, J. B., Lehman, S. J., Verhulst, K. R., Miller, C. E., Duren, R. M., Yadav, V., Newman, S., and Sloop, C. D.: Large and seasonally varying biospheric $CO_2$ fluxes in the Los Angeles megacity revealed by atmospheric radiocarbon, P. Natl. Acad. Sci. USA, 117, 26681–26687, https://doi.org/10.1073/pnas.2005253117, 2020.

Myhre, G., Shindell, D., Bréon, F.-M., Collins, W., Fuglestvedt, J., Huang, J., Koch, D., Lamarque, J.-F., Lee, D., Mendoza, B., Nakajima, T., Robock, A., Stephens, G., Takemura, T., and Zhang, H.: 2013: Anthropogenic and Natural Radiative Forcing, in: Climate Change 2013:

The Physical Science Basis. Contribution of Working Group I to the Fifth Assessment Report of the Intergovernmental Panel on Climate Change, vol. 9781107057, edited by: Stocker, T. F., Qin, D., Plattner, Q.-K., Tignor, M. M. B., Allen, S. K., Boschung, J., Nauels, A., Xia, Y., Bex, V., and Midgley, P. M., Cambridge University Press, 659–740, https://doi.org/10.1017/CBO9781107415324.018, 2013.

MNP LLP: Spring 2019 Wildfire review, Government of Alberta, available at: https://wildfire.alberta.ca/resources/reviews/documents/af-spring-2019-wildfire-review-final-report.pdf (last access: 19 January 2022), 2020.

Mossop, G. D.: Geology of the Athabasca Oil Sands, Science, 207, 145–152, https://doi.org/10.1126/SCIENCE.207.4427.145, 1980.

Ocko, I. B., Sun, T., Shindell, D., Oppenheimer, M., Hristov, A. N., Pacala, S. W., Mauzerall, D. L., Xu, Y., and Hamburg, S. P.: Acting rapidly to deploy readily available methane mitigation measures by sector can immediately slow global warming, Environ. Res. Lett., 16, 054042, https://doi.org/10.1088/1748-9326/ABF9C8, 2021.

Penner, T. J. and Foght, J. M.: Mature fine tailings from oil sands processing harbour diverse methanogenic communities, Can. J. Microbiol., 56, 459–470, https://doi.org/10.1139/W10-029, 2010.

Reimer, P. J., Brown, T. A., and Reimer, R. W.: Discussion: Reporting and Calibration of Post-Bomb $^{14}C$ Data, Radiocarbon, 46, 1299–1304, https://doi.org/10.1017/S0033822200033154, 2004.

Rooney, R. C., Bayley, S. E., and Schindler, D. W.: Oil sands mining and reclamation cause massive loss of peatland and stored carbon, P. Natl. Acad. Sci. USA, 109, 4933–4937, 2012.

Rubino, M., Etheridge, D. M., Thornton, D. P., Howden, R., Allison, C. E., Francey, R. J., Langenfelds, R. L., Steele, L. P., Trudinger, C. M., Spencer, D. A., Curran, M. A. J., van Ommen, T. D., and Smith, A. M.: Revised records of atmospheric trace gases $CO_2$ , $CH_4$, $N_2O$, and $\delta^{13}C\text{-}CO_2$ over the last 2000 years from Law Dome, Antarctica, Earth Syst. Sci. Data, 11, 473–492, https://doi.org/10.5194/essd-11-473-2019, 2019.

Saidi-Mehrabad, A., He, Z., Tamas, I., Sharp, C. E., Brady, A. L., Rochman, F. F., Bodrossy, L., Abell, G. C., Penner, T., Dong, X., Sensen, C. W., and Dunfield, P. F.: Methanotrophic bacteria in oilsands tailings ponds of northern Alberta, ISME J., 75, 908–921, https://doi.org/10.1038/ismej.2012.163, 2013.

Saunois, M., Stavert, A. R., Poulter, B., Bousquet, P., Canadell, J. G., Jackson, R. B., Raymond, P. A., Dlugokencky, E. J., Houweling, S., Patra, P. K., Ciais, P., Arora, V. K., Bastviken, D., Bergamaschi, P., Blake, D. R., Brailsford, G., Bruhwiler, L., Carlson, K. M., Carrol, M., Castaldi, S., Chandra, N., Crevoisier, C., Crill, P. M., Covey, K., Curry, C. L., Etiope, G., Frankenberg, C., Gedney, N., Hegglin, M. I., Höglund-Isaksson, L., Hugelius, G., Ishizawa, M., Ito, A., Janssens-Maenhout, G., Jensen, K. M., Joos, F., Kleinen, T., Krummel, P. B., Langenfelds, R. L., Laruelle, G. G., Liu, L., Machida, T., Maksyutov, S., McDonald, K. C., McNorton, J., Miller, P. A., Melton, J. R., Morino, I., Mëller, J., Murguia-Flores, F., Naik, V., Niwa, Y., Noce, S., O'Doherty, S., Parker, R. J., Peng, C., Peng, S., Peters, G. P., Prigent, C., Prinn, R., Ramonet, M., Regnier, P., Riley, W. J., Rosentreter, J. A., Segers, A., Simpson, I. J., Shi, H., Smith, S. J., Steele, L. P., Thornton, B. F., Tian, H., Tohjima, Y., Tubiello, F. N., Tsuruta, A., Viovy, N., Voulgarakis, A., Weber, T. S., van Weele, M., van der Werf, G. R., Weiss, R. F., Worthy, D., Wunch, D., Yin, Y., Yoshida, Y., Zhang, W., Zhang, Z., Zhao, Y., Zheng, B., Zhu, Q., Zhu, Q., and Zhuang, Q.: The Global Methane Budget 2000–2017, Earth Syst. Sci. Data, 12, 1561–1623, https://doi.org/10.5194/essd-12-1561-2020, 2020.

Shahimin, M. F. M., Foght, J. M., and Siddique, T.: Preferential methanogenic biodegradation of short-chain n-alkanes by microbial communities from two different oil sands tailings ponds, Sci. Total Environ., 553, 250–257, https://doi.org/10.1016/j.scitotenv.2016.02.061, 2016.

Sherwood, O. A., Schwietzke, S., Arling, V. A., and Etiope, G.: Global Inventory of Gas Geochemistry Data from Fossil Fuel, Microbial and Burning Sources, version 2017, Earth Syst. Sci. Data, 9, 639–656, https://doi.org/10.5194/essd-9-639-2017, 2017.

Siddique, T., Fedorak, P. M., and Foght, J. M.: Biodegradation of short-chain n-alkanes in oil sands tailings under methanogenic conditions, Environ. Sci. Technol., 40, 5459–5464, https://doi.org/10.1021/es060993m, 2006.

Siddique, T., Fedorak, P. M., Mackinnon, M. D., and Foght, J. M.: Metabolism of BTEX and naphtha compounds to methane in oil sands tailings, Environ. Sci. Technol., 41, 2350–2356, https://doi.org/10.1021/es062852q, 2007.

Siddique, T., Penner, T., Semple, K., and Foght, J. M.: Anaerobic Biodegradation of Longer-Chain n-Alkanes Coupled to Methane Production in Oil Sands Tailings, Environ. Sci. Technol., 45, 5892–5899, https://doi.org/10.1021/ES200649T, 2011.

Siddique, T., Penner, T., Klassen, J., Nesbø, C., and Foght, J. M.: Microbial communities involved in methane production from hydrocarbons in oil sands tailings, Environ. Sci. Technol., 46, 9802–9810, https://doi.org/10.1021/es302202c, 2012

Small, C. C., Cho, S., Hashisho, Z., and Ulrich, A. C.: Emissions from oil sands tailings ponds: Review of tailings pond parameters and emission estimates, J. Petrol. Sci. Eng., 127, 490–501, https://doi.org/10.1016/j.petrol.2014.11.020, 2015.

Stein, A. F., Draxler, R. R., Rolph, G. D., Stunder, B. J. B., Cohen, M. D., and Ngan, F.: NOAA's HYSPLIT Atmospheric Transport and Dispersion Modeling System, B. Am. Meteorol. Soc., 96, 2059–2077, https://doi.org/10.1175/BAMS-D-14-00110.1, 2015.

Stock, B. C., Jackson, A. L., Ward, E. J., Parnell, A. C., Phillips, D. L., and Semmens, B. X.: Analyzing mixing systems using a new generation of Bayesian tracer mixing models, PeerJ, 6, e5096, https://doi.org/10.7717/PEERJ.5096, 2018.

Stuiver, M. and Polach, H. A.: Discussion Reporting of $^{14}$C Data, Radiocarbon, 19, 355–363, https://doi.org/10.1017/S0033822200003672, 1977.

Takamura, K.: Microscopic structure of athabasca oil sand, Can. J. Chem. Eng., 60, 538–545, https://doi.org/10.1002/CJCE.5450600416, 1982.

Tilley, B. and Muehlenbachs, K.: Isotopically Determined Mannville Group Gas Families, in: CSPG/CSEG Convention 2007, 14–17 May 2007, Calgary, Alberta, Canada, 2007.

Townsend-Small, A., Tyler, S. C., Pataki, D. E., Xu, X., and Christensen, L. E.: Isotopic measurements of atmospheric methane in Los Angeles, California, USA: Influence of “fugitive” fossil fuel emissions, J. Geophys. Res.-Atmos., 117, 1–11, https://doi.org/10.1029/2011JD016826, 2012.

Townsend-Small, A., Botner, E. C., Jimenez, K. L., Schroeder, J. R., Blake, N. J., Meinardi, S., Blake, D. R., Sive, B. C., Bon, D., Crawford, J. H., Pfister, G., and Flocke, F. M.: Using stable isotopes of hydrogen to quantify biogenic and thermogenic atmospheric methane sources: A case study from the Colorado Front Range, Geophys. Res. Lett., 43, 11462–11471, https://doi.org/10.1002/2016GL071438, 2016.

Turnbull, J. C., Zondervan, A., Kaiser, J., Norris, M., Dahl, J., Baisden, T., and Lehman, S.: High-Precision Atmospheric $^{14}CO_2$ Measurement at the Rafter Radiocarbon Laboratory, Radiocarbon, 57, 377–388, https://doi.org/10.2458/AZU_RC.57.18390, 2015a.

Turnbull, J. C., Sweeney, C., Karion, A., Newberger, T., Lehman, S. J., Tans, P. P., Davis, K. J., Lauvaux, T., Miles, N. L., Richardson, S. J., Cambaliza, M. O., Shepson, P. B., Gurney, K., Patarasuk, R., and Razlivanov, I.: Toward quantification and source sector identification of fossil fuel $CO_2$ emissions from an urban area: Results from the INFLUX experiment, J. Geophys. Res.-Atmos., 120, 292–312, https://doi.org/10.1002/2014JD022555, 2015b.

Turner, A. J., Frankenberg, C., and Kort, E. A.: Interpreting contemporary trends in atmospheric methane, P. Natl. Acad. Sci. USA, 116, 2805–2813, https://doi.org/10.1073/PNAS.1814297116, 2019.

Ward, E. J., Semmens, B. X., and Schindler, D. E.: Including Source Uncertainty and Prior Information in the Analysis of Stable Isotope Mixing Models, Environ. Sci. Technol., 44, 4645–4650, https://doi.org/10.1021/ES100053V, 2010.

Whalen, M., Tanaka, N., Henry, R., Deck, B., Zeglen, J., Vogel, J. S., Southon, A., Shemesh, A., Fairbanks, R., and Broecker, W.: Carbon-14 in Methane Sources in Atmospheric Methane: The contribution from fossil carbon, Science, 245, 286–290, https://doi.org/10.1126/science.245.4915.286, 1989.

Whiticar, M. J.: Carbon and hydrogen isotope systematics of bacterial formation and oxidation of methane, Chem. Geol., 161, 291–314, https://doi.org/10.1016/S0009-2541(99)00092-3, 1999.

Whiticar, M. J., Faber, E., and Schoell, M.: Biogenic methane formation in marine and freshwater environments: $CO_2$ reduction vs. acetate fermentation—Isotope evidence, Geochim. Cosmochim. Acta, 50, 693–709, https://doi.org/10.1016/0016-7037(86)90346-7, 1986.

You, Y., Staebler, R. M., Moussa, S. G., Beck, J., and Mittermeier, R. L.: Methane emissions from an oil sands tailings pond: a quantitative comparison of fluxes derived by different methods, Atmos. Meas. Tech., 14, 1879–1892, https://doi.org/10.5194/amt-14-1879-2021, 2021.

York, D., Evensen, N. M., Lopez Martinez, M., and De Basabe Delgado, J.: Unified equations for the slope, intercept, and standard errors of the best straight line, Am. J. Phys., 72, 367–375, 2004.

Zazzeri, G., Xu, X., and Graven, H.: Efficient Sampling of Atmospheric Methane for Radiocarbon Analysis and Quantification of Fossil Methane, Environ. Sci. Technol., 55, 8541, https://doi.org/10.1021/ACS.EST.0C03300, 2021.

Zhou, L., Li, K. P., Mbadinga, S. M., Yang, S. Z., Gu, J. D., and Mu, B. Z.: Analyses of n-alkanes degrading community dynamics of a high-temperature methanogenic consortium enriched from production water of a petroleum reservoir by a combination of molecular techniques, Ecotoxicology, 21, 1680–1691, https://doi.org/10.1007/s10646-012-0949-5, 2012.

Zimnoch, M., Jelen, D., Galkowski, M., Kuc, T., Necki, J., Chmura, L., Gorczyca, Z., Jasek, A., and Rozanski, K.: Partitioning of atmospheric carbon dioxide over Central Europe: insights from combined measurements of $CO_2$ mixing ratios and their carbon isotope composition, Isot. Environ. Healt. S., 48, 421–433, https://doi.org/10.1080/10256016.2012.663368, 2012.

Zondervan, A., Hauser, T. M., Kaiser, J., Kitchen, R. L., Turnbull, J. C., and West, J. G.: XCAMS: The compact $^{14}C$ accelerator mass spectrometer extended for $^{10}Be$ and $^{26}Al$ at GNS Science, New Zealand, Nucl. Instrum. Meth. B, 361, 25–33, https://doi.org/10.1016/J.NIMB.2015.03.013, 2015.

## 6. Discussion

Some of the largest potentially vulnerable stores of soil carbon are currently found in permafrost soils and wetlands at high northern latitudes (Dean, et al., 2018). These regions have experienced a pronounced warming in the last century and are predicted to continue warming in the coming century (IPCC, 2013). Carbon isotopes can help us answer how these carbon stores will be processed in the environment by giving insight on the sources of key carbon fractions such as $CH_4$ (Trumbore, 2009). In this thesis I applied radiocarbon in $CH_4$, aided by the use of $^{13}C$, to elucidate the origin of $CH_4$ emissions in Canadian ecosystems through three different case studies, formatted as peer-reviewed manuscripts. In this section I discuss the main findings that ensued from each of the three manuscripts in the context of the specific application of radiocarbon, the current literature and its gaps, our main results and their significance, the limitations of our results, and future directions of research that stem from these limitations.

Radiocarbon measurements in organic carbon exported to lakes and rivers (i.e., as DOC and POC) can provide evidence of the destabilization of soil organic carbon (SOC) that has remained previously frozen for hundreds to thousands of years. Several studies have shown that old (i.e., pre-1950) DOC and POC are transferred to rivers from high-latitude soils whether by the warming of deeper soil layers and from erosion (Neff, et al., 2006; Wild, et al., 2019). However, few groups had examined the age of DOC or POC in thermokarst lakes at the time this thesis was written, despite the prevalence of these lakes in high-latitude landscapes (Dean, et al., 2018). While DOC and POC transfer SOC across high-latitude ecosystems, $CO_2$ and $CH_4$ can transfer SOC directly from the lake sediments to the atmosphere. As with DOC and POC, radiocarbon measurements in $CO_2$ and $CH_4$ provide evidence of the microbial metabolization of the destabilized permafrost SOC that is contained in aquatic systems. Previous work has established that thermokarst lakes are conduits for the emission of permafrost SOC deposits as $CH_4$ to the atmosphere mainly in the form of bubbles, but a recently growing body of literature has demonstrated that contributions from young carbon to diffused $CH_4$ emitted from these lakes are much more important than previously recognized (Elder, et al., 2018; Walter Anthony , et al., 2016; Estop-Aragonés, et al., 2020). Although the body of literature analyzing the radiocarbon content of the different types of $CH_4$ emissions has been growing in the recent past (Estop-Aragonés, et al., 2020), there is still a large geographic gap and the need to do studies that incorporate results from these carbon fractions simultaneously, so that a more direct comparison of pathways is made.

In the first manuscript, we generated a comprehensive dataset on the ages and therefore sources of $CH_4$ and $CO_2$ (in the form of DIC) in several lakes and rivers of Eastern Canada affected by permafrost thaw. We found that the age of $CH_4$ and $CO_2$ was heavily influenced by the soil type (peat soils or mineral soils) and emission pathway, but it remained relatively constant throughout the seasons. For instance, we observed that dissolved $CH_4$ tended towards modern ages while ebullition $CH_4$ was generally sourced by old carbon pools. We provided information on the age of DOC and POC and found that POC contained a larger proportion of older carbon pools than DOC in most cases, and we found that POC and DOC ages varied between soil types and season. With these results, we generated one of the most complete radiocarbon datasets for lakes and rivers in Eastern Canada, covering the key carbon fractions involved in the cycling of carbon in aquatic systems, different $CH_4$ transport mechanisms, and different seasons. We filled an important gap in the literature as at the time this thesis was written, most studies were concentrated in few sites in

Alaska and Eastern Siberia, focused on one $CH_4$ emission pathway (i.e., ebullition or diffusion), or sampled during the growing season only (Estop-Aragonés, et al., 2020).

There were some limitations in the study design that will affect how we can extrapolate the results explained in the previous paragraph. The first issue was that because we focused on obtaining a large number of measurements in every lake, the sampling was reduced to a small number of lakes and even a smaller number of rivers. This means that the results of this study cannot necessarily be taken as representative of thermokarst lakes of Eastern Canada or even of the region, since lakes in the region encompass different types of lake while our sampling was mostly focused on peatland lakes. Moreover, the sampled lakes are all located in a sporadic permafrost region, even though Eastern Canada contains a broad range of permafrost environments, from regions covered by continuous permafrost to permafrost free regions. Similarly, we focused in obtaining data from many carbon fractions, which meant that our sampling was reduced to a representative water sample located in the center of the lake around one and a half meter below the surface. Realistically, this is not necessarily representative of the whole lake since there are vertical and horizontal spatial differences within the lakes, for example, the biogeochemical conditions and structure of the organic matter vary above and below the oxycline.

There are several directions for research future that stem from this research. First of all, sampling other representative types of lakes such as non-peatland thermokarst lakes could allow to build a more complete picture of the transport and emission of permafrost SOC through lakes in Eastern Canada. Similarly, sampling in the same type of lakes but in areas of discontinuous or continuous permafrost would help determine the effect of permafrost cover in SOC mineralization. Currently, there are few studies directly comparing the ages of carbon fractions from the same type of thermokarst lake but in regions of different permafrost coverage (Matveev, Laurion, Deshpande, Bhiry, & Vincent, 2016; Matveev, Laurion, & Vincent, 2018). Second, studies of the carbon pool age in peatland lakes would greatly benefit from adding measurements from the surrounding bog, as a significant part of the organic matter in the lake can originate in in the bog, because $CO_2$ and $CH_4$ could be transported laterally from the bog, and because carbon dynamics in the peatland lakes is strongly influenced by the carbon dynamics in the surrounding peatland.

Field measurements provide a real-time picture of how carbon pools are being processed in the environment at the moment of sampling but do not inform on how these carbon pools will be processed in the future. In other words, we need to know how the mineralization of the different carbon pools respond to climate parameters such as temperature in order to build projections of future permafrost loss and climate feedback. One way to achieve this goal is to incubate lake sediments in the laboratory and manipulate the parameters that are expected to respond to climate change, then measure the effect of the target parameter in $CH_4$ production or $CH_4$ consumption. The advantage of this method is that it is possible to change one parameter at a time while keeping others constant reducing the effects of confounding variables. However, measuring rates of production $CH_4$ by itself does not necessarily inform from what carbon pool the microbial communities are producing this $CH_4$. Because radiocarbon measurements in $CH_4$ can provide information on the carbon pool that microbes are metabolizing, we can add radiocarbon measurements to the $CH_4$ produced in laboratory incubation experiments to assess how permafrost or other carbon pools will be processed under increased temperatures, simulating global warming.

Previous experimental work has shown that $CH_4$ production rates are strongly dependent on temperature, and that the magnitude of the change in $CH_4$ production is also regulated by other parameters such as substrate availability (Treat, et al., 2015; Heslop, et al., 2015). The production rates of anaerobic $CH_4$ have been extensively explored for permafrost soils (Treat, et al., 2015), but much less is known about $CH_4$ production rates of lakes in permafrost regions (Heslop, et al., 2015). Where data of $CH_4$ production rates at different temperatures in lakes is scarce, there is a lack of studies evaluating the radiocarbon ages of $CH_4$ produced from lake sediments at different temperatures. The few radiocarbon datasets that are available have measured radiocarbon of incubation $CO_2$ produced from permafrost soil respiration (Vaughn & Torn, 2019). In this previous study, the age of respiration $CO_2$ increases (becomes older) at increased temperatures.

In our second manuscript, we produced one of the firsts datasets to analyze together $CH_4$ production rates along with the $\Delta^{14}C$ values of the produced $CH_4$ in thermokarst lake sediments at different temperatures. The data included $CH_4$ production rates and $\Delta^{14}C$ values of six different thermokarst lakes at three different temperatures, including the lakes analyzed in Chapter 3. Our results showed that the production rates of $CH_4$ increased significantly with warming and were influenced by the landscape position of the site, as the sediment had varying C:N ratios and therefore varying organic matter quality. We observed that the $\Delta^{14}C$ values of $CH_4$ responded to temperature, increasing at higher temperatures. The $\Delta^{14}C$ values were also influenced by the production rate of $CH_4$, with older carbon appearing to be transformed to $CH_4$ more slowly.

Despite increasing our understanding on how different carbon pools will be processed in the near future as global temperatures increase, there were several limitations in our dataset and experimental set up. Our main limitation was the incubation set up. We observed drastically different responses between experiments, mainly because the travel restrictions during the global COVID pandemic prevented us from collecting fresh sediment in the field so for the second incubation we ended up using the sediment that was used for the first incubation and was stored in the fridge for around one year. This most likely caused a depletion of labile substrates and a change in the composition of the microbial community that resulted in the presence of anaerobic oxidation of $CH_4$ in the second incubation. Inhibiting the activity of microbial communities that are capable of $CH_4$ oxidation in this case could potentially allow for better replicability of the experiments and more accurate $CH_4$ production rates, or simply using sediment that was recently collected. Other experimental limitations were that the duration of the different incubations varied, and that we used a different sampling method in the second field campaign that might have resulted in the samples from the third incubation to be exposed to oxygen. Specifically, I used Whirlpak bags instead of Nalgene bottles to collect the sediments in the second field campaign.

In terms of scope, we focused mainly in interpreting the data associated to the production of $CH_4$, because $CH_4$ has a greater warming potential compared to $CO_2$, even though the anerobic microbial decomposition of permafrost organic carbon results in the production of both $CO_2$ and $CH_4$ (Bethke, Sanford, Kirk , Jin , & Flynn, 2011). While we did analyze $CO_2$ and $\Delta^{14}C_{CO2}$ at the end of the experiments, we did not add $CO_2$ controls or measured $CO_2$ concentrations through the experiment, which limited our interpretation of these results. Moreover, $CH_4$ emissions from lakes depend not only in the production of $CH_4$ but also in the consumption of $CH_4$ (Zhu, et al., 2020). We only analyzed $CH_4$ production partly because the production of $CH_4$ has a greater sensitivity to temperature when compared to $CH_4$ oxidation, however analyzing more accurately these other components is crucial to understand how $CH_4$ emissions will respond to global warming.

Several directions for future work can stem from this research project. First, measuring the response of anaerobic $CO_2$ production rates more accurately along with $CH_4$ can provide a more complete picture of greenhouse gas emissions from lakes but also from this information it is possible to quantify the mineralization of organic carbon, as in Gudasz et al., (2010). Incorporating radiocarbon measurements in these two parameters, it might be even possible to calculate and make projections of the mineralization of permafrost organic carbon in lake sediments because radiocarbon can inform of the carbon pool that sources both gases. Second, since the composition of the microbial community proved to be highly sensitive to time elapse since collection, it might be worth to evaluate the response of $\Delta^{14}C_{CH4}$ to temperature in a shorter incubation experiment. For example, I suspect that ending the incubations around day 40, corresponding to the observed maximum $CH_4$ production rate, could produce enough $CH_4$ to yield informative results that reflect the microbial community in the field.

In the discussion of Chapter 4, we hypothesized that changes in the structure of the sediment microbial community could result in changes in the carbon pools utilized to produce $CH_{4,}$ but there are no current studies evaluating this hypothesis. A future study can, therefore, be designed to evaluate how the different community structures (e.g., a hydrogenotrophy dominant versus an acetotrophy dominant community) influence the use of carbon pools of different radiocarbon ages. A way to do this would be to supply a certain nutrient such as acetate or hydrogen in order to simulate the growth of methanogens associated to the different pathways, as in Blake, Tveit, Ovreas, Head and Gray (2015), and measure $CH_4$ production and $\Delta^{14}C_{CH4}$. Last, because $CH_4$ emissions from lakes depend not only in the production of $CH_4$ but also in the consumption of $CH_{4,}$ assessing how aerobic and anaerobic $CH_4$ oxidation will respond to temperature is crucial to understand how $CH_4$ emissions will respond to global warming.

Up to now, I have discussed how the studied lakes and rivers in Canadian ecosystems, especially in wetlands, respond to changes in environmental conditions induced by global warming and climate change. However, in addition to being vulnerable to changes in climate, Canadian ecosystems are also susceptible to disturbances from human activities. In wetlands, these disturbances include the building of roads and dams, peat extraction, development of agriculture, forestry, and mining (Volik, et al., 2020). Such is the case of the Athabasca Oil Sands Region (AOSR), in which the development of oil sands mines is expected to result in the loss of over 300 $km^2$ of peatlands (Rooney, Bayley, & Schindler, 2012). The recovery and processing of the shallow oil deposits in the AOSR is done through an energy intensive technique that requires crushing and mixing of the bitumen with diluents and storing the residues in tailings ponds (Larter & Head, 2014). Methane is directly emitted from some of these steps, especially the crushing of mine material and the microbial decomposition of tailings residuals, but also from gas leaks from facilities equipment (Baray , et al., 2018). Because these emissions constitute an important percentage of Canada's total greenhouse gas emissions, it is imperative to assess how the relative contributions from anthropogenic and natural $CH_4$ sources change in regions impacted by the development of mines.

Currently, the quantification of $CH_4$ emissions from the oil sands are done through each company's self-reporting to Environment and Climate Change Canada (ECCC) through the Greenhouse Gas Reporting Program (GHGRP), but there are not many sources of external monitoring that can verify the accuracy of these reports. The previous studies that have quantified the contribution of wetland versus anthropogenic $CH_4$ emissions at a provincial level have estimated that wetlands $CH_4$ emissions in Alberta are roughly half of the total anthropogenic emissions (Baray, et al., 2021). However, at the moment this thesis was written, there was a lack of studies assessing the contributions of anthropogenic and natural sources at a regional level. One of the few available studies had as goal to quantify anthropogenic emissions from the AOSR specifically but did not consider natural emissions in the region such as wetlands (Baray , et al., 2018). This study, conducted six years before our study, was the main reference we had to contextualize our results from the third manuscript.

Both $\Delta^{14}C$ and $\delta^{13}C$ measurements of atmospheric $CH_4$ can help partition natural and anthropogenic sources at region levels and therefore address the knowledge gaps mentioned in the previous paragraph, but the simultaneous use of these two isotopes for partitioning $CH_4$ sources in the atmosphere has not been widely applied (Townsend-Small, Tyler, Pataki, Xu, & Christensen , 2012). This is in part because applying the use of these two isotopes for source attribution is technically challenging requiring large amounts of air to the get accurate measurements but also because the presence of unquantified regional nuclear $CH_4$ fluxes can complicate the use of mixing models (Zazzeri, Xu, & Graven H., 2021; Graven , Hocking, & Zazzeri, 2019). In our study, we had two important advantages to overcome the challenges of using $\delta^{13}C$ and $\Delta^{14}C$ measurements in $CH_4$. In the first place, the $CH_4$ source endmembers in our site had distinct $\delta^{13}C$ and $\Delta^{14}C$ values due to their different formation processes and substrate ages: the $CH_4$ tailings ponds emissions are produced microbially from radiocarbon depleted substrates, while wetlands are microbially produced from contemporary substrates and emissions from mines are thermogenic. Secondly, $^{14}C$ emissions from nuclear reactors are limited in our study site because there are no nuclear reactors in the region, and even if there were, Canada uses pressurized heavy-water reactors that do not leak radio methane to the atmosphere.

Despite the exploratory character of Chapter 5, the results reported in this thesis indicated that the emissions from wetlands contributed only 10% of atmospheric $CH_4$, while anthropogenic emissions constituted the majority of regional $CH_4$ emissions. We were further able to determine, although with large uncertainties, that around 40% of the anthropogenic emissions were originating from the tailings ponds and the other 60% from other fossil fuel emissions such as the mines surfaces. These results do not only support previous characterizations of $CH_4$ emissions in the region (Baray , et al., 2018), but also provided the first estimate of the importance of wetland emissions in the AOSR. Furthermore, we showed that the simultaneous use of the two carbon isotopes is a feasible option for long term monitoring in the area and potentially other areas if the limitations in the study are addressed.

There were several important limitations in this study, partly because it was one of the first attempt to use this method for regional methane emissions source apportionment, but at the same time it also opened multiple avenues for future research. The first limitation was that there is a very limited set of $\delta^{13}C$ values for the $CH_4$ sources in the Athabasca, and in particular there are no measurements on the $\delta^{13}C$ and $\Delta^{14}C$ of the $CH_4$ that is produced in tailings ponds, but also from local wetlands and surface mines. Because of this, we used large ranges of endmember isotopic values for our mixing models and the results had really large uncertainties. Second, because atmospheric radiocarbon measurements are expensive and challenging, we collected and analyzed a total of fourteen samples. This decreases the accuracy of the results, and only covers a brief time window. For example, we determined that a few of our samples were originating from the northern mines, but the low sample size did not allow us to give a conclusive interpretation on the correlation and source $\delta^{13}C$ value. In addition to these limitations, there is a lack of data at different times of the year in our sampling and existing datasets, as we assessed the $CH_4$ sources in summer similarly to Baray, et al.  (2018), and there is also a need to couple this tool to data of $CH_4$ fluxes in the region in order to quantify $CH_4$ emissions from these key sources.

With this in mind, a logical first step in future research would be to isotopically characterize common sources of $CH_4$ in the Athabasca region to reduce the uncertainty in future source appointments in the region. Then, adding a larger number of samples or collecting samples from only one wind direction, and using additional tracers as ethane could strengthen the confidence in future research work. Additionally, sampling in winter would fill the gap on how the $CH_4$ source partitioning changes seasonally, as microbial activity is dependent on temperature and therefore both wetland and tailings pond emissions probably vary throughout the year. Last, monitoring total $CH_4$ fluxes in the region will allow to provide a quantitative estimation of $CH_4$ fluxes from each of the main $CH_4$ sources instead of just the proportional contribution. These avenues for future research are focused in expanding our knowledge on the Athabasca region, but there is also the potential for using this technique in other places and settings. For example, a previous study used isotopic measurements in $CO_2$ to calculate the contribution from urban biogenic sources in Los Angeles (Miller, et al., 2020). The same could be used to calculate contribution from urban biogenic sources of $CO_2$ and $CH_4$ in Canadian cities.

## 7. Concluding summary

The exploitation of the land and fossil resources during the Anthropocene has led to a rapid accumulation of $CH_4$ in the atmosphere that has contributed to changes in global climate. Natural ecosystems are expected to respond to these changes by either increasing or decreasing $CH_4$ emissions, but the mechanisms are complex and $CH_4$ feedbacks to climate change are not very well constrained. In this thesis, I explored the role of climate change in $CH_4$ emissions from two Canadian ecosystems using carbon isotopes to characterize the sources of $CH_4$ and processes in which it is produced. This goal was achieved through three case studies that were published or submitted as peer-revied manuscripts and form the chapters in this thesis.

In the first manuscript, my colleagues and I analyzed what carbon pools sourced DOC, DIC, POC, and $CH_4$ in thermokarst lakes and rivers of subarctic Quebec. We used radiocarbon to characterize the carbon fractions because “old” carbon is associated to permafrost soil. The results indicated that there was a reservoir of old organic carbon in the peatland lakes and the ebullition $CH_4$, but dissolved $CO_2$ and $CH_4$ in all lakes were disproportionally sourced by a contemporary source of carbon. We also found that the radiocarbon ages of all fractions varied with soil type, gas emission pathway, or season.

In the second manuscript, we tested how the rate of production of $CH_4$ and the use of different carbon pools to produce $CH_4$ would change under global warming. We answered this question by assembling incubation experiments at increasing temperatures and measuring $CH_4$ production rates and $\Delta^{14}C_{CH4}$. We showed that both the $CH_4$ production rate and $\Delta^{14}C_{CH4}$ increased with warming, that the reactivity of organic carbon is linked to the age of organic carbon substrate, and that landscape position might influence $CH_4$ production because the composition of organic substrates is different in the different sites of the permafrost thaw gradient.

These first two manuscripts added to the body of literature concerning $CH_4$ emissions from thermokarst lakes. Previous work had established that thermokarst lakes are conduits for permafrost soil carbon deposits to the atmosphere, but a more recent growing body of literature has demonstrated that contributions from contemporary carbon pools are much more significant than previously recognized. This has implications in assessing what impact the processing of carbon in thermokarst lakes will have in climate. This thesis supports this body of literature and demonstrates that while pre-1950 deposits are significantly contributing to $CH_4$ emissions, contemporary carbon is likely to have a predominant role in emissions from these ecosystems, even in scenarios of increased warming.

In the third manuscript, we examined if we could use $^{13}C$ and $^{14}C$ measurements to determine the proportional contributions of natural and anthropogenic $CH_4$ emissions in the Athabasca oil sands region in Alberta. We showed that around 90 % of emissions in the region stem from human activities related to the mining of bitumen deposits and determined that this method can potentially be used for long term monitoring of emissions if the uncertainties in source signatures can be lowered. These results have practical applications. First, it is feasible to couple the method to results of total $CH_4$ fluxes in the region to quantify $CH_4$ point emissions. These results can be particularly important for policy makers because they can be used to validate emission inventories and they can help identify mitigation targets. Moreover, while my research project focused on emissions from the Athabasca oil sands mining region, the results can still provide context for attribution studies in different settings.

## References

Baray , S., Darlington, A., Gordon, M., Hayden, K., Leithead, A., Li, S.-M., . . . McLaren, R. (2018). Quantification of methane sources in the Athabasca Oil Sands Region of Alberta by aircraft mass balance. *Atmospheric Chemistry and Physics, 18*, 7361-7378.

Baray, S., Jacob, D., Massakkers, J., Sheng, J.-X., Sulprizio, M., Jones, D., . . . McLaren, R. (2021). Estimating 2010-2015 Anthropogenic and Natural Methane Emissions in Canada using ECCC Surface and GOSAT Satellite Observations. *Atmospheric Chemistry and Physics*, 1-40. doi:https://doi.org/10.5194/ACP-2020-1195

Bastviken, D., Cole, J., Pace, M., & Tranvik, L. (2004). Methane emissions from lakes: Dependence on lake characteristics, two regional assessments, and a global estimate. *Global biogeochemical cycles, 18*.

Berg, A., Sheffield, J., & Milly, P. (2016). Divergent surface and total soil moisture projections under global warming. *Geophysical research letters, 44*(1), 236-244.

Bethke, C., Sanford, R., Kirk , M., Jin , Q., & Flynn, T. (2011). The thermodynamic ladder in geomicrobiology. *American Journal of Science, 311*, 183-210.

Blake, L., Tveit, A., Ovreas, L., Head, I., & Gray, N. (2015). Response of methanogens in Arctic sediments to temperature and methanogenic substrate availability. *PLOS one, 10*(6).

Bouchard, F., Laurion, I., Preskienis, V., Fortier, D., Xu, X., & Whiticar, M. (2015). Modern to millennium-old greenhouse gases emitted from ponds and lakes of the Eastern Canadian Arctic (Bylot Island, Nunavut). *Biogeosciences, 12*, 7279-7298.

Bowling, D., Pataki, D., & Randerson, J. (2008). Carbon isotopes in terrestrial ecosystem pools and CO2 fluxes. *New Phytologist*, *178*(1), 24-40.

Bridgham, S., Cadillo-Quiroz, H., Keller, J., & Zhuang, Q. (2013). Methane emissions from wetlands: biogeochemical, microbial, and modeling perspectives from local to global scales. *Global Change Biology, 19,* 1325-1346.

Chang, H., Xu, X., Fang, C., Li, B., & Nie, M. (2021). Differences in the temperature dependence of wetland CO2 and CH4 emissions vary with water table depth. *Nature Climate Change*(11), 766-771.

Chanton, J., Glaser P.H. , Chasar , L., Burdige, D., Hines, M., Siegel, D., . . . Cooper, W. (2008). Radiocarbon evidence for the importance of surface vegetation on fermentation and methanogenesis in contrasting types of boreal peatlands. *Global biogeochemical Cycles, 22*(4).

Christensen, T., Johansson, T., Akerman, H., & Mastepanov, M. (2004). Thawing sub-arctic permafrost: Effects of vegetation and methane emissions. *Geophysical Research Letters, 31*.

Conrad, R. (2005). Quantification of methanogenic pathways using stable carbon isotopic signatures: a review and a proposal. *Organic geochemistry, 36*, 739-752.

Conrad, R. (2020). Importance of hydrogenotrophic, aceticlastic and methylotrophic methanogenesis for methane production in terrestrial, aquatic and other anoxic environments: A mini review. *Pedosphere, 30*(1), 25-39.

Cook, B., Smerdon, J., Seager, R., & Coats, S. (2014). Global warming and 21st century drying. *Climate Dynamics, 43*(9), 2607-2627.

Dean, J., Middelburg, J., Rockmann, T., Aerts, R., Blauw, L., Egger, M., . . . Dolman, A. (2018). Methane feedbacks to the global climate system in a warmer world. *Reviews of geophysics, 56*, 207-250.

Dean, J., van der Velde, Y., Garnett, M., Dinsmore, K., Baxter, R., Lessels , J., . . . Billet, M. (2018). Abundant pre-industrial carbon detected in Canadian Arctic headwaters: implications for the permafrsot carbon feedback. *Environmental Research Letters, 13*(3), 034024.

Dlugokencky, E. (2021, December 23). *Trends in atmospheric methane*. Retrieved from NOAA/GML: https://gml.noaa.gov/ccgg/trends_ch4/

Eisma, R., Vermeulen, A., & Van der Borg, K. (1995). 14CH4 emissions from nuclear power plants in northwestern Europe. *Radiocarbon, 37*(2), 475-483.

Elder, C., Xu, X., Walker, J., Schnell, J., Hinkel, K., Townsend-Small, A., . . . Czimczik, C. (2018). Greenhouse gas emissions from diverse Arctic Alaskan lakes are dominated by young carbon. *Nature climate change, 8*, 166-171.

Estop-Aragonés, C., Olefeldt, D., Abbott, B., Chanton, J., Czimczik, C., Dean , J., . . . Walter Anthony, K. (2020). Assessing the potential for mobilization of old soil carbon after permafrost thaw: a synthesis of 14C measurements from the northern permafrost region. *Global biogeochemical cycles*(34).

Farquhar, G. (1989). Carbon Isotope Discrimination and Photosynthesis. *Annual review of plant physiology and plant molecular biology, 40*(1), 503-537.

Fletcher, S. M., & Schaefer, H. (2019). Rising methane: A new climate challenge. *Science, 364*(6444), 932-933.

Graven , H., Hocking, T., & Zazzeri, G. (2019). Detection of fossil and biogenic methane at regional scales using atmospheric radiocarbon. *Earth's future, 7*(3), 283-299.

Graven, H. (2015). Impact of fossil fuel emissions on atmospheric radiocarbon and various applications of radiocarbon over this century. *Proceedings of the national academy of sciences, 112*(31), 9542-9545.

Greene, S., Walter Anthony, K., Archer, D., Sepulveda-Jauregui, A., & Martinez Cruz, K. (2014). Modeling the impediment of methane ebullition bubbles by seasonal ice. *Biogeosciences, 11*, 6791-6811.

Gudasz, C., Bastviken, D., Steger, K., Premke, K., Sobek, S., & Tranvik, L. (2010). Temperature-controlled organic carbon mineralization in lake sediments. *Nature, 466*(7305), 478-481.

Hammer, S., & Levin, I. (2017). Monthly mean atmospheric D14CO2 at Jungfraujoch and Schauinsland from 1986 to 2016. *heiDATA [data set]*. doi:https://doi.org/10.11588/data/10100

Harmon, G. (1953). The geochemistry of the stable carbon isotopes. *Geochimica et cosmochimica acta, 3*(2-3), 53-92.

Harmon, G. (1954). Carbon 13 in plants and the relationships between carbon 13 and carbon 14 variations in nature. *The journal of geology, 62*(2), 115-149.

Head, I., Jones, M., & Larter, S. (2003). Biological activity in the deep subsurface and the origin of heavy oil. *Nature, 426*(6964), 344-352.

Heslop, J., Walter Anthony, K., Sepulveda Jauregui, A., Martinez Cruz, K., Bondurant, A., Grosse, G., & Jones, M. (2015). Thermokarst lake methanogenesis along a complete talik profil. *Biogeosciences, 12*(14), 4317-4331.

Heslop, J., Walter Anthony, K., Winkel, M., Sepulveda-Jauregui, A., Martinez-Cruz, K., Bondurant, A., . . . Liebner, S. (2020). A synthesis of methane dynamics in thermokarst lake environments. *Earth-Science Reviews, 210*.

Hmiel, B., Petrenki, V., Dyonisius, M., Buizert, C., Smith, A., Place, P., . . . Dlugokencky, E. (2020). Preindustrial 14CH4 indicates greater anthropogenic fossil CH4 emissions. *Nature, 578*, 409-412.

IPCC. (2013). Contribution of working group I to the fifth assessment report of the intergovernmental panel on climate change. In T. Stocker, D. Qin, G. Plattner, M. Tignor, S. Allen, J. Boschung, . . . P. Midgley (Eds.), *Climate Change 2013: The Physical Science Basis.* (p. 1535). Cambridge and New York: Cambridge University Press.

Kharbush, J., Close, H., Van Mooy, B., Arnosti, C., Smittenberg, R., Le Moigne, F., . . . Mohr, W. (2020). Particulate organic carbon deconstructed: molecular and chemical composition of particulate organic carbon in the ocean. *Frontiers in Marine Sciences*.

Kirschke, S., Bousquet, P., Ciais, P., Saunois, M., Canadell, J. G., Dlugokencky, E. J., . . . Zeng, G. (2013). Three decades of global methane sources and sinks. *Nature geosciences*, 813-823. doi:https://doi.org/10.1038/ngeo1955

Knittel, K., & Boetius, A. (2009). Anaerobic oxidation of methane: progress with an unknown process. *Annual Review of microbiology, 63*, 311-334.

Konhauser, K. (2007). *Introduction to geomicrobiology.* Oxford: Blackwell Science Ltd.

Kuhn, M., Varner, R., Bastviken, D., Crill, P., MacIntyre, S., Turetsky, M., . . . Olefeldt, D. (2021). BAWLD-CH4: a comprehensive dataset of methane fluxes from breal and arctic ecosystems. *Earth System Science Data*, *13*(1), 5151-5189.

Larter , S., & Head, I. (2014). Oil sands and heavy oil: origin and exploitation. *Elements, 10*(4), 277-283.

Lassey, K., Lowe, D., & Smith, A. (2007). The atmospheric cycling of radiomethane and the "fossil fraction" of the methane source. *Atmospheric chemistry and physics, 7*(1988), 2141-2149.

Le Mer , J., & Roger, P. (2001). Production, oxidation, emission and consumption of methane by soils: a review. *European Journal of Soil Biology, 37*(1), 25-50.

Lofton , D., Whalen, S., & Hershey, A. (2014). Effect of temperature on methane dynamics and evaluation of methane oxidation kinetics in shallow Arctic Alaskan lakes. *Hydrobiologia, 721*, 209-222.

Lopez, M., Sherwood, O., Dlugokencky, E., Kesler, R., Giroux, L., & Worthy, D. (2017). Isotopic signatures of anthropogenic CH4 sources in Alberta. *Atmospheric Environment*, 280-288.

Lowe, D., Brenninkmeijer, C., Manning, M., Sparks, R., & Wallace, G. (1998). Radiocarbon determination of atmospheric methane at Baring Head, New Zealand. *Nature, 332*, 522-525.

Lowry, D., Holmes, C., Rata , N., O Brien , P., & Nisbet, E. (2001). London methane emissions: Use of diurnal changes in concentration and d13C to identify urban sources and verify inventories. *Journal of geophysical research, 106*, 7427-7448.

Maazallahi, H., Fernandez, J., Menoud, M., Zavala-Araiza, D., Weller, Z., Schwietzke, S., . . . Rockmann, T. (2020). Methane mapping, emission quantification, and attribution in two European cities: Utrecht (NL) and Hamburg (DE). *Atmospheric Chemistry and Physics, 20*, 14717-14740.

Matveev, A., Laurion, I., & Vincent, W. (2018). Methane and carbon dioxide emissions from thermokarst lakes on mineral soils. *Arctic Science, 4*(4), 584-604.

Matveev, A., Laurion, I., Deshpande, B., Bhiry, N., & Vincent, W. (2016). High methane emissions from thermokarst lakes in subarctic peatlands. *Limnology and Oceanography, 61*(S1), 150-164.

McCalley, C., Hodgkins, S., Wher, R., Kim, E.-H., Mondav, R., Crill , P., . . . Saleska , S. (2014). Methane dynamics regulated by microbial community response to permafrost thaw. *Nature, 514*, 478-481.

Miller, J., Lehman, S., Verhults, K., Miller, C., Duren, R., Yadav, V., . . . Sloop, C. (2020). Large and seasonally varying biospheric CO2 fluxes in the Los Angeles megacity revealed by atmospheric radiocarbon. *Proceedings of the National Academy of Sciences, 117*(43), 26681-26687.

Neff, J., Finlay, J., Zimov, S., Davydov, S., Carrasco, J., Schuur, E., & Davydova, A. (2006). Seasonal changes in the age and structure of dissolved organic carbonin Siberian rivers and stream. *Geohysical research letters, 33*(23).

O'Connor, F., Boucher, O., Gedney, N., Jones, C., Folberth, G., Coppell, R., . . . Johnson, C. (2010). Possible role of wetlands, permafrost, and methane hydrates in the methane cycle under future climate change: a review. *Reviews of geophysics, 48*(4).

Olefeldt , D., Goswami, S., Grosse, G., Hayes , D., Hugelius, G., Kuhry, P., . . . Turetsky, M. (2016). Circumpolar distribution and carbon storage of thermokarst landscapes. *Nature communications, 7*(1), 1-11.

Olson, I. (1970). The use of oxalic acid as a standard. *Radiocarbon variations and absolute chronology*, 17.

Park, R., & Epstein, S. (1960). Carbon isotope fractionation during photosynthesis. *Geochim. et Cosmochim. Acta, 21*.

Parmentier, F.-J., Christensen , T., Lotte Sorensen , L., Rysgaard , S., McGuire, A., Miller, P., & Walker, D. (2013). The impact of lower sea-ice extent on Arctic greenhouse-gas exchange. *Nature Climate Change, 3*, 195-202.

Pienitz, R., Doran , P., & Lamoureux, S. (2008). Origin and geomorphology of lakes in the polar regions. In *Polar lakes and rivers: limnology of arctic and antarctic aquatic ecosystems* (pp. 25-42). Oxford University Press.

Preskenis, V., Laurion, I., Bouchard, F., Douglas, P., Billet, M., Fortier, D., & Xu, X. (2021). Seasonal patterns in greenhouse gas emissions from lakes and ponds. *Limnology and oceanography*, *66*, S117-S141.

Prowse, T., Wrona, F., Reist, J., Gibson, J., Hobbie, J., Levesque, L., & Vincent, W. (2002). Climate change effects on hydroecology of arctic freshwater ecosystems. *AMBIO: A journal of the Human Environment, 35*, 347-358.

Rooney, R., Bayley, S., & Schindler, D. (2012). Oil sands mining and reclamation cause massive loss of peatland and stored carbon. *Proceeding of the National Academy of Sciences, 109*(13), 4933-4937.

Saunois, M., Bousquet, P., Poulter, B., Peregon, A., Ciais, P., Canadell, J. G., . . . Zhu, Q. (2016). The global methane budget 2000-2012. *Earth System Science Data, 8*(2), 697-751. Retrieved from https://doi.org/10.5194/essd-8-697-2016

Saunois, M., Stavert, A. R., Poulter, B., Bousquet, P., Canadell, J. G., Jackson, R. B., . . . Zhuang, Q. (2020). The global methane budget 2000-2017. *Earth System Science Data, 12*(13), 1561-1623. doi:https://doi.org/10.5194/essd-12-1561-2020

Schaefer, H. (2019). On the causes and consequences of recent trends in atmospheric methane. *Current Climate Change Reports, 5*, 259-274.

Schaefer, H., Mikaloff Fletcher, S., Veidt, C., Lassey , K., Brailsford, G., Bromley, T., . . . White , J. (2016). A 21st-century shift from fossil-fuel to biogenic methane emissions indicated by 13CH4. *Science, 352*(6281).

Schuur, E., Carbone, M., Hicks Pries, C., Hopkins, F., & Natali, S. (2016). Radiocarbon in Terrestrial Sytems. In E. Schuur, E. Druffel, & S. Trumbore, *Radiocarbon and Climate Change.* Springer.

Schuur, E., McGuire, A., Schadel, C., Grosse, G., Harden, J., Hayes, D., . . . Vonk, J. (2015). Climate change and the permafrost carbon feedback. *Nature*, *520*, 171-179.

Seekel, D., Lapierre, J., & Cheruvelil, K. (2018). A geography of lake carbon cycling. *Limnology and oceanography Letters, 3*, 49-56.

Sherwood, O., Schwietzke, S., Arling, V., & Etiope, G. (2017). Global inventory of gas geochemistry data from fossil fuel, microbial and burning sources, version 2017. *Earth system science data* , *9*(2), 639-656.

Sinha, E., Michalak, A., & Balaji, V. (2017). Eutrophication will increase during the 21st century as a result of precipitation changes. *Science, 357*(6349), 405-408.

Small, C., Cho, S., Hashisho , Z., & Ulrich, A. (2015). Emissions from oil sands tailings ponds: Review of tailings pond parameters and emission estimates. *Journal of petroleum science and engineering, 127*, 490-501.

Smith, L., Sheng, Y., & MacDonald, G. (2007). A first pan-arctic assessment of the influence of glaciation, permafrost, topography and peatlands on the northern hemisphere lake distribution. *permafrost and periglacial processes, 18*, 201-208.

Stuiver, M., & Polach, H. (1977). Discussion reporting of 14C data. *Radiocarbon, 19*(3), 355-363.

Tank, S., Striegl, R., McClelland, J., & Kokelj, S. (2016). Multi-decadal increases in dissolved organic carbon and alkalinity flux from the Mckenzie drainage basin to the Arctic Ocean. *Environmental research letters, 11*(5).

Tank, S., Vonk, J., Walvoord, M., McClelland , J., Laurion , I., & Abbott , B. (2020). Landscape matters: predicting the biogeochemical effects of permafrost thaw on aquatic networks with a state factor approach. *Permafrost and periglacial process, 31*, 358-370.

Thornton, B., Wik, M., & Crill, P. (2015). Climate-forced changes in available energy and methane bubbling from subarctic lakes. *Geophysical Research Letters, 42*(6), 1936-1942.

Townsend-Small, A., Botner, C., Jimenez, K., Schroeder, J., Blake, N., Meinardi, S., . . . Flocke, F. (2016). Using stable isotopes of hydrogen to quantify biogenic and thermogenic atmospheric methane sources: A case study from the Colorado Front Range. *Geophysical Research Letters*, *43*(21).

Townsend-Small, A., Tyler, S., Pataki, D., Xu, X., & Christensen , L. (2012). Isotopic measurements of atmospheric methane in Los Angeles, California, USA: Influence of "fugitive" fossil fuel emissions. *Journal of Geophysical Research: Atmospheres*, *117*.

Treat, C., Natali, S., Ernakovich, J., Iversen, C., Lupascu, M., McGuire, A., . . . Waldrop, M. (2015). A pan-Arctic synthesis of CH4and CO2production fromanoxic soil incubations. *Global Change Biology, 21*(7), 2787–280.

Trumbore, S. (2009). Radiocarbon and soil dynamics. *Annual Review of Earth and Planetary Sciences, 37*(1), 47-66.

Turner, A., Frankerburg , C., & Kort, E. (2019). Interpreting contemporary trends in atmospheric methane. *Proceedings of the National Academy of Science, 116*, 2905-2813.

Valentine, D., & Reeburgh, W. (2000). New perspectives on anaerobic methane oxidation. *Environmental microbiology, 2*(5), 477-484.

Vaughn, L., & Torn, M. (2019). 14C evidence that millennial and fast-cycling soil carbon are equally sensitive to warming. *nature climate change, 9*, 467-471.

Volik, O., Elmes, M., Petrone, R., Kessel, E., Green, A., Cobbaert, D., & Price, J. (2020). Wetlands in the Athabasca Oil Sands Region: the nexus between wetland hydrological function and resource extraction. *Environmental reviews, 28*(3), 246-261.

Vonk, J., Sanchez-Garcia, L., van Dongen, B., Alling, V., Kosmach, D., Charkin, A., . . . Gustafsson, O. (2012). Activation of old carbon by erosion of coastal and subsea permafrost in Arctic Siberia. *Nature, 489*, 137-140.

Walter Anthony , K., Daanen, R., Anthony, P., Schneider von Demling , T., Ping, C., Chanton, J., & Grosse , G. (2016). Methane emissions proportional to permafrost carbon thawed in Arctic lakes since the 1950s. *Nature geoscience, 9*, 679-682.

Whiticar, M. (1999). Carbon and hydrogen isotope systematics of bacterial formation and oxidation of methane. *Chemical geology, 161*(1), 219-314.

Wik, M., Varner, R., Walter Anthony, K., MacIntyre, S., & Batsviken , D. (2016). Climate-sensitive northern lakes and ponds are critical components of methane release. *nature geoscience, 0*, 99-105.

Wild, B., Andersson, A., Broder, L., Vonk, J., Hugelius , G., McClelland, J., . . . Gustafsson, O. (2019). Rivers across the Siberian Arctic unearth the patternsof carbon release from thawing permafrost. *Proceedings of the National Academy of Sciences, 1116*(21), 10280-10285.

Zazzeri, G., Xu, X., & Graven H. (2021). Efficient Sampling of Atmospheric Methane for Radiocarbon Analysis and Quantification of Fossil Methane. *Environmental Science & Technology, 55*(13), 8535-8541.

Zhu, X.-c., Di, D.-r., Ma , M., & Shi, W.-y. (2019). Stable Isotopes in Greenhouse gases from Soil: A Review of Theory and Application. *Atmosphere, 10*(7), 377.

Zhu, Y., Purdy, K., Eyice, O., Shen, L., Harpenslager, S., Yvon-Durocher, G., . . . Trimmer, M. (2020). Disproportionate increase in freshwater methane emissions induced by experimental warming. *Nature climate change, 10*(7), 685–690.

## Appendix

### A1. Dataset and supporting information of Chapter 3

**Table 0.1. Fraction modern carbon and radiocarbon age of the carbon fractions analysed in Chapter 3.**

| **Site (Replicate)** | **Date of collection** | **Fraction** | **FMC** | **(±s)** | **$^{14}$C age (yrs BP)** | **(±s)** |
|---|---|---|---|---|---|---|
| KWK12 | August_2018 | CH4 ebullition | 1.0579 | 0.0046 | Modern | NA |
| KWK1 | August_2018 | CH4 ebullition | 1.0511 | 0.0048 | Modern | NA |
| KWK12 | August_2018 | CH4 dissolved | 1.0438 | 0.0046 | Modern | NA |
| KWK1 | August_2018 | CH4 dissolved | 0.9824 | 0.0043 | 143 | 35 |
| KWK1 | August_2019 | CH4 dissolved | NA | NA | NA | NA |
| KWK12 | August_2019 | CH4 dissolved | NA | NA | NA | NA |
| KWK12 | August_2018 | DIC | 1.0368 | 0.0048 | Modern | NA |
| KWK1 | August_2018 | DIC | 0.9648 | 0.004 | 288 | 33 |
| KWK1 | August_2019 | DIC | 1.0381 | 0.0044 | Modern | 34 |
| KWK12 | August_2019 | DIC | 1.0214 | 0.0051 | Modern | 40 |
| SAS2A (2) | August_2018 | CH4 ebullition | 0.8053 | 0.0037 | 1740 | 37 |
| SAS2B (2) | August_2018 | CH4 ebullition | 0.8536 | 0.0037 | 1272 | 35 |
| SAS2C (2) | August_2018 | CH4 ebullition | 0.8629 | 0.0038 | 1185 | 35 |
| SAS2A | August_2019 | CH4 ebullition | 0.798 | 0.0023 | 1812 | 24 |
| SAS2B (1) | August_2019 | CH4 ebullition | 0.8726 | 0.0025 | 1094 | 23 |
| SAS2B (2) | August_2019 | CH4 ebullition | 0.8221 | 0.0025 | 1573 | 24 |
| SAS2C (1) | August_2019 | CH4 ebullition | 0.8472 | 0.0062 | 1332 | 59 |
| SAS2C (2) | August_2019 | CH4 ebullition | 0.8854 | 0.0026 | 978 | 24 |
| SAS2A | August_2018 | Ebullition CO2 | 0.9971 | 0.0018 | 25 | 15 |
| SAS2C | August_2018 | Ebullition CO2 | 0.9525 | 0.0017 | 390 | 15 |
| SAS2A | August_2019 | Ebullition CO2 | 0.9402 | 0.0085 | 495 | 73 |
| SAS2B | August_2019 | Ebullition CO2 | 0.9542 | 0.0028 | 376 | 24 |
| SAS2C | August_2019 | Ebullition CO2 | 0.9652 | 0.0028 | 285 | 23 |
| SAS2A | August_2018 | CH4 dissolved | 1.0005 | 0.0046 | Modern | NA |

| | | | | | | |
|---|---|---|---|---|---|---|
| SAS2B | August_2018 | CH4 dissolved | 0.9407 | 0.0041 | 491 | 35 |
| SAS2C | August_2018 | CH4 dissolved | 0.966 | 0.0044 | 278 | 37 |
| SAS2A | February_2019 | CH4 dissolved | 0.9976 | 0.0046 | 19 | 37 |
| SAS2B | February_2019 | CH4 dissolved | 0.9604 | 0.0044 | 324 | 37 |
| SAS2C | February_2019 | CH4 dissolved | 0.962 | 0.0042 | 311 | 35 |
| SAS2A | August_2019 | CH4 dissolved | 0.9926 | 0.0045 | 60 | 37 |
| SAS2B | August_2019 | CH4 dissolved | 0.9305 | 0.0043 | 579 | 37 |
| SAS2C | August_2019 | CH4 dissolved | 0.9548 | 0.0044 | 372 | 37 |
| SAS2A | August_2018 | DIC | 0.4123 | 0.0014 | 7117 | 27 |
| SAS2B | August_2018 | DIC | 0.9953 | 0.0038 | 38 | 31 |
| SAS2C | August_2018 | DIC | 0.9344 | 0.0026 | 545 | 22 |
| SAS2A | August_2019 | DIC | 0.9844 | 0.0087 | 126 | 71 |
| SAS2B | August_2019 | DIC | 0.9339 | 0.0056 | 549 | 48 |
| SAS2C | August_2019 | DIC | 0.9673 | 0.0146 | 267 | 121 |
| SAS2A | February_2019 | DIC | 0.9493 | 0.0048 | 418 | 41 |
| SAS2B | February_2019 | DIC | 0.9117 | 0.0049 | 743 | 43 |
| SAS2C | February_2019 | DIC | 0.9476 | 0.0046 | 432 | 39 |
| SAS river upstream | February_2019 | DIC | 0.8829 | 0.0046 | 1001 | 42 |
| SAS river downstream | February_2019 | DIC | 0.8764 | 0.0046 | 1060 | 42 |
| Non peatland river 1 | August_2019 | DIC | 1.0136 | 0.0028 | Modern | 22 |
| Non peatland river 2 | August_2019 | DIC | 1.0083 | 0.0024 | Modern | 19 |
| KWK1 | August_2019 | DOC | 1.0793 | 0.0038 | Modern | 28 |
| KWK12 | August_2019 | DOC | 1.0801 | 0.0044 | Modern | 33 |
| KWK12 | August_2018 | DOC | 1.0609 | 0.0029 | Modern | NA |
| KWK1 | August_2018 | DOC | 1.0623 | 0.0029 | Modern | NA |
| SAS2A | August_2019 | DOC | 0.9208 | 0.0068 | 662 | 59 |
| SAS2B | August_2019 | DOC | 0.8679 | 0.0049 | 1138 | 46 |
| SAS2C | August_2019 | DOC | 0.9596 | 0.0094 | 331 | 79 |
| SAS2A | August_2018 | DOC | 0.9147 | 0.0025 | 716 | 22 |
| SAS2B | August_2018 | DOC | 0.8598 | 0.0024 | 1213 | 22 |

| | | | | | | |
|---|---|---|---|---|---|---|
| SAS2C | August_2018 | DOC | 0.914 | 0.0025 | 723 | 22 |
| SAS2A | February_2019 | DOC | 0.8654 | 0.0037 | 1162 | 34 |
| SAS2B | February_2019 | DOC | 0.834 | 0.0035 | 1458 | 34 |
| SAS2C | February_2019 | DOC | 0.905 | 0.0039 | 802 | 34 |
| Non peatland river 1 | August_2019 | DOC | 1.0636 | 0.0034 | Modern | 26 |
| Non peatland river 2 | August_2019 | DOC | 1.0766 | 0.0031 | Modern | 23 |
| SAS river upstream | February_2019 | DOC | 0.9644 | 0.0041 | 291 | 34 |
| SAS river downstream | February_2019 | DOC | 0.954 | 0.0041 | 378 | 34 |
| SAS2A | August_2019 | POC | 0.895 | 0.0026 | 891 | 23 |
| SAS2B | August_2019 | POC | 0.8343 | 0.0031 | 1455 | 30 |
| SAS2C | August_2019 | POC | 0.8697 | 0.0026 | 1122 | 24 |
| KWK1 | August_2019 | POC | 0.9884 | 0.0029 | 94 | 24 |
| KWK12 | August_2019 | POC | 0.9148 | 0.0033 | 715 | 29 |
| Non peatland river 1 | August_2019 | POC | 0.9305 | 0.0043 | 579 | 37 |
| Non peatland river 2 | August_2019 | POC | 0.9097 | 0.0052 | 760 | 46 |
| SAS2A | August_2018 | POC | 0.8804 | 0.0124 | 1023 | 113 |
| SAS2B | August_2018 | POC | 0.7862 | 0.017 | 1932 | 174 |
| SAS2C | August_2018 | POC | 0.8663 | 0.012 | 1153 | 112 |
| KWK12 | August_2018 | POC | 0.9326 | 0.0152 | 560 | 131 |
| KWK1 | August_2018 | POC | 0.9162 | 0.0154 | 703 | 135 |
| SAS2A | February_2019 | POC | 0.7506 | 0.0146 | 2305 | 156 |
| SAS2B | February_2019 | POC | 0.7007 | 0.0144 | 2857 | 165 |
| SAS2C | February_2019 | POC | 0.7394 | 0.014 | 2425 | 152 |
| SAS River upstream | February_2019 | POC | 0.6833 | 0.0197 | 3060 | 232 |
| SAS River downstream | February_2019 | POC | 0.724 | 0.019 | 2594 | 210 |
| SAS2A | August_2019 | Sediment OC | 0.7197 | 0.0021 | 2642 | 23 |
| SAS2B | August_2019 | Sediment OC | 0.7839 | 0.0023 | 1956 | 23 |

| | | | | | | |
|---|---|---|---|---|---|---|
| SAS2C | August_2019 | Sediment OC | 0.8077 | 0.0024 | 1716 | 24 |
| KWK1 | August_2019 | Sediment OC | 1.093 | 0.003 | Modern | 22 |
| KWK12 | August_2019 | Sediment OC | 1.0698 | 0.003 | Modern | 23 |
| SAS2A | August_2018 | Sediment OC | 0.6515 | 0.0021 | 3442 | 25 |
| SAS2B | August_2018 | Sediment OC | 0.5884 | 0.0021 | 4260 | 29 |
| SAS2C | August_2018 | Sediment OC | 0.669 | 0.002 | 3229 | 24 |
| KWK12 | August_2018 | Sediment OC | 0.8841 | 0.0038 | 990 | 34 |
| KWK1 | August_2018 | Sediment OC | 0.8827 | 0.0042 | 1002 | 39 |

**Table 0.2. $\delta^{13}$C and concentration of DOC, DIC, POC, $CH_4$, and sediment OC.** This table shows the composition for the carbon fractions dissolved organic carbon (DOC), dissolved inorganic carbon (DIC), total particulate carbon (TPC), particulate organic carbon (POC), ebullition and dissolved methane ($CH_4$), sediment organic carbon (OC), and sediment carbon (C).

| **Site** | **Date of collection** | **Fraction** | **δ13C-VPDB (‰)** | **(±)** | **Concentration (ppm)** | **(±)** |
|---|---|---|---|---|---|---|
| KWK1 | August_2019 | DOC | -28.99 | 0.2 | 10.48 | 0.5 |
| KWK12 | August_2019 | DOC | -29.05 | 0.2 | 7.92 | 0.5 |
| KWK12 | August_2018 | DOC | -29.33 | 0.2 | 9.3 | 0.5 |
| KWK1 | August_2018 | DOC | -29.19 | 0.2 | 7.1 | 0.5 |
| SAS2A | August_2019 | DOC | -27.24 | 0.2 | 18.29 | 0.5 |
| SAS2B | August_2019 | DOC | -27.01 | 0.2 | 23.50 | 0.5 |
| SAS2C | August_2019 | DOC | -27.81 | 0.2 | 14.03 | 0.5 |
| SAS2A | August_2018 | DOC | -27.56 | 0.2 | 23.99 | 0.5 |
| SAS2B | August_2018 | DOC | -27.28 | 0.2 | 27.01 | 0.5 |
| SAS2C | August_2018 | DOC | -27.45 | 0.2 | 18.9 | 0.5 |
| SAS2A | February_2019 | DOC | -27.14 | 0.2 | 31.11 | 0.5 |
| SAS2B | February_2019 | DOC | -27.33 | 0.2 | 31.68 | 0.5 |
| SAS2C | February_2019 | DOC | -28.35 | 0.2 | 24.89 | 0.5 |
| Non peatland river 1 | August_2019 | DOC | -27.03 | 0.2 | 14.81 | 0.5 |

| | | | | | | |
|---|---|---|---|---|---|---|
| Non peatland river 2 | August_2019 | DOC | -27.55 | 0.2 | 9.44 | 0.5 |
| SAS river upstream | February_2019 | DOC | -29.04 | 0.2 | 7.89 | 0.5 |
| SAS river downstream | February_2019 | DOC | -29.07 | 0.2 | 8.32 | 0.5 |
| Great Whale River MS1 | February_2019 | DOC | -16.33 | 0.2 | 22.67 | 0.5 |
| KWK1 | August_2019 | DIC | -21.01 | 0.2 | 2.98 | 0.5 |
| KWK12 | August_2019 | DIC | -14.63 | 0.2 | 4.07 | 0.5 |
| KWK12 | August_2018 | DIC | -17.79 | 0.2 | 4.23 | 0.5 |
| KWK1 | August_2018 | DIC | -16.48 | 0.2 | 1.81 | 0.5 |
| SAS2A | August_2019 | DIC | -4.98 | 0.2 | 13.78 | 0.5 |
| SAS2B | August_2019 | DIC | -4.83 | 0.2 | 20.20 | 0.5 |
| SAS2C | August_2019 | DIC | -7.22 | 0.2 | 7.82 | 0.5 |
| SAS2A | August_2018 | DIC | -4.68 | 0.2 | 30.98 | 0.5 |
| SAS2B | August_2018 | DIC | -5.48 | 0.2 | 27.21 | 0.5 |
| SAS2C | August_2018 | DIC | -5.23 | 0.2 | 18.27 | 0.5 |
| SAS2A | February_2019 | DIC | -8.29 | 0.2 | 20.68 | 0.5 |
| SAS2B | February_2019 | DIC | -7.75 | 0.2 | 20.78 | 0.5 |
| SAS2C | February_2019 | DIC | -9.76 | 0.2 | 11.17 | 0.5 |
| Non peatland river 1 | August_2019 | DIC | -18.41 | 0.2 | 1.38 | 0.5 |
| Non peatland river 2 | August_2019 | DIC | -15.74 | 0.2 | 1.29 | 0.5 |
| SAS river upstream | February_2019 | DIC | -12.93 | 0.2 | 4.8 | 0.5 |
| SAS river downstream | February_2019 | DIC | -13.02 | 0.2 | 6.48 | 0.5 |
| Great whale River MS1 | February_2019 | DIC | -7.51 | 0.2 | 1.49 | 0.5 |
| SAS2A | August_2018 | CH4 dissolved | -64.6 | 0.1 | 6.76 | 0.4 |
| SAS2B | August_2018 | CH4 dissolved | -60.0 | 0.1 | 10.78 | 0.9 |
| SAS2C | August_2018 | CH4 dissolved | -60.5 | 0.1 | 8.01 | 0.3 |
| KWK12 | August_2018 | CH4 dissolved | -54.7 | 0.1 | 0.09 | 0.0 |
| KWK1 | August_2018 | CH4 dissolved | NA | NA | 0.21 | 0.0 |
| SAS2A | February_2019 | CH4 dissolved | -66.0 | 0.1 | NA | NA |
| SAS2B | February_2019 | CH4 dissolved | -68.6 | 0.1 | NA | NA |
| SAS2C | February_2019 | CH4 dissolved | -65.4 | 0.1 | NA | NA |
| SAS2A | August_2019 | CH4 dissolved | -62.9 | 0.1 | 6.97 | 0.2 |
| SAS2B | August_2019 | CH4 dissolved | -59.5 | 0.1 | 9.68 | 0.3 |
| SAS2C | August_2019 | CH4 dissolved | -56.5 | 0.1 | 4.14 | 0.1 |

|  |  |  |  |  |  |  |
|---|---|---|---|---|---|---|
| KWK1 | August_2019 | CH4 dissolved | NA | NA | 0.00 | 0.0 |
| KWK12 | August_2019 | CH4 dissolved | NA | NA | 0.00 | 0.0 |
| SAS2A | August_2019 | TPC | -28.9 | 0.1 | 2.69 | NA |
| SAS2B | August_2019 | TPC | -28.8 | 0.1 | 1.75 | NA |
| SAS2C | August_2019 | TPC | -31.4 | 0.1 | 1.61 | NA |
| KWK1 | August_2019 | TPC | -35.9 | 0.1 | 1.00 | NA |
| KWK12 | August_2019 | TPC | -34.6 | 0.1 | 0.93 | NA |
| Non peatland river 1 | August_2019 | TPC | -28.1 | 0.1 | NA | NA |
| Non peatland river 2 | August_2019 | TPC | -27.9 | 0.1 | NA | NA |
| KWK1 | August_2019 | POC | -36.3 | 0.1 | 0.09 | NA |
| SAS2A | August_2019 | POC | -29.2 | 0.1 | 4.71 | NA |
| SAS2A | August_2018 | TPC | -29.5 | 0.1 | NA | NA |
| SAS2B | August_2018 | TPC | -28.5 | 0.1 | NA | NA |
| SAS2C | August_2018 | TPC | -29.3 | 0.1 | NA | NA |
| KWK12 | August_2018 | TPC | -36.1 | 0.1 | NA | NA |
| KWK1 | August_2018 | TPC | -30.5 | 0.1 | NA | NA |
| SAS2A | January_2019 | TPC | -29.6 | 0.1 | NA | NA |
| SAS2B | January_2019 | TPC | -29.7 | 0.1 | NA | NA |
| SAS2C | January_2019 | TPC | -30.7 | 0.1 | NA | NA |
| SAS River upstream | January_2019 | TPC | -30.0 | 0.1 | NA | NA |
| SAS River downstream | January_2019 | TPC | -29.5 | 0.1 | NA | NA |

**Table 0.3 $\delta^{13}$C and concentration of $CH_4$, $CO_2$, and sediment OC.** This table contains $\delta^{13}$C and concentration of ebullition methane ($CH_4$) and carbon dioxide ($CO_2$), sediment organic carbon (OC), and sediment carbon (C).

| **Site** | **Date of collection** | **Fraction** | **δ13C-VPDB (‰)** | **(±)** | **Concentration (%)** | **(±)** |
|---|---|---|---|---|---|---|
| SAS2A(1) | August_2019 | Ebullition CO2 | -12.9 | 0.3 | 0.21 | 0.01 |
| SAS2A(2) | August_2019 | Ebullition CO2 | -13.6 | 0.3 | 1.13 | 0.002 |
| SAS2B(1) | August_2019 | Ebullition CO2 | -10.7 | 0.3 | 2.66 | 0.002 |

|  |  |  |  |  |  |  |
|---|---|---|---|---|---|---|
| SAS2B(2) | August_2019 | Ebullition CO2 | -10.9 | 0.3 | 0.83 | 0.001 |
| SAS2C(1) | August_2019 | Ebullition CO2 | -11.0 | 0.3 | 0.76 | 0.08 |
| SAS2C(2) | August_2019 | Ebullition CO2 | -10.8 | 0.3 | 1.44 | 0.17 |
| SAS2A (2) | August_2018 | Ebullition CO2 | NA | NA | 0.52 | NA |
| SAS2B (2) | August_2018 | Ebullition CO2 | NA | NA | 0.34 | NA |
| SAS2C (2) | August_2018 | Ebullition CO2 | NA | NA | 0.49 | NA |
| KWK12 | August_2018 | Ebullition CO2 | NA | NA | 0.22 | NA |
| KWK1 | August_2018 | Ebullition CO2 | NA | NA | 0.17 | NA |
| SAS2A | August_2019 | Sediment C | -27.3 | 0.1 | 25.60 | NA |
| SAS2A | August_2019 | Sediment OC | -27.3 | 0.1 | 26.73 | NA |
| SAS2B | August_2019 | Sediment C | -27.7 | 0.1 | 24.77 | NA |
| SAS2C | August_2019 | Sediment C | -27.8 | 0.1 | 32.51 | NA |
| KWK1 | August_2019 | Sediment C | -31.9 | 0.1 | 2.30 | NA |
| KWK12 | August_2019 | Sediment C | -32.8 | 0.1 | 4.54 | NA |
| KWK1 | August_2019 | Sediment OC | -31.9 | 0.1 | 1.60 | NA |
| SAS2A | August_2018 | Sediment C | NA | NA | 24.38 | NA |
| SAS2B | August_2018 | Sediment C | NA | NA | 30.79 | NA |
| SAS2C | August_2018 | Sediment C | NA | NA | 40.39 | NA |
| KWK1 | August_2018 | Sediment C | NA | NA | 0.68 | NA |
| KWK12 | August_2018 | Sediment C | NA | NA | 2.00 | NA |
| SAS2A(1) | August_2019 | Ebullition CH4 | -60.8 | 0.3 | 0.37 | 0.0 |
| SAS2A(2) | August_2019 | Ebullition CH4 | -62.9 | 0.3 | 11.1 | 0.2 |
| SAS2B(1) | August_2019 | Ebullition CH4 | -68.0 | 0.3 | 27.45 | 0.5 |
| SAS2B(2) | August_2019 | Ebullition CH4 | -64.8 | 0.3 | 5.84 | 0.0 |
| SAS2C(1) | August_2019 | Ebullition CH4 | -65.8 | 0.3 | 24.45 | 0.1 |
| SAS2C(2) | August_2019 | Ebullition CH4 | -64.8 | 0.3 | 30.11 | 0.2 |
| SAS2A (2) | August_2018 | Ebullition CH4 | -60.1 | 0.1 | 8.14 | NA |
| SAS2B (2) | August_2018 | Ebullition CH4 | -60.4 | 0.1 | 17.9 | NA |
| SAS2C (2) | August_2018 | Ebullition CH4 | -60.9 | 0.1 | 12.55 | NA |
| KWK12 | August_2018 | Ebullition CH4 | -71.4 | 0.1 | 14.64 | NA |
| KWK1 | August_2018 | Ebullition CH4 | -69.7 | 0.1 | 2.28 | NA |

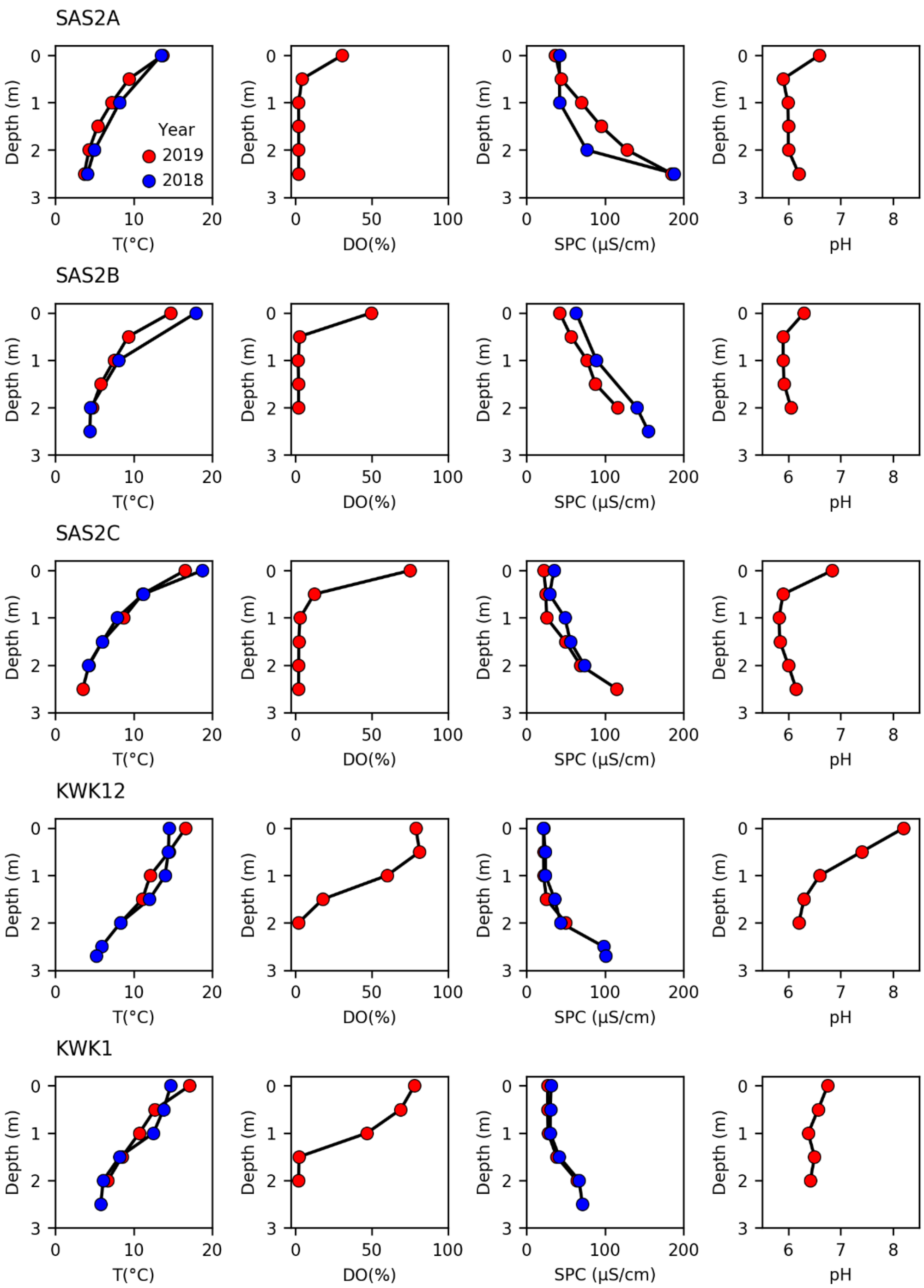

**Figure 0.1. Summer stratification profiles of the five thermokarst lakes sampled in summer 2018 and 2019.**

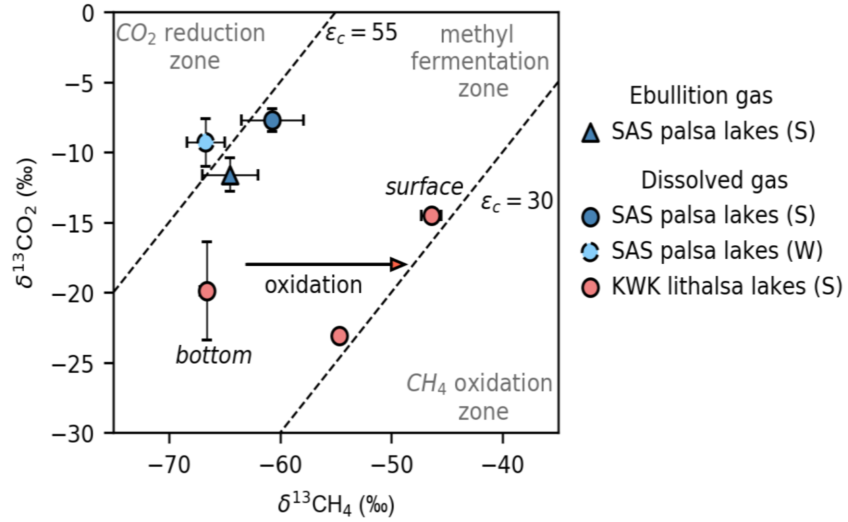

**Figure 0.2. Plot of dissolved and ebullition $\delta^{13}CH_4$ and $\delta^{13}CO_2$ with isotope separation lines ($\varepsilon c = \delta^{13}CO_2 - \delta^{13}CH_4$), after Whiticar (1999).** The arrow shows the $CH_4$ oxidation trajectory. Error bars are smaller than symbols where not shown. The surface and bottom εc values for the lithalsa lakes were obtained from Matveev et al. (2018).

### Calculation of the dissolved $\delta^{13}CO_2$

Gaseous carbon dioxide ($CO_2$ (g)) dissolves in the presence of water ($CO_2$ (aq)) and forms carbonic acid ($H_2CO_3$; equation 6). Because the concentration of $CO_2$ (aq) far exceeds the concentration of $H_2CO_3$, we use $CO_2^*\ (aq)$ to denote the sum of both $CO_2(aq)$. Similarly, $CO_2$*(aq) and $HCO_3^-$ dissociate in water as shown in equations 7 and 8.

$$\boldsymbol{CO_2(g) \rightleftharpoons CO_2^*\ (aq)} \quad \textbf{Equation 6}$$

$$\boldsymbol{CO_2^*(aq) \rightleftharpoons HCO_3^- + H^+} \quad \textbf{Equation 7}$$

$$\boldsymbol{HCO_3^- \rightleftharpoons CO_3^{2-} + H^+} \quad \textbf{Equation 8}$$

The concentration of each equilibrium species depends on the dissociation constants $K_1$, $K_2$, and pH. Using the dissociation constants values, pH values, and the DIC concentration value, we calculated the concentration of $CO_2^*\ (aq), HCO_3^-, and\ CO_3^{2-}$ , knowing that DIC is the sum of these three species. The dissociation constant values for the carbonate equilibrium in pure water were obtained from Harned and Davis (1943), and Harned and Scholes (1941):

$$\boldsymbol{K_1 = \frac{[H^+][HCO_3^-]}{[CO_2^*\,(aq)]} = 10^{-[-126.34+\frac{6320.81}{T(K)}+19.568\ln T(K)]}} \qquad \textbf{Equation 9}$$

$$\boldsymbol{K_2 = \frac{[H^+][CO_3^{2-}]}{[HCO_3^-]} = 10^{-[-90.18+\frac{5143.692}{T(K)}+14.61\ln T(K)]}} \qquad \textbf{Equation 10}$$

Then, we calculated the fractionation factors [$\alpha_{AB} = (\varepsilon_{AB}/1000) + 1$], between $H_2CO_3$ and $CO_2$* (aq), and between $CO_3^{2-}$ and $CO_2$* (aq) from the per mil fractionation factors ε calculated by Zhang et al. (1995):

$$\boldsymbol{\varepsilon_{CO_2^*\,(aq)-CO_2\,(g)} = (0.0049\ \pm 0.0015)\,T} \text{ (°C)} \boldsymbol{- (1.31\ \pm 0.005)} \text{ ‰} \qquad \textbf{Equation 11}$$

$$\boldsymbol{\varepsilon_{HCO_3^-\,(aq)-CO_2\,(g)} = -(0.1141\ \pm 0.0028)\,T} \text{ (°C)} \boldsymbol{+ (10.78\ \pm 0.04)} \text{ ‰} \qquad \textbf{Equation 12}$$

$$\boldsymbol{\varepsilon_{CO_2^3\,(aq)-CO_2\,(g)} = -(0.052\ \pm 0.021)\,T} \text{ (°C)} \boldsymbol{+ (7.22\ \pm 0.38)} \text{ ‰} \qquad \textbf{Equation 13}$$

The dissolved $\delta^{13}CO_2$ can be then calculated from the following equation, which was derived from a mass balance of the $^{13}C/^{12}C$ ratios expressed in terms of $\delta^{13}CO_2^*$ [$\delta^{13}C_A = ((R_A / R_{standard}) - 1) * 1000$], and the fractionation factors [$\alpha_{AB} = (^{13}R_A/^{13}R_B)$].

$$\boldsymbol{\left(\frac{\delta^{13}C_{CO_2^*}}{1000} + 1\right) = \frac{[DIC](\frac{\delta^{13}C_{DIC}}{1000}+1)}{[CO_2^*\,(aq)] + [HCO_3^-]\alpha_{HCO_3^- - CO_2^*\,(aq)} + [CO_3^{2-}]\,\alpha_{CO_3^{2-} - CO_2^*\,(aq)}}} \qquad \textbf{Equation 14}$$

**Table 0.4. Dissolved $\delta^{13}CO_2$ values calculated from $\delta DI^{13}C$, DIC concentration, pH, and temperature.**

| Site | Date of collection | $\delta DI^{13}C$ (‰) | DIC Concentration (ppm) | pH | T (°C) | $\delta^{13}CO_2$ (aq) |
|---|---|---|---|---|---|---|
| SAS2A | August 2019 | -4.98 | 13.78 | 6 | 5.4 | -7.632 |
| SAS2B | August 2019 | -4.83 | 20.2 | 5.92 | 5.8 | -7.118 |
| SAS2C | August 2019 | -7.22 | 7.82 | 5.84 | 6 | -9.182 |
| SAS2A | August 2018 | -4.68 | 30.98 | 5.9 | 6.1 | -6.879 |
| SAS2B | August 2018 | -5.48 | 27.21 | 5.9 | 6 | -7.679 |
| SAS2C | August 2018 | -5.23 | 18.27 | 5.9 | 6 | -7.430 |
| SAS2A | January 2019 | -8.29 | 20.68 | 5.06 | 2 | -8.687 |
| SAS2B | January 2019 | -7.75 | 20.78 | 4.78 | 2 | -7.962 |
| SAS2C | January 2019 | -9.76 | 11.17 | 5.65 | 2 | -11.163 |
| KWK1 | August 2018 | -17.79 | 4.23 | 6.5 | 8.2 | -23.119 |

## A2. Dataset and supporting information of Chapter 4

### Table 0.5. Production rates, $\delta^{13}C$ and $\Delta^{14}C$ values of incubation $CH_4$.

| **Incubation number** | **Incubation time (days)** | **Site** | **Temperature (°C)** | **Replicate** | **Sediment added (g dw)** | **mgC extracted** | **Production rate (umol $CH_4$ $gdw^{-1}$ $days^{-1}$ )** | **$\delta^{13}C$ (‰)** | **±** | **$\Delta^{14}C$ (‰)** | **±** |
|---|---|---|---|---|---|---|---|---|---|---|---|
| 1 | 105 | SAS2B | 4 | 1 | 0.48 | 0.21 | 0.2685 | -16.27 | 0.15 | 23.64 | 2.22 |
| 1 | 105 | SAS2B | 4 | 2 | 0.48 | 0.16 | 0.1935 | | | 15.23 | 2.20 |
| 1 | 105 | SAS2C | 4 | 1 | 0.77 | 0.06 | 0.0481 | | | -127.85 | 3.05 |
| 1 | 105 | SAS2C | 4 | 2 | 0.77 | 0.06 | 0.0481 | | | -131.19 | 3.07 |
| 1 | 105 | KWK1 | 4 | 1 | 4.55 | 0.18 | 0.0234 | | | 55.84 | 2.29 |
| 1 | 105 | SAS2B | 12 | 1 | 0.46 | 0.35 | 0.4473 | -18.18 | 0.15 | 14.55 | 2.26 |
| 1 | 105 | SAS2C | 12 | 1 | 0.76 | 0.08 | 0.0599 | | | -98.49 | 2.67 |
| 1 | 105 | SAS2C | 12 | 2 | 0.76 | 0.08 | 0.0647 | | | -115.38 | 2.57 |
| 1 | 105 | KWK1 | 12 | 1 | 4.38 | 0.23 | 0.0311 | | | 71.79 | 2.36 |
| 1 | 105 | KWK1 | 12 | 2 | 4.29 | 0.22 | 0.0302 | | | 56.56 | 2.36 |
| 1 | 105 | SAS2B | 22 | 1 | 0.47 | 0.57 | 0.7333 | -21.65 | 0.15 | -0.41 | 2.31 |
| 1 | 105 | SAS2B | 22 | 2 | 0.49 | 0.53 | 0.6448 | -22.38 | 0.15 | -12.17 | 2.32 |
| 1 | 105 | SAS2C | 22 | 1 | 0.76 | 0.34 | 0.2619 | -29.46 | 0.15 | -59.79 | 2.05 |
| 1 | 105 | SAS2C | 22 | 2 | 0.79 | 0.14 | 0.1078 | | | -109.80 | 1.99 |
| 1 | 105 | KWK1 | 22 | 1 | 4.25 | 0.37 | 0.0525 | -25.80 | 0.15 | 48.51 | 2.34 |
| 1 | 105 | KWK1 | 22 | 2 | 4.55 | 0.28 | 0.0365 | -22.81 | 0.15 | 57.01 | 2.30 |
| 2 | 219 | SAS2A | 4 | 1 AND 3 | 2.65 | 0.04 | 0.0041 | | | -404.26 | 4.86 |
| 2 | 219 | SAS2A | 4 | 2 | 1.35 | 0.03 | 0.0072 | | | -426.14 | 5.35 |
| 2 | 218 | SAS2A | 12 | 2 | 1.38 | 0.05 | 0.0113 | | | -298.70 | 4.49 |
| 2 | 218 | SAS2A | 12 | 3 AND 1 | 2.65 | 0.10 | 0.0108 | | | -317.32 | 1.90 |
| 2 | 217 | SAS2A | 22 | 2 | 1.36 | 0.14 | 0.0304 | -46.76 | 0.1 | -258.94 | 1.55 |
| 2 | 217 | SAS2A | 22 | 3 AND 1 | 2.76 | 0.12 | 0.0121 | | | -306.13 | 1.74 |
| 2 | 218 | SAS2B | 12 | 1 | 0.50 | 0.19 | 0.1076 | -61.13 | 0.1 | -546.09 | 1.15 |

| | | | | | | | | | | | |
|---|---|---|---|---|---|---|---|---|---|---|---|
| 2 | 218 | SAS2B | 12 | 3 AND 2 | 0.93 | 0.13 | 0.0407 | | | -504.92 | 1.64 |
| 2 | 217 | SAS2B | 22 | 1 | 0.52 | 0.38 | 0.2077 | -60.37 | 0.1 | -223.71 | 1.12 |
| 2 | 217 | SAS2B | 22 | 3 | 0.50 | 0.31 | 0.1763 | -60.97 | 0.1 | -206.99 | 1.15 |
| 2 | 218 | SAS2C | 12 | 1 | 0.82 | 0.11 | 0.0401 | | | -571.59 | 1.63 |
| 2 | 218 | SAS2C | 12 | 2 AND 3 | 1.60 | 0.18 | 0.0319 | -52.20 | 0.1 | -511.91 | 1.17 |
| 2 | 219 | SAS2C | 22 | 3 | 0.83 | 0.18 | 0.0605 | | | -302.07 | 1.17 |
| 3 | 224 (166 without timelag) | SAS2A | 22 | 2 | 0.73 | 0.269 | 0.138846 | -50.8 | 0.1 | -371.3 | 1.1 |
| 3 | 224 (166 without timelag) | SAS2A | 22 | 3 | 0.73 | 0.186 | 0.096097 | -52.1 | 0.1 | -330.7 | 1.3 |
| 3 | 224 (87 without timelag) | SAS2C | 22 | 2 | 0.66 | 0.046 | 0.049662 | | | -779.3 | 6.5 |
| 3 | 224 (87 without timelag) | SAS2C | 22 | 3 | 0.66 | 0.016 | 0.017214 | | | -550.2 | 14.2 |
| 3 | 224 (166 without timelag) | SAS2X | 22 | 1 | 1.20 | 0.068 | 0.021568 | | | -677.4 | 4.0 |
| 3 | 224 (166 without timelag) | SAS2X | 22 | 2 AND 3 | 2.56 | 0.055 | 0.008067 | | | -666.7 | 5.3 |

**Table 0.6. Production rates, δ$^{13}$C and Δ$^{14}$C values of incubation CO$_2$.**

| **Incubation number** | **Incubation time (days)** | **Site** | **Temperature (°C)** | **Replicate** | **Sediment added (g dw)** | **mgCO2 extracted** | **Production rate (umol CO2 gdw$^{-1}$ days$^{-1}$)** | **d$^{13}$C (‰)** | **±** | **Δ$^{14}$C (‰)** | **±** |
|---|---|---|---|---|---|---|---|---|---|---|---|
| 1 | 105 | SAS2B | 4 | 1 | 0.475 | 0.012 | 0.102 | | | -81.64 | 30.65 |
| 1 | 105 | SAS2B | 4 | 2 | 0.485 | 0.032 | 0.133 | | | -52.88 | 3.94 |
| 1 | 105 | SAS2B | 12 | 1 | 0.461 | 0.021 | 0.105 | | | -154.71 | 14.19 |
| 1 | 105 | SAS2B | 20 | 1 AND 2 | 0.955 | 0.110 | 0.111 | | | -113.21 | 2.12 |
| 1 | 105 | SAS2C | 4 | 1 AND 2 | 1.542 | 0.022 | 0.182 | | | -207.99 | 6.60 |

| | | | | | | | | | | | |
|---|---|---|---|---|---|---|---|---|---|---|---|
| 1 | 105 | SAS2C | 12 | 1 AND 2 | 1.526 | 0.079 | 0.143 | | | -125.70 | 2.45 |
| 1 | 105 | SAS2C | 20 | 1 | 0.763 | 0.223 | 0.449 | | | -71.05 | 2.08 |
| 1 | 105 | SAS2C | 20 | 2 | 0.794 | 0.073 | 0.301 | | | -140.26 | 2.52 |
| 1 | 105 | KWK1 | 20 | 1 | 4.248 | 0.450 | 0.518 | -8.23 | 0.15 | 49.64 | 2.35 |
| 1 | 105 | KWK1 | 20 | 2 | 4.555 | 0.012 | 0.534 | | | -75.44 | 9.39 |
| 2 | 219 | SAS2A | 4 | 1 AND 3 | 2.60 | 0.929 | 0.102 | -23.88 | 0.10 | -627.89 | 0.75 |
| 2 | 219 | SAS2A | 4 | 2 | 1.35 | 0.629 | 0.133 | -23.63 | 0.10 | -593.16 | 0.75 |
| 2 | 218 | SAS2A | 12 | 2 | 1.38 | 0.505 | 0.105 | -22.16 | 0.10 | -455.36 | 1.19 |
| 2 | 218 | SAS2A | 12 | 3 AND 1 | 2.60 | 1.005 | 0.111 | -21.82 | 0.10 | -460.34 | 1.08 |
| 2 | 217 | SAS2A | 22 | 2 | 1.36 | 0.862 | 0.182 | -19.56 | 0.10 | -334.82 | 0.98 |
| 2 | 217 | SAS2A | 22 | 3 AND 1 | 2.60 | 1.288 | 0.143 | -21.13 | 0.10 | -381.48 | 1.08 |
| 2 | 218 | SAS2B | 12 | 1 | 0.50 | 0.788 | 0.449 | -21.19 | 0.10 | -489.57 | 0.96 |
| 2 | 218 | SAS2B | 12 | 3 AND 2 | 0.90 | 0.946 | 0.301 | -22.51 | 0.10 | -482.99 | 0.80 |
| 2 | 217 | SAS2B | 22 | 1 | 0.52 | 0.940 | 0.518 | -14.77 | 0.10 | -281.66 | 1.05 |
| 2 | 217 | SAS2B | 22 | 3 | 0.50 | 0.934 | 0.534 | -15.78 | 0.10 | -274.04 | 1.06 |
| 2 | 218 | SAS2C | 12 | 1 | 0.82 | 0.808 | 0.283 | -24.35 | 0.10 | -567.72 | 0.75 |
| 2 | 218 | SAS2C | 12 | 2 AND 3 | 1.60 | 0.973 | 0.174 | -22.90 | 0.10 | -563.00 | 0.82 |
| 2 | 219 | SAS2C | 22 | 3 | 0.83 | 0.808 | 0.276 | -21.69 | 0.10 | -414.63 | 0.97 |
| 3 | 188 | SAS2A | 22 | 2 | 0.73 | 1.018 | 0.464 | -20.07 | 0.10 | -407.44 | 1.01 |
| 3 | 188 | SAS2A | 22 | 3 | 0.73 | 1.031 | 0.469 | -21.04 | 0.10 | -453.78 | 0.93 |
| 3 | 96 | SAS2C | 22 | 2 | 0.66 | 0.786 | 0.771 | -24.63 | 0.10 | -588.27 | 0.75 |
| 3 | 96 | SAS2C | 22 | 3 | 0.66 | 0.837 | 0.829 | -25.70 | 0.10 | -616.98 | 0.82 |
| 3 | 206 | SAS2X | 22 | 1 | 1.20 | 1.068 | 0.271 | -20.33 | 0.10 | -362.57 | 1.03 |
| 3 | 206 | SAS2X | 22 | 2 and 3 | 5.11 | 0.815 | 0.048 | -20.66 | 0.10 | -444.73 | 0.91 |

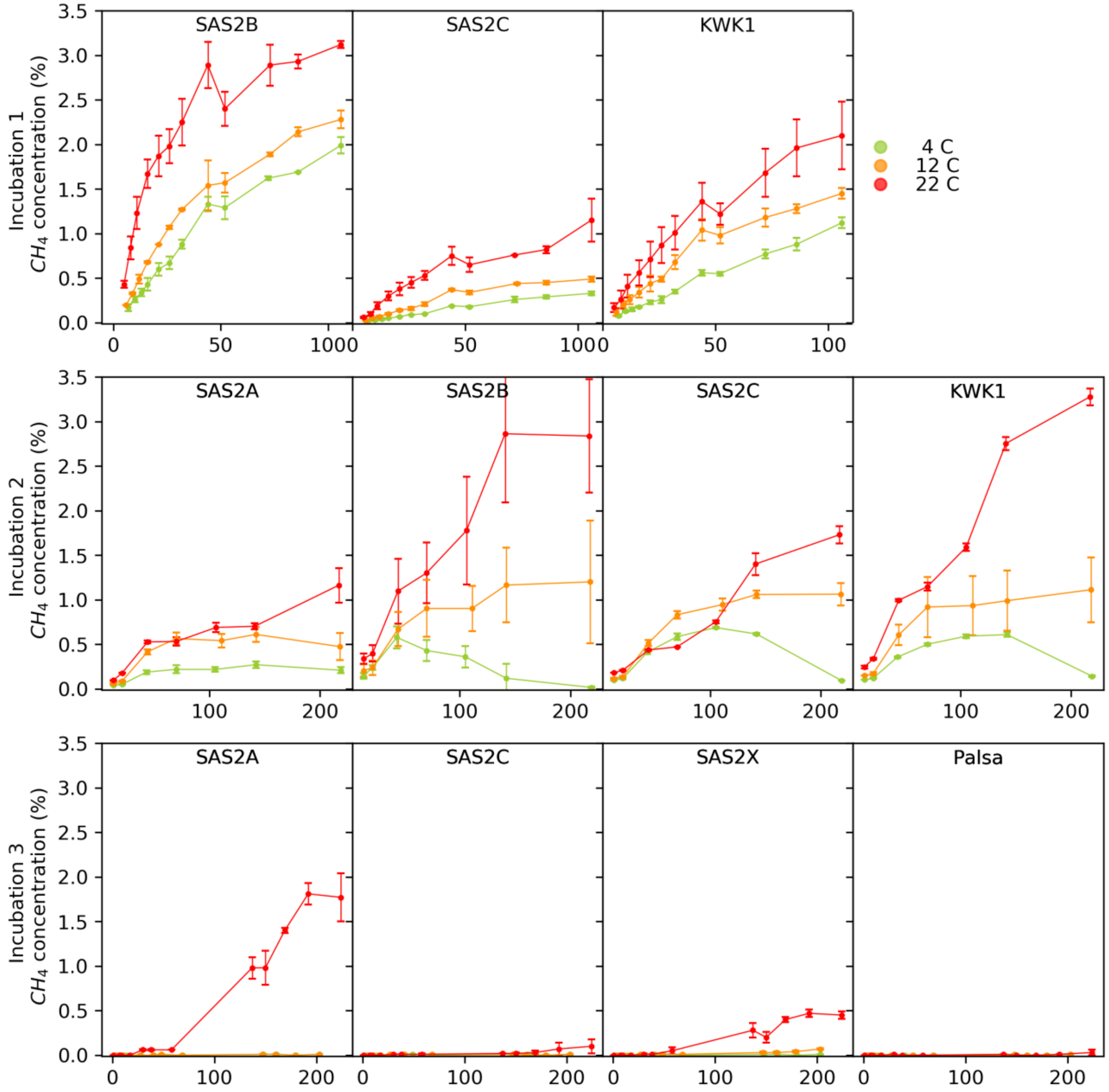

**Figure 0.3. Incubation $CH_4$ concentration profiles.** The plots show the cumulative headspace concentrations of $CH_4$ for the total duration of the incubation experiments including the time lag in the third incubation. First incubation lasted 105 days, the second 219 days and the third 266 days.